AUTOIGNITON CHARACTERISTICS OF PRIMARY REFERENCE FUELS AND THEIR MIXTURES

THESIS

Presented in Partial Fulfillment of the Requirements for

the Degree Master of Science in the Graduate

School of The Ohio State University

By

A. Tyler Little, B.S.

*****

The Ohio State University

2008

Master's Examination Committee:

Professor Ahmet Selamet, Advisor

Professor John Yu

Approved by

Advisor

Department of Mechanical Engineering

ABSTRACT

Internal combustion (IC) engine knock is characterized by uncontrolled autoignition of a mixture of fuel and oxidizer, whereas homogeneous charge compression ignition (HCCI) relies on controlling the autoignition to achieve a favorable engine performance. This study investigates the autoignition of Primary Reference Fuels (PRFs) using the kinetic model by Curran *et al*. (2002). The CHEMKIN (2006) software is used to facilitate solutions in a constant volume reactor and a variable volume reactor representing an internal combustion engine. Both models assume homogeneous mixing of fuel and oxidizer. Experimental data for shock tube ignition delay times and HCCI engine pressures and temperatures have been obtained from literature. First, shock tube data is compared with the present predictions in the constant volume adiabatic reactor for a range of inlet temperatures and fuel octane numbers. CHEMKIN's IC engine model with a heat transfer correlation is then used to reproduce the engine experimental data. Finally, a parametric study of the effect of inlet pressure, inlet temperature, octane number, fuel/air equivalence ratio, and exhaust gas recirculation (EGR) on the autoignition of PRF/air mixtures is conducted.

The kinetic model used in conjunction with the adiabatic constant volume reactor captures ignition delay trends of variation with temperature and fuel. However, the model predicts longer ignition delay for the majority of temperatures and octane numbers compared to the shock tube experiments. Important trends in the experimental HCCI engine data are also reproduced well by the model, yet difficulties are encountered while attempting to model the engine data. It is reasoned that these difficulties are primarily due to the non-ideal conditions, such as mixture and temperature inhomogeneities, existing in the experiments. A number of interesting characteristics are demonstrated in the parametric study. In particular, it is discovered that PRFs can exhibit single or two-stage ignition depending on the inlet temperature. The total ignition delay corresponding to the second stage ignition is observed to be dependent upon the energy released during the first stage reactions. Inlet pressure and temperature, octane number, and equivalence ratio all affect the first stage energy release. Thermodynamic and chemical effects are identified for the EGR constituents CO_2, H_2O, and N_2. The thermodynamic effect resulting from addition of CO_2 or H_2O is to inhibit temperature rise of the gas mixture resulting from compression by the piston or energy released by chemical reactions. This is due to the larger specific heat c_p of these species compared to air. N_2 has a slightly lower c_p than air and thus its addition may actually enhance temperatures. Introduction of each diluent has the chemical effect of reducing O_2 mole fraction, which delays ignition. A separate chemical effect of ignition enhancement is also identified for H_2O.

ACKNOWLEDGMENTS

I would like to thank my advisor, Prof. Ahmet Selamet, for the opportunity and support he has provided for my graduate study. His counsel and guidance have been invaluable to my education and will continue to be for my future endeavors. I am especially appreciative of the time he has committed and attention to detail he has shown in the development of this thesis. Additionally, I would like to thank Prof. John Yu for serving on my defense committee. I also wish to express sincere gratitude to my family for the love and support they have shown over the course of my education. And last, but certainly not least, I would like to thank my fiancé for her love and encouragement.

VITA

July 1, 1983	Born – Athens, OH
2007	B.S. Mechanical Engineering, The Ohio State University.
2007 – present	Graduate Research Associate, The Ohio State University.

FIELDS OF STUDY

Major Field: Mechanical Engineering

TABLE OF CONTENTS

LIST OF TABLES

LIST OF FIGURES

CHAPTER 1

INTRODUCTION

Hydrocarbon combustion in internal combustion (IC) engines remains the primary source of propulsion for land vehicles. High oil prices and increasingly strict emissions regulations motivate research in the area and as a result many promising technologies have emerged. For example, hybrid-electric and flex-fuel vehicles are becoming popular as automotive companies increase production after years of research. Efforts are currently being made to develop even more radical technologies such as fuel cell and fully electric powertrains, which do not rely on hydrocarbon combustion directly. Many are attracted to such projects because they believe they offer solutions to emissions problems and heavy foreign oil dependence. However, these supporters often fail to consider the energy life-cycle. Electric vehicles most likely would rely on coal combustion to charge batteries which generates large amounts of CO_2, and the hydrogen required for "zero emissions" fuel cell vehicles does not exist naturally in the earth's atmosphere and therefore requires production using some other energy source, presumably nuclear or fossil fuel based. While these technologies may offer some benefits, they should not be viewed as permanent solutions. A more realistic outlook is to utilize a variety of technologies that improve efficiency and emissions. For this reason

the combustion of hydrocarbon fuels in an engine environment remains a subject that merits investigation.

It can be shown that the fuel conversion efficiency of a four-stroke spark ignition (SI) engine is given by

$$\eta = 1 - \frac{1}{r_c^{\gamma-1}}, \tag{1.1}$$

where r_c is the compression ratio representing the ratio of the maximum to minimum cylinder volume and γ is the ratio of specific heats for ideal gases. Assuming constant γ, efficiency increases with r_c, however, limits are imposed on the compression ratio by knocking combustion. Knock is essentially the uncontrolled spontaneous ignition, or autoignition, of a portion of the charge within an engine cylinder in which energy is released at a faster than normal rate. This rapid energy release can cause substantial damage to the engine structure. Knock is governed primarily by the temperature of the compressed gas and hence as r_c increases, so does pressure and temperature. Consequently, knock is arguably the largest barrier to efficiency improvements in SI engines.

Knock at its most fundamental level is a chemical kinetics phenomenon. In fact, the study of any combustion system requires knowledge of the kinetic interaction of its molecules which can involve thousands of reactions among a large number of species. A significant effort in combustion research involves the development of models to represent the chemical kinetics of fuel oxidation. Applied to automotive combustion, an accurate

model can be useful for predicting the onset of knock as well as other important concerns such as pollutant formation. Methods for suppressing knock are currently the subject of much investigation relying heavily on not only experimental but also computational studies via kinetic models.

Homogeneous charge compression ignition (HCCI) is a promising technology for IC engines that is in many ways kinetically similar to knock. HCCI relies on controlled autoignition via compression of a homogeneously mixed fuel and oxidizer. It is attractive because it possesses the positive qualities of both compression ignition (CI) and SI engines, namely high efficiency similar to CI engines and low emissions of particulates and NO_x that can be achieved with aftertreatment in SI engines. Despite nearly 30 years of research, HCCI engines are yet to reach the mass production level primarily due to difficulties in controlling the ignition event over a wide range of speeds and load conditions. However, advancements in control methods such as electronic sensors and exhaust gas recirculation (EGR) may allow HCCI engines to become a practical technology. EGR involves the recirculation of inert exhaust gas into the engine intake which acts as an energy absorber during compression, inhibiting the temperature rise. It has also been proposed as a method of suppressing knock in SI engines.

Several efforts have investigated the phenomenon of autoignition in an environment similar to that of an engine. Hu and Keck (1987) developed a branched chain kinetic model consisting of 18 reactions to correlate experimental data of explosion limits of saturated hydrocarbons in a constant volume bomb and homogeneous

autoignition in a rapid compression machine (RCM). The mechanism reproduced much of the low and intermediate temperature chemistry and predicted the well known two-stage ignition. Key branching agents and reactions as well as terminating reactions governing the first and second stage ignition were identified. Tanaka *et al*. (2003) expanded the Hu and Keck mechanism to 55 reactions by including those important to the high temperature regime responsible for the majority of energy release. They also included an interaction between primary reference fuels (PRFs) *n*-heptane (*n*-C_7H_{16}) and *iso*-octane (*i*-C_8H_{18}) to facilitate the use of fuels with varying octane number (ON). Comparisons with RCM experiments using fuels representing a wide range of ON (Tanaka *et al*., 2003) have shown excellent agreement.

Curran *et al*. (2002) developed a complex reaction mechanism of 4236 reactions to describe the oxidation of PRF mixtures over a broad range of conditions. The mechanism represents a compilation of their previous work on *n*-heptane and *iso*-octane oxidation. Using experimental results of ignition behind a reflected shock wave, they were able to accurately describe low, intermediate, and high temperature chemistry and predict much of the intermediate product formation that is characteristically lacking in smaller mechanisms. Model comparisons with experiment were favorable for various flow reactors, a jet-stirred reactor, and a shock tube. Modeling of a motored engine revealed some agreement with experimentally determined critical compression ratios. Andrae *et al*. (2005) attempted to expand the mechanism by Curran and co-workers by including 132 co-oxidation reactions between *n*-heptane and *iso*-octane. They attempted to model both the compression and expansion of HCCI combustion as opposed to strictly

compression as in the RCM. Results with the co-oxidation reactions showed an improvement with comparisons to experimental data, however, the adiabatic modeling used in their study fails to represent actual experimental conditions.

An accurate kinetic model should have the capability of predicting the autoignition event and thus the onset of knock. Methods to suppress knock have been the subject of research for some time. Traditional techniques for knock suppression include retardation of spark timing and/or fuel enrichment to limit the charge temperature. However, fuel enrichment is detrimental to fuel consumption and also to emissions as a result of the departure from stoichiometric operation needed for efficient three-way catalytic conversion. Several studies have investigated the potential of using EGR as a knock suppressant. To avoid the power loss associated with replacing a portion of the intake air with diluent gases, EGR is often used in turbocharged engines. Brüstle and Hemmerlein (1994) studied EGR in a turbocharged engine and found that it could be used to raise the mean effective pressure or increase the compression ratio. Grandin *et al*. (1998) investigated the use of cooled EGR in a turbocharged SI engine and observed a decreased combustion rate leading to lower peak cylinder pressure and temperature which were favorable to knock suppression. Diana *et al*. (1996) used EGR in a naturally aspirated engine and discovered that an increase in r_c from 10 to 13 could be achieved using 11% EGR with spark timing set for maximum brake torque. A recent investigation by Sjöberg *et al*. (2007) attempted to quantify the thermodynamic and chemical effects of EGR and its major constituents on HCCI autoignition. The primary mechanisms identified as being responsible for retarding the start of combustion were a

thermodynamic cooling effect due to the high specific heat capacities of CO_2 and H_2O, and an O_2 reduction effect resulting from a portion of the intake air being displaced by the EGR gases. It was also discovered that H_2O had a chemical effect of enhancing autoignition which negated its thermodynamic cooling effects for PRF 80 but had less of an impact on *iso*-octane and gasoline. The effect of trace species such as CO, NO, and unburned hydrocarbons were also found to possess both enhancement and suppression tendencies depending of the type of fuel used.

The objective of this work is to study the spontaneous ignition and combustion of a homogeneous mixture of PRF and air. It is therefore relevant to the analysis of autoignition as it pertains to engine knock and HCCI combustion. The detailed chemical kinetic model by Curran *et al*. (2002) describing the oxidation of PRFs capable of representing a wide range of fuel octane numbers is used in conjunction with CHEMKIN (2006) to simulate the combustion. Experimental data of ignition delay times in a shock tube reactor are first compared to constant volume homogeneous reactor calculations to assess accuracy of the kinetic model in predicting the ignition event in an easily controlled environment. The kinetic model is then extrapolated to the more complex environment of an engine. Experimental data representing a range of engine geometry and operating conditions is taken from literature. Upon validation of the kinetic model, the effect of operating parameters, such as inlet pressure and temperature, octane number, equivalence ratio, and EGR, on the autoignition event and combustion are investigated.

CHAPTER 2

HYDROCARBON COMBUSTION AND MODELING

2.1 Reaction Kinetics

Combustion of a fuel and oxidizer generally involves reaction of many different species whose formation and destruction are interdependent. The rates in which reactions proceed are primarily dictated by collisions of two molecules that may have the capability to react. Therefore, the most common elementary reactions used in modeling are bimolecular in that two species collide and react to form two new species. To illustrate, consider an arbitrary bimolecular second order reaction

$$A + B \rightarrow C + D\,. \tag{2.1}$$

The rate at which such a reaction proceeds is proportional to the concentration of the reactant species,

$$\frac{d[A]}{dt} = -k[A][B]\,, \tag{2.2}$$

where the notation [*S*] denotes the molar concentration of species *S*. The rate constant *k* is a function of temperature *T* and is the parameter used to describe each elementary reaction composing the entire kinetic mechanism. A reaction will only take place, however, if the colliding molecules possess an adequate amount of energy called the

activation energy E_A. Kinetic theory shows that the fraction of all collisions that possess energy greater than E_A is given by the Boltzmann factor $\exp\left(\frac{-E_A}{\overline{R}T}\right)$. Determination of reaction rates also requires that the frequency of molecular collisions be taken into account in the form of a pre-exponential factor A. The rate constant k is then typically expressed in a modified Arrhenius form as

$$k = AT^b \exp\left(\frac{-E_A}{\overline{R}T}\right), \tag{2.3}$$

where A, b, and E_A are parameters determined experimentally and $\overline{R}$ is the universal gas constant. The exponent b becomes particularly important in systems where temperatures vary widely. Kinetic model construction is accomplished by including all the reactions believed to significantly contribute to the energy release and formation of products. Accompanying each reaction are unique values of the parameters in Eq. (2.3).

Most combustion processes are governed by chain reactions initiated via the production of unstable radicals from the dissociation of one of the reacting species. The radicals then initiate a relatively fast chain of steps reacting with other molecules. A simple chain propagating reaction involves the production of one radical for each consumed, however, in chain branching reactions two or more radicals are generated from the consumption of one. This leads to a rapid buildup of radical concentration and hence a very fast overall reaction explosive in character. An explosive gas mixture, then, is one that supports very fast reaction kinetics and hence rapid energy release. A system will be explosive if chain branching is faster than the chain termination, which occurs

when the reaction of two radicals or a radical reacting with another molecule form a stable species. Termination can also be achieved with the formation of a radical with lower activity that cannot propagate the chain.

The oxidation of saturated hydrocarbons of the form C_nH_{2n+2} has been described by Fristrom and Westenberg (1965) to occur in two thermal zones. In the primary reaction zone, fuel molecules are attacked and reduced to CO, H_2, H_2O, and various radicals (H, O, OH). It is also here that other intermediates are formed. In the secondary reaction zone, oxidation of CO and H_2 occurs. They suggest that in oxygen-rich saturated hydrocarbon flames, lower order hydrocarbons form according to

$$OH + C_nH_{2n+2} \rightarrow H_2O + C_nH_{2n+1} \Rightarrow C_{n-1}H_{2n-2} + CH_3, \tag{2.4}$$

while in fuel-rich flames

$$H + C_nH_{2n+2} \rightarrow H_2 + C_nH_{2n+1} \tag{2.5}$$

is the scheme. These characteristics have been confirmed by Dryer and Glassman (1978) via high-temperature flow reactor studies which also revealed that the fuel is consumed prior to the majority of the energy release. This evidence led Glassman (1996) to characterize the general oxidation of hydrocarbons in three steps: (1) following ignition where H atoms are formed from the fuel molecules to react with oxygen and populate the radical pool of OH, H, and O, the primary fuel disappears with little or no energy release producing unsaturated hydrocarbons and H_2, with some hydrogen being oxidized to water; (2) the unsaturated hydrocarbons are further oxidized to CO and H_2, and

essentially all hydrogen is simultaneously oxidized to water; and (3) finally, most of the heat from the overall reaction is released from the oxidation of CO to CO_2.

2.2 Ignition

For a specific fuel/oxidizer mixture, conditions exist in which the system will undergo explosive reaction (spontaneous ignition). The explosion limits are formed by pressure and temperature boundaries as illustrated in Fig. 2.1 taken from Glassman (1996). Much of the understanding of hydrogen-oxygen oxidation developed through the study of explosion limits (Lewis and von Elbe, 1951). For hydrocarbons, as either pressure or temperature is increased the general tendency of the mixture to become explosive increases. Of the saturated hydrocarbons C_nH_{2n+2}, methane (CH_4) exhibits the highest resistance to explosion due to the comparatively large energy required to break the C-H bond. For higher order hydrocarbons, the chain reaction initiation is dominated by the breaking of a C-C bond, which is substantially weaker than the C-H bonds in the molecule. Inflections exist in the explosion limit curves for saturated hydrocarbons with $n > 2$. These inflections are a result of the negative temperature coefficient (NTC) of reaction rate in which chain branching and terminating steps are in competition as temperature increases (Glassman, 1996). This phenomenon manifests itself in the form of a two-stage ignition. The first stage ignition termination is a result of the inhibited branching, termed degenerate branching. This mechanism is commonly referred to as the low temperature kinetic scheme because of the modest temperature rise associated with it. The chain terminating step becomes dominant and prevents the mixture from completely reacting to reach its adiabatic flame temperature. The system then returns to

the non-explosive regime, and an induction time follows until branching again becomes dominant resulting in the second-stage or hot ignition where the majority of heat is released.

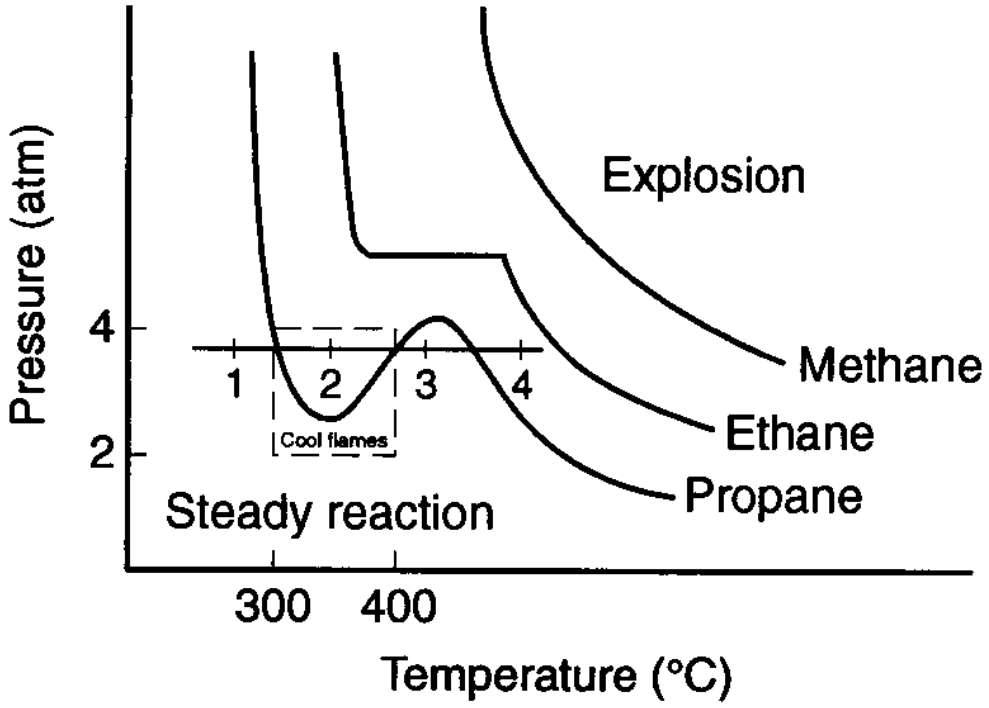

Figure 2.1: Explosion Limit Characteristics of Stoichiometric Hydrocarbon-Air Mixture (Glassman, 1996).

Low temperature hydrocarbon oxidation has been studied extensively for the last fifty years with the goal of determining an appropriate kinetic scheme. The early works of Semenov (1958), Benson (1981), and Cox and Cole (1985) have contributed greatly to current knowledge. Today, the construction of kinetic mechanisms to model the autoignition of saturated hydrocarbon fuels closely follows the work of Hu and Keck (1987). They describe the general sequence of reactions responsible for two-stage

ignition as follows. Reaction is initiated by the abstraction of a hydrogen atom H from the saturated hydrocarbon molecule RH forming the alkyl radical R (C_nH_{2n+1}) and HO_2:

$$RH + O_2 \rightarrow R + HO_2 . \quad \text{(R1)}$$

The main chain cycle is begun with subsequent oxidation of the alkyl radical forming the peroxy alkyl radical RO_2:

$$R + O_2 \rightleftarrows RO_2 \quad \text{(R2)}$$

which then undergoes internal hydrogen abstraction to produce ROOH:

$$RO_2 \rightleftarrows ROOH . \quad \text{(R3)}$$

Oxidation of ROOH ensues by the addition of oxygen to form O_2ROOH:

$$ROOH + O_2 \rightleftarrows O_2ROOH \quad \text{(R4)}$$

which subsequently decomposes irreversibly into OROOH and the hydroxyl radical OH:

$$O_2ROOH \rightarrow OH + OROOH . \quad \text{(R5)}$$

The cycle is completed when the hydroxyl radical reacts with a fuel molecule producing an alkyl radical and H_2O:

$$OH + RH \rightarrow R + H_2O . \quad \text{(R6)}$$

The associated branching reaction is

$$\mathrm{OROOH} \rightarrow \mathrm{ORO} + \mathrm{OH}\,. \qquad \text{(R7)}$$

Reactions (R1-R7) describe the low temperature kinetic scheme in which the temperature rises rapidly until the competing reaction

$$\mathrm{R} + \mathrm{O_2} \rightarrow \mathrm{olefin} + \mathrm{HO_2} \qquad \text{(R8)}$$

becomes faster than (R2) thus terminating the first stage of ignition. (R8) is the mechanism responsible for degenerate branching, which is followed by the reactions

$$\mathrm{HO_2} + \mathrm{HO_2} \rightarrow \mathrm{HOOH} + \mathrm{O_2} \qquad \text{(R9)}$$

and

$$\mathrm{HOOH} + \mathrm{M} \rightarrow 2\mathrm{OH} + \mathrm{M} \qquad \text{(R10)}$$

where M represents any third body in the system. The branching of hydrogen peroxide HOOH (or H_2O_2) to produce 2OH accelerates the reaction into the explosive regime leading to the hot second stage ignition.

2.3 Knock and HCCI Combustion

Heywood (1988) describes two modes of abnormal combustion in an internal combustion (IC) engine: (1) *knock* is the term used to describe the spontaneous ignition of the end gas ahead of the propagating flame front and (2) *surface ignition* is the ignition of the fuel/air mixture by a hot spot on the combustion chamber walls, spark plug, or combustion chamber deposit. The latter is a problem easily solved with attention to engine design and fuel and lubricant quality. Therefore, most current research on the

subject is concerned with the former, spontaneous ignition of the premixed end gas, or simply knock in spark ignition (SI) engines which generates high frequency, large amplitude pressure oscillations within the cylinder. This phenomenon manifests itself with audible "pinging" or "knocking" sounds transmitted through the engine structure, hence its name. Knock is problematic for multiple reasons, including the severe damage it can cause to engine components. Since the spontaneous ignition is highly dependent on pressure-temperature histories (see Sec. 2.2), fuel chemistry as well as engine design and operating conditions govern the onset of knock. Therefore, knock also affects efficiency as a result of the limit that must be imposed on engine compression ratios.

Two explanations for the phenomenon of knock are commonly recognized: (1) the autoignition theory and (2) the detonation theory (Heywood, 1988). The autoignition theory maintains that all or part of the end gas ahead of the propagating flame front spontaneously ignites prior to being reached by the flame front as a result of high pressures and temperatures achieved during compression. The detonation theory supposes that the flame front accelerates to sonic velocity consuming the end gas much more quickly than in normal combustion. High speed photographic studies (Nakagawa *et al*., 1984, Smith *et al*., 1984) have supported the autoignition theory and thus it is more widely accepted.

Homogeneous charge compression ignition (HCCI) represents an emerging technology in which a pre-mixed lean fuel/air mixture undergoes controlled autoignition. HCCI engines have the potential to achieve (1) part-load efficiencies similar to

compression ignition (CI) diesel engines, (2) the specific power output of SI engines, and (3) very low NO_x and particulate emissions without the need for expensive aftertreatment devices. A lean mixture allows the engine to operate unthrottled similar to that of a diesel engine, thereby increasing the efficiency by eliminating flow losses associated with throttling. The use of high compression ratios needed for autoignition also contribute to efficiency improvements. The homogeneous mixture permits SI operation at high loads and generates fewer particulate emissions overcoming two major disadvantages of diesel engines (Thring, 1989). Unlike conventional SI or CI engines, combustion occurs simultaneously throughout the cylinder volume rather than with a propagating flame front. As a result, the combustion duration is shorter and occurs at lower temperatures producing less NO_x emissions (Epping *et al*., 2002).

The fundamental chemistry of HCCI and knock by autoignition in SI engines are identical (Epping *et al*., 2002). The principal energy release follows the second stage ignition which commences as a result of the branching of hydrogen peroxide H_2O_2 (or HOOH) into two highly reactive hydroxyl radicals OH as given by (R10) of Sec. 2.2. The temperature required for H_2O_2 decomposition is approximately 1050-1100 K. Therefore, the temperature history within an engine cylinder plays an important role in determining the autoignition event. Indeed, the primary difficulty associated with HCCI is the control of ignition timing and hence temperature histories, which are highly dependent on pressure, fuel, and mixture composition. Consequently, the study of HCCI is in many ways analogous to the onset of knock.

2.4 Chemical Kinetic Models

Kinetic models can be useful for any application involving chemical reactions. As such, they have become particularly valuable to the automotive industry. Knocking combustion has been the primary barrier to efficiency improvements in IC engines since their inception and it continues to be a major obstacle despite many technological advances. The chemistry and physics involved in knock are similar to those of HCCI (see Sec. 2.3). Several kinetic models attempting to simulate the autoignition of hydrocarbon/air mixtures in an engine environment have been developed (Hu and Keck, 1987, Curran *et al*., 2002, Tanaka *et al*., 2003, and Zheng *et al*., 2004). Zheng *et al*. (2004) have categorized kinetic models into five groups according to their level of complexity (Table 2.1). The most complex are the detailed models which attempt to incorporate all known reactions and intermediate species contributing to the heat release and product formation. Theoretically, detailed models provide the most comprehensive and accurate representation of the reaction kinetics. As a result the computational demand can be high. This is particularly problematic when attempting to couple chemical reaction with a complex flow environment. Currently only very simple kinetic mechanisms are capable of being combined with intricate computational fluid dynamics (CFD) calculations due to computing limitations. Such difficulties motivate the development of smaller kinetic models. However, a model that is universally applicable for different combustion environments should be capable of reproducing the intermediate chemical behavior of hydrocarbon oxidation (Dryer, 1991) thus requiring additional

reaction steps and placing constraints on model reduction. Indeed, many mechanisms are validated only for a specified range of conditions due to these considerations.

Category	Description	Species	Reactions
Detailed	The latest "comprehensive" reaction set	100's	1000's
Lumped	Uses a lumped description for larger species	100's	1000's
Reduced	A subset of the detailed model	10's	10's – 100's
Skeletal	Employs class chemistry and lumping concepts	10's	10's
Global	Utilizes global reactions to minimize reaction set	< 10	< 10

Table 2.1: Categories of Chemical Kinetic Models (Zheng *et al*., 2004).

Once the appropriate reactions for a kinetic model have been selected, further complications arise in the determination of the rate constants of Eq. (2.3). Typically in mechanism construction, the majority of rate constants is taken from literature or previously developed submechanisms that have proven to be accurate. However, estimations are frequently required, particularly for mechanisms featuring a large number of intermediate steps. Sensitivity analyses are then carried out to determine the dependence of the solution on the estimated parameter allowing a measure of uncertainty to be determined. Equally important to the accuracy of the model, though, is the thermodynamic data. Several extensive compilations exist as a result of years of research (Kee *et al*., 1987, Chase, 1998, and McBride *et al*., 2002), yet data for many short-lived intermediate hydrocarbon species remain unknown. In such cases, the group additivity methods of Benson (1976), in which properties of a complex species are estimated by summing individual molecular and bond properties, are usually employed. Despite the challenges associated with model formulation, a large number of detailed kinetic

mechanisms for hydrocarbon oxidation exist. An extensive review of these is provided by Simmie (2003).

CHAPTER 3

CHEMKIN

3.1 Description

CHEMKIN (2006) is a computer program designed to facilitate the solution of complex chemical kinetics problems. It features a large variety of flame simulators and reactor models, including the *closed homogeneous reactor* and *closed internal combustion engine simulator* used in the present work. The software includes an extensive library of gas-phase kinetics, surface kinetics, gas transport, and thermodynamic data. In the pre-processing stage, the user is required to create a chemistry set that specifies applicable data. It is here that the kinetic mechanism with each elementary reaction and associated parameters A, b, and E_A (Eq. 2.3) are loaded into a gas-phase kinetics file. The thermodynamic data file can then be loaded from the internal library. Complicated mechanisms with a variety of species may require external thermodynamic data not supplied by CHEMKIN. The user can specify physical parameters, inlet conditions, and solver and output controls within a user interface. These model specific input parameters are conveniently written to an input file by CHEMKIN using the FORTRAN program AURORA for well stirred (homogeneous) reactors. If the user wishes to input further information not provided as options within the interface, supplemental input can be entered in the input file via keyword format. Details of

keyword syntax and rules can be found in the CHEMKIN manual (2006). When the model set-up is complete and the run executed, CHEMKIN will solve the governing equations for mass and energy of each species according to the parameters identified within the input file. The governing equations of homogeneous reactors and details of the CHEMKIN modules used in this study are provided next in Sections 3.2-3.4.

3.2 Governing Equations for Homogeneous Reactor Models

Governing equations for a homogeneous reactor system are based on conservation of mass, energy, and species. This includes net generation of chemical species within the reactor volume and net loss of species and mass to surfaces in the reactor. If it is assumed that there are no species deposits on the reactor walls, the inlet and outlet mass flow rates are equal and the mass conservation of each species takes the form

$$\dot{m}\left(X_S^o - X_S^i\right) - \dot{\omega}_S V M_S = 0\,, \tag{3.1}$$

where the subscript S denotes a particular species; $\dot{m}$ is the total mass flow rate of the mixture; X_S^i and X_S^o are inlet and outlet mass fractions, respectively; $\dot{\omega}_S$ is the molar rate of production of S per unit volume; V is the reactor volume; and M_S is the molecular weight of S. For steady state conditions, residence time can be defined in place of mass flow rate as

$$\tau = \frac{\rho V}{\dot{m}}, \tag{3.2}$$

where density ρ is determined from the ideal gas equation of state,

$$\rho = \frac{pM}{\bar{R}T} \tag{3.3}$$

with p denoting pressure, T the temperature, and $\bar{R}$ the universal gas constant. In the case of a closed reactor, the mass flow rate is zero, therefore residence time is not applicable or necessary.

Similarly, conservation of energy for an open system with no rate of change of energy is

$$\dot{Q} - \dot{W} = \dot{m}\sum_{S=1}^{N}\left(X_S^o h_S^o - X_S^i h_S^i\right). \tag{3.4}$$

Here, h_S^i and h_S^o are the inlet and outlet specific enthalpies of S, respectively, $\dot{Q}$ is the rate of heat transfer into the system (reactor), $\dot{W}$ is the rate of work done by the system, and N is the total number of species. For a closed system, Eq. (3.4) becomes

$$Q - W = m\sum_{S=1}^{N}\left(X_S^P u_S^P - X_S^R u_S^R\right), \tag{3.5}$$

where Q and W represent the total heat into the reactor and net work done by the system, respectively. The right side is the mass m times the difference between the summation of the internal energy u for the products and the reactants.

The conservation laws form a set of N + 1 nonlinear algebraic equations that account for the production of N species and their associated energies in Eqs. (3.1) and (3.4) or (3.5) as well as the temperature, which appears implicitly in terms of enthalpy or

internal energy. The system of equations is solved according to the Newton algorithm method discussed in the CHEMKIN manual (2006).

3.3 Constant Volume Closed Homogeneous Reactor Model

A constant volume closed homogeneous reactor is used for calculation of ignition delay times. Kinetic model rate parameters are often optimized according to ignition delay comparisons with experimental shock tube results. One advantage of using shock tubes to study autoignition of fuel/air mixtures is that the compression time is sufficiently short (~ 1 ns) to reduce any influences of the compression process such as heat transfer (Fieweger *et al*., 1997 and Würmel *et al*., 2007). The ignition delay times measured are typically on the scale of 10^{-4} to 10^{-3} seconds, however, extension to lower temperatures lengthens this time and an adiabatic assumption may come into question at sufficiently low temperatures. Nonetheless, it is common practice to neglect heat loss when calculating ignition delays for comparison to shock tube results, as will be followed in the present work.

The closed homogeneous reactor user interface within CHEMKIN requires specification of the type of problem to be solved. To simulate autoignition in a shock tube, a constant volume solution of the energy equation (Eq. 3.5) is appropriate. The initial temperature and pressure are required inputs along with initial mixture composition. Since surface chemistry is neglected, the actual reactor volume is not important, and if not specified, a default value of 1 cm^3 is used. CHEMKIN provides the option of defining ignition time as the time of maximum heat release (indicated by the

inflection point of the temperature profile) or the time of maximum concentration of a particular species, or both. Additionally, a user-defined ignition time can be specified via the Ignition Criterion User Routine.

3.4 The Internal Combustion Engine Model

3.4.1 Physical Parameters

The IC engine model simulates combustion of a single-zone, homogeneous mixture under autoignition conditions in a closed reactor. The model is therefore relevant to the studies of fuel autoignition, engine knock, and HCCI engines. Figure 3.1 is a schematic of the model. The cylinder bore is represented by D, the connecting rod length and crank arm radius are given by L_C and L_A, respectively, and θ is the angle through which the crank arm rotates. Since the model is valid only for closed systems, the appropriate time for simulation is the interval in which both the intake and exhaust valves are closed.

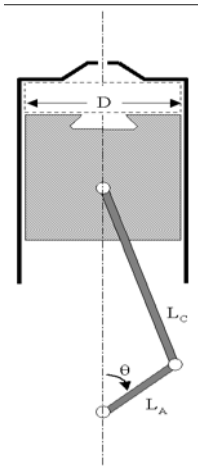

Figure 3.1: Schematic of an IC Engine Cylinder.

The time dependence of the cylinder volume is given (Heywood, 1988) by

$$V(t) = V_c\left[1 + \frac{r_c - 1}{2}\left(R + 1 - \cos\theta - \sqrt{R^2 - \sin^2\theta}\right)\right], \tag{3.6}$$

where V_c is the clearance volume, r_c is the compression ratio, and $R = L_C/L_A$. The maximum displaced volume

$$V_d = \frac{\pi}{2} D^2 L_A \tag{3.7}$$

is used to define the compression ratio

$$r_c = \frac{V_d + V_c}{V_c}. \tag{3.8}$$

With the engine speed N measured in rpm, the time derivative of the volume is

$$\frac{dV}{dt} = 2\pi N V_c \left(\frac{r_c - 1}{2}\right)\sin\theta\left[\frac{1 + \cos\theta}{\sqrt{R^2 - \sin^2\theta}}\right]. \tag{3.9}$$

Utilizing Eqs. (3.6-3.9), the general governing equations for species and energy conservation (Eqs. 3.1 and 3.4 or 3.5) can be solved.

3.4.2 Heat Transfer

Options to specify heat transfer to the walls in the cylinder include: (1) a constant heat transfer rate, (2) a piecewise heat transfer rate profile, (3) a user subroutine, or (4) a heat transfer correlation. For the heat transfer correlation, the convective heat transfer to the cylinder walls is simply written as

$$\dot{Q} = hA\left(T - T_{wall}\right), \tag{3.10}$$

where T_{wall} is the wall temperature and A is the total surface area, including the time-varying cylinder liner area and the end surfaces which are assumed to be circular. The convective heat transfer coefficient h can be found from

$$Nu \equiv \frac{hD}{k}, \tag{3.11}$$

where k is the gas thermal conductivity, and the Nusselt number Nu is determined from

$$Nu = aRe^{b}Pr^{c}, \tag{3.12}$$

where

$$Re \equiv \frac{D\overline{S}_p\rho}{\mu} \tag{3.13}$$

and

$$Pr \equiv \frac{c_p\mu}{k} \tag{3.14}$$

are the Reynolds and Prandtl numbers, respectively. The constants a, b, and c are defined by the user, $\overline{S}_p = 4\pi NL_A$ is the mean piston speed, ρ is the gas density, μ is the gas viscosity, and c_p is the specific heat of the gas at constant pressure.

An extension of the heat transfer correlation described above is the Woschni correlation (1967) which provides a more accurate representation of the cylinder gas

velocity. The mean piston speed in Eq. (3.13) is replaced by an average cylinder gas velocity given by

$$w = \left(C_{11} + C_{12} \frac{v_s}{\overline{S}_p} \right) \overline{S}_p + C_2 \frac{V_d T_i}{p_i V_i} \left(p - p_m \right). \tag{3.15}$$

Here, C_{11}, C_{12}, and C_2 are modeling parameters specified by the user, v_s is the swirl velocity, V_d is the displaced volume, p is the instantaneous cylinder pressure, p_m is the motored cylinder pressure at the same crank angle as p, and T_i, p_i, and V_i are the initial (or inlet) temperature, pressure, and volume inside the cylinder, respectively, whose values are given in Chap. 5. The expression for the convective heat transfer coefficient can then be written as

$$h = aD^{b-1} \frac{k}{\mu^b} w^b \rho^b . \tag{3.16}$$

CHAPTER 4

FUEL AND KINETIC MODEL

The tendency of a fuel to autoignite is measured by its octane number (ON). Octane numbers are defined by the tendency of two primary reference fuels (PRFs) to ignite. *n*-Heptane (*n*-C_7H_{16}) and *iso*-octane (*i*-C_8H_{18}) are assigned octane numbers of 0 and 100, respectively, where the smaller ON represents a greater propensity for autoignition. Where the investigation of ignition timing is important, a fuel with any ON in the range 0-100 is easily modeled by the appropriate combination of PRFs. With this realization, several studies have aimed to develop chemical kinetic models describing the oxidation of PRFs. These mechanisms can vary in complexity from fewer than ten to thousands of reactions. The most complex or detailed mechanisms attempt to include all the important reactions and species, including intermediates, which contribute to the overall oxidation process. Reduced models are driven by the desire to minimize the computational demand required of the detailed mechanisms, particularly when coupled with computational fluid dynamics (CFD) calculations. Since the present work examines only single-zone models, the use of a detailed kinetic mechanism is feasible.

Perhaps the most widely used kinetic model for PRF oxidation is the Lawrence Livermore National Laboratory (LLNL) mechanism by Curran *et al*. (2002). It is comprised of 1034 species and 4236 reactions. This includes all reactions known to be

relevant to both high and low temperature kinetics. Thermodynamic parameters have been determined based on numerous works, including Benson (1976), Ritter and Bozzelli (1991), Lay *et al*. (1995), Lay and Bozzelli (1997), and Knyazev and Slagle (1998). The mechanism has been validated with experimental data from flow reactors, jet-stirred reactors, and shock tubes. It has also compared favorably to autoignition experiments in a cooperative fuels research (CFR) engine though the extent of investigation reported has been limited.

CHAPTER 5

MODEL AND EXPERIMENTAL COMPARISONS

5.1 Ignition Delay in a Constant Volume Reactor

Fieweger and co-workers (1997) have measured ignition delay times of PRF mixtures in a shock tube using the reflected shock technique. Their maximum measuring time of 12 ms represents a time scale comparable to that available for autoignition in an engine. The shock tube was constructed to support pressures up to 700 bar resulting from the ignited fuel/air mixture. Pressure data was obtained via acceleration-compensated piezoelectric transducers. Temperature behind the reflected shock was calculated from the velocity of the incident shock taking into account real gas properties. Ignition delay was defined as the time interval from the passing of the reflected shock past the pressure transducer to time of explosion of the gas, which was easily determined from the pressure records.

Figure 5.1 shows experimental data from Fieweger *et al*. (1997) and model predictions using the constant volume homogeneous reactor in CHEMKIN of the dependence of ignition delay on temperature for four different PRF mixtures at 40 bar and fuel/air equivalence ratio $\phi = 1.0$. Ignition delay was defined in CHEMKIN to be the time of maximum heat release, corresponding to explosion of the gas mixture. In

general, the kinetic model calculations are similar to experimental data and capture the overall trend of temperature influence for each fuel. However, it is observed that the model consistently predicts a longer ignition delay, particularly considering that values are plotted on a logarithmic scale, even though heat loss is neglected. For a different view, the contents of Fig. 5.1 plotted linearly in Fig. 5.2. As discussed in Sec. 3.3, an adiabatic assumption is generally considered valid provided that time scales are sufficiently small. The largest disagreement between experiment and model occurs at lower temperatures or longer ignition delay times. At approximately 700 K, the model predicts an ignition delay of more than 1.5 times greater than that measured for *iso*-octane (PRF 100). Since neglecting heat loss in model calculations would tend to decrease ignition delay compared to experiment, the overpredictions at low temperatures are particularly alarming. This suggests that the low temperature kinetics of the model may be less accurate than those at higher temperatures.

5.2 HCCI Engine Combustion

Experimental data of homogeneous charge compression ignition (HCCI) engine combustion has been gathered from various works in literature. An attempt has been made to collect data with a range of fuel octane numbers as well as engine operating parameters and conditions. This data is compared with the detailed kinetic model by Curran *et al.* (2002) using the IC engine model in CHEMKIN.

HCCI engine combustion of PRF 20 (20% *i*-C_8H_{18}, 80% *n*-C_7H_{16}) representing octane number 20 has been studied at Drexel University by Zheng *et al*. (2004). A single

cylinder, four-stroke, air cooled research engine with physical parameters given in Table 5.1 was used to collect the data. For brevity, this engine will be referred to as the "PRF 20 engine". The engine was operated at N = 750 rpm with inlet manifold pressure of 1 atm at ϕ = 0.4. The inlet temperature was varied from 393-453 K and volumetric efficiencies of 71% and 89% were used. Complete vaporization and mixing were assured by injecting the fuel into the air stream of the heated inlet manifold sufficiently far upstream of the intake valve. Cylinder pressure data were collected via a wall mounted piezoelectric transducer. Temperature was then calculated from this data using a thermodynamic model.

PRF 84 (84% *i*-C_8H_{18}, 16% *n*-C_7H_{16}) representing octane number 84 was studied by Kalghatgi *et al.* (2003) in a single cylinder, four stroke, water cooled HCCI engine with port fuel injection. Specs for this engine, denoted the "PRF 84 engine", are provided in Table 5.1. The data that follows represents operation at N = 900 rpm, intake air temperature and pressure of 393 K and 1 bar, respectively, and $\lambda = 1/\phi = 3.5$. The fuel was injected at bottom dead center (180° BTDC) and cylinder pressure was measured with a piezoelectric transducer.

	PRF 20 Engine	PRF 84 Engine
Compression Ratio	8.17	16.7
Bore (mm)	76.2	127
Stroke (mm)	82.6	154
Inlet Valve Closing	125° BTDC	139° BTDC
Exhaust Valve Opening	133° ATDC	121° ATDC

Table 5.1: Experimental Engine Specifications.

The Woschni correlation with the gas velocity correction of Eq. (3.15) has been used to model heat transfer in the calculations. Due to the uncertainty associated with heat transfer modeling, multiple parameters are evaluated in an attempt to estimate the actual heat loss associated with the physical engine. Following Woschni (1967), Heywood (1988) provides parameters for (1) the gas exchange period, (2) the compression period, and (3) the combustion and expansion period of the four-stroke cycle. Since the IC Engine Model is a batch (closed) reactor, the gas exchange period is neglected and the start of simulation corresponds to the time of inlet valve closing in the experimental engine. Additionally, since the experimental engines did not incorporate swirling flow, the coefficient C_{12} of Eq. (3.15) can be neglected. C_2 then becomes the only differing parameter between periods (2) and (3) with values of 0 and 0.324 cm/s.K, respectively. Inspection of Fig. 5.3 reveals that C_2 has no bearing on the compression period and therefore justifies the use of 0.324 cm/s.K for the entire simulation period.

A different set of values for the heat transfer correlation is used in a tutorial provided by CHEMKIN (2006). They estimate heat loss during the combustion and expansion period to be much larger with C_2 = 3.24 cm/s.K. Additionally, a smaller exponent of 0.71 is used for b in Eq. (3.13) compared to that of 0.8 suggested by Woschni and reported by Heywood. The complete list of parameter values characterizing the heat transfer correlation is provided in Table 5.2 for both CHEMKIN and Heywood. Both models are used in conjunction with varying inlet temperatures to deduce the best representation of the actual engine heat transfer and for evaluating the accuracy of the

kinetic mechanism in CHEMKIN's IC engine model. In all calculations, a wall temperature of 400 K was used.

Parameter	CHEMKIN	Heywood
a	0.035	0.035
b	0.71	0.80
c	0.0	0.0
C_{11}	2.28	2.28
C_{12}	--	--
C_2	3.24 cm/s.K	0.324 cm/s.K

Table 5.2: Heat Transfer Correlation Parameters.

Figures 5.4 and 5.5 provide model pressure and temperature predictions vs. crank angle (CAD), respectively, for PRF 20 along with the experimental data. Top dead center (TDC) is represented by 0 CAD. Using exact experimental inlet conditions for model calculations results in a significantly delayed ignition time. This is likely a result of hot spots in the charge due to residual gases in a real engine. Ignition will start at these hot spots where temperature is higher than the bulk gas temperature (Gu *et al*., 2003), and therefore ignition will advance from that of a truly homogeneous mixture. Andrae *et al*. (2005) has suggested adding a temperature difference ΔT between the bulk gas and the hot spots to the inlet temperature in modeling studies. In an attempt to estimate this, two approaches were used. First, ignition timing was approximated from the experimental data as the point of maximum temperature increase rate $\frac{dT}{d\theta}$. The temperature corresponding to this CAD was designated as the experimental ignition temperature. The same approach was used to approximate the model ignition temperature, which would

presumably be larger. The hot spot temperature difference ΔT was defined as the difference between the two. It should be expected that ignition temperature is nearly independent of inlet temperature for given inlet conditions, fuel, and engine configuration. This approach of course assumes that the model accurately predicts the temperature at which ignition occurs. Due to the limited resolution of both sets of data, however, it was difficult to determine precise values and this method to determine ΔT was no longer used in the present study.

In a similar effort, Zheng *et al*. (2002) has approximated ignition time as the CAD corresponding to the intersection of the tangent of the negative temperature coefficient (NTC) region with the tangent of the maximum pressure rise of the pressure vs. CAD curve as illustrated in Fig. 5.6. The same approach was attempted here with the designation of the ignition temperature as the temperature corresponding to this ignition time and ΔT as the difference between model and experimental ignition temperatures. Fig. 5.7 shows that $\Delta T \approx 230$ K using the heat transfer parameters reported by Heywood, which seems unreasonable. Furthermore, consistent values were not measured while varying inlet temperature and heat transfer parameters. Since such a temperature difference proved difficult to measure using the pressure rise tangents, this method for estimating ΔT was also abandoned. Instead, the approach taken here is to guess a value until the calculated temperature profile approximates, to within 5 K, that measured late in the compression stroke but before the ignition. By trial and error, it was discovered that $\Delta T = 40$ K ($T_{in} = 463$ K) approximated the temperature well at 40° BTDC, the point where experimental data is made available. As observed from Figs. 5.4 and 5.5, this

temperature increase improves agreement of ignition timing, however, the model still predicts ignition about 8° later than the experiment with CHEMKIN heat transfer and 11° later with Heywood. It is also observed that the model displays the well-known two-stage ignition which is common of saturated compounds (Tanaka *et al*., 2003). The interval between the first and second stage ignition is approximately 22 CAD for experiment and both models.

Figure 5.8 depicts the temperature while isolating the effects of each different heat transfer parameter with T_{in} = 463 K. It is easily seen that C_2 used by Heywood (0.324 cm/s.K) better approximates the heat loss during the expansion process where the majority of heat release due to chemical reaction has already occurred, thereby neutralizing any inaccuracies of the kinetic model. However, b = 0.71 used in the CHEMKIN tutorial more closely approximates the time of ignition observed in the experimental data than does b = 0.80 from Heywood. Nevertheless, a judgment about the validity of its use should be reserved due to the uncertainty in the accuracy of the kinetic model, particularly in terms of ignition time. It should also be noted that the experimental data of Figs. 5.4-5.8 are with volumetric efficiency of 89%. Since the model is unable to replicate flow characteristics and thus volumetric efficiency, it may be a source of error to explain discrepancies in ignition timing.

Chang *et al*. (2004) examined the suitability of using the Woschni heat transfer correlation when modeling HCCI engines and modified the expression for the convective heat transfer coefficient (Eq. 3.16) to be

$$h = \alpha L^{b-1} w^b p^b T^{-b'} \tag{5.1}$$

with

$$w = \left(C_{11} + C_{12} \frac{v_s}{\overline{S_p}} \right) \overline{S_p} + \frac{C_2}{6} \frac{V_d T_i}{p_i V_i} \left(p - p_m \right). \tag{5.2}$$

They hypothesized that the gas velocity increase during combustion as evidenced in the pressure factor of Eq. (3.15) is not as large for HCCI as it is for spark ignition since the combustion occurs simultaneously at multiple locations and is driven primarily by kinetics rather than turbulent flame phenomena. To account for this, C_2 was reduced to 1/6 the value used by Woschni based on experimental measurements. Additional refinements to Woschni's correlation were made by replacing the bore diameter with the instantaneous cylinder height L as the characteristic length for Re, including pressure and temperature explicitly in place of density through the ideal gas law, and neglecting the effect of variable gas properties. Woschni's value of $b = 0.8$ was maintained with the exception of the negative temperature exponent, which was optimized to $b' = 0.73$ from iterative curve fitting. The constant α was used to scale according to different engine geometries. They found that their correlation showed better agreement with experimentally measured heat fluxes in an HCCI engine than did the original expression by Woschni. Unfortunately, the user interface of CHEMKIN allows specification of b only as it appears in Eq. (3.12), which prevents assignment of a different exponent to T. Additionally, the instantaneous cylinder height cannot be used as the characteristic length because CHEMKIN calls for a constant value. (It should be noted that Chang *et al.*

observed only a slight effect due to changing of the characteristic length.) Nonetheless, the value C_2 = (0.324 cm/s.K)/6 = 0.054 cm/s.K was used in the gas velocity expression, which is the only deviation from Woschni's original correlation. The temperature profile is shown in Fig. 5.8 for PRF 20 with this change. This value better approximates the cooling rate during expansion than does Woschni's value of 0.324 cm/s.K and thus will be used in subsequent calculations.

Experimental and model results for pressure and temperature vs. CAD for PRF 84 are shown in Figs. 5.9 and 5.10, respectively. In working with the same data, Andrae *et al*. (2005) have chosen 25 K to represent the hot spot temperature difference at these conditions. However, the modeling in that work was adiabatic and thus ΔT should consider not only residual gas hot spots but also the temperature decrease due to heat loss in the experimental engine. Therefore, when modeling with heat transfer, ΔT would presumably need to be larger. Pressure and temperature profiles are shown for ΔT = 25 K and 35 K (T_{in} = 418 K and 428 K) using C_2 = 0.054 cm/s.K. Since temperatures are over predicted for the compression process even for ΔT = 25 K (see Fig. 5.10), ΔT is not determined by matching temperature profiles as before. Rather, the value of 35 K comes from the relation

$$\left(\frac{\Delta T}{T_{peak}-T_{in}}\right)_{PRF\,84}=\left(\frac{\Delta T}{T_{peak}-T_{in}}\right)_{PRF\,20} \tag{5.3}$$

where T_{in} and T_{peak} are the experimental inlet and peak cylinder temperatures, respectively, and ΔT = 40 K for PRF 20 as previously designated. Peak temperatures are

approximately 1880 K and 1600 K for the PRF 20 and PRF 84 engines, respectively. This is a somewhat crude estimation technique, but it at least recognizes the effect of peak temperature on residual gas hot spot temperature and inlet temperature on ΔT. T_{in} = 418 K predicts ignition time approximately 3° later than the experiment while using b = 0.71, a conservative value considering that it causes earlier ignition than b = 0.8. Both b = 0.71 and 0.80 are shown for T_{in} = 428 K, and ignition time is approximately 1° and 4° late, respectively. To avoid further ambiguity and to establish a consistent set of parameters, a value of b = 0.80 will be used in the following calculations. This selection is motivated by the widespread acceptance and use of the Woschni correlation in engine modeling. Ignition time is consistently later with this value of b; however, as observed in Figs. 5.1 and 5.2, ignition delay calculations in a constant volume reactor compared with shock tube data suggest inaccuracies of the kinetic model which would be consistent with the HCCI engine modeling discrepancies. A summary of the parameters used to model the PRF 20 and PRF 84 engines based on the preceding discussions is given in Table 5.3 along with the specs in Table 5.1, and the pressure profiles using these values are shown with the experimental data for both engines in Fig. 5.11. These values are adopted as the baseline for the parameter studies of Chap. 6.

	PRF 20 Engine	PRF 84 Engine
N	750 rpm	900 rpm
ϕ	0.4	0.286
ΔT	40 K	35 K
T_{in}	463 K	428 K
P_{in}	1 atm	1 bar
a	0.035	0.035
b	0.80	0.80
c	0.0	0.0
C_{11}	2.28	2.28
C_{12}	--	--
C_2	0.054 cm/s.K	0.054 cm/s.K
T_{wall}	400 K	400 K

Table 5.3: IC Engine Modeling Parameters in CHEMKIN.

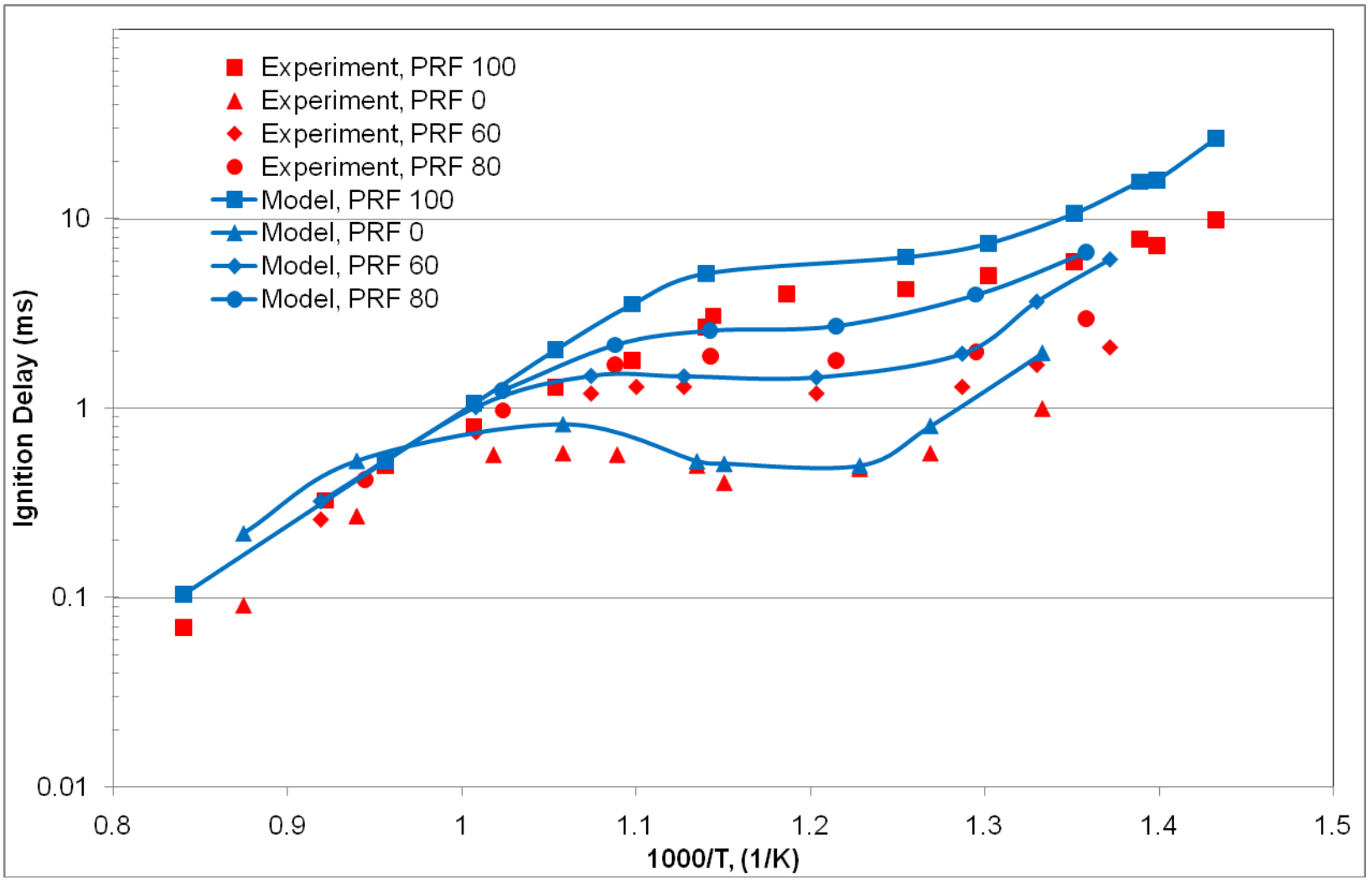

Figure 5.1: Logarithmic Ignition Delay vs. 1000/T, Experiment and Model for 4 Fuels, $P = 40$ bar, $\phi = 1.0$.

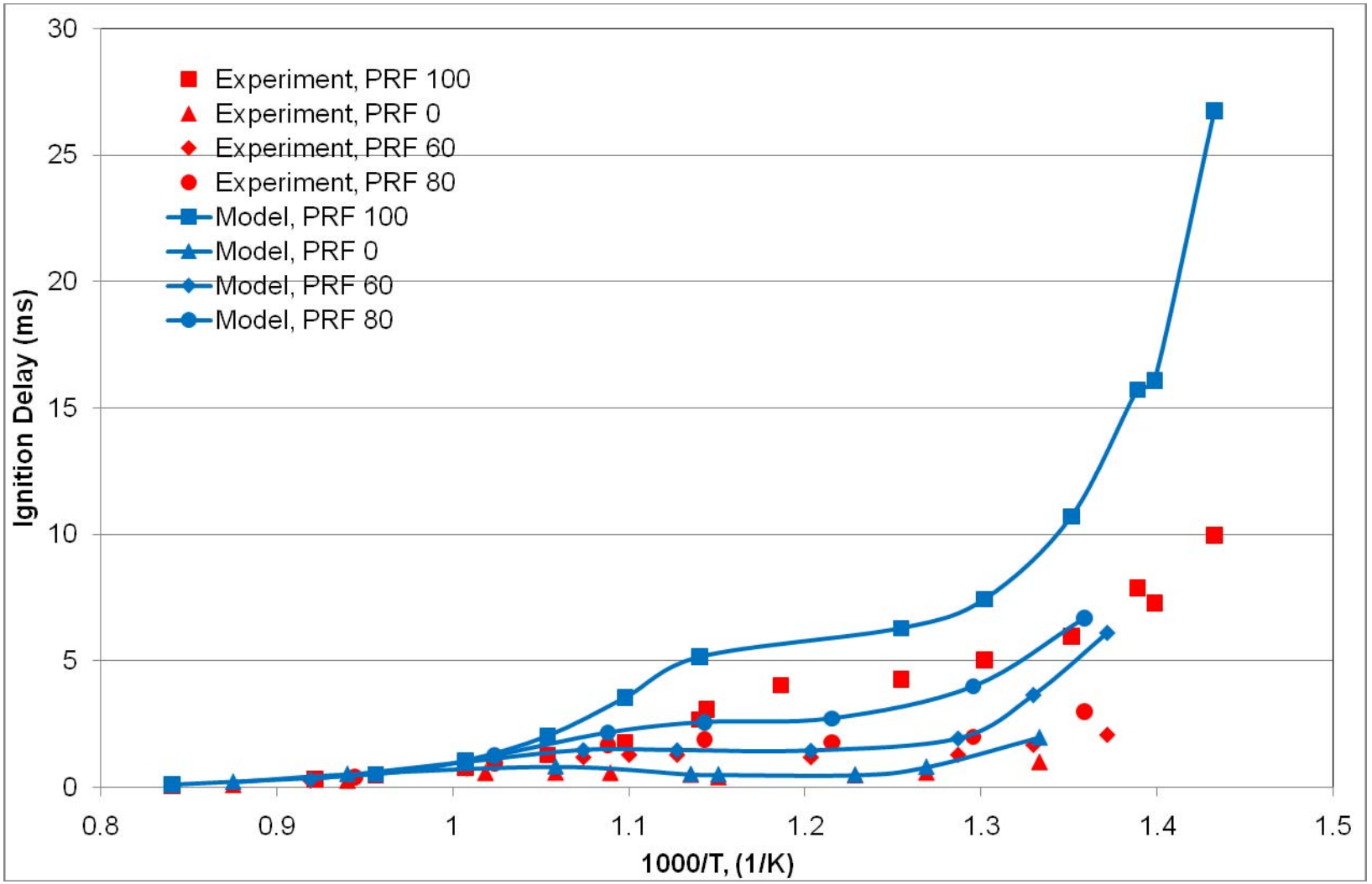

Figure 5.2: Linear Ignition Delay vs. 1000/T, Experiment and Model for 4 Fuels, $P = 40$ bar, $\phi = 1.0$.

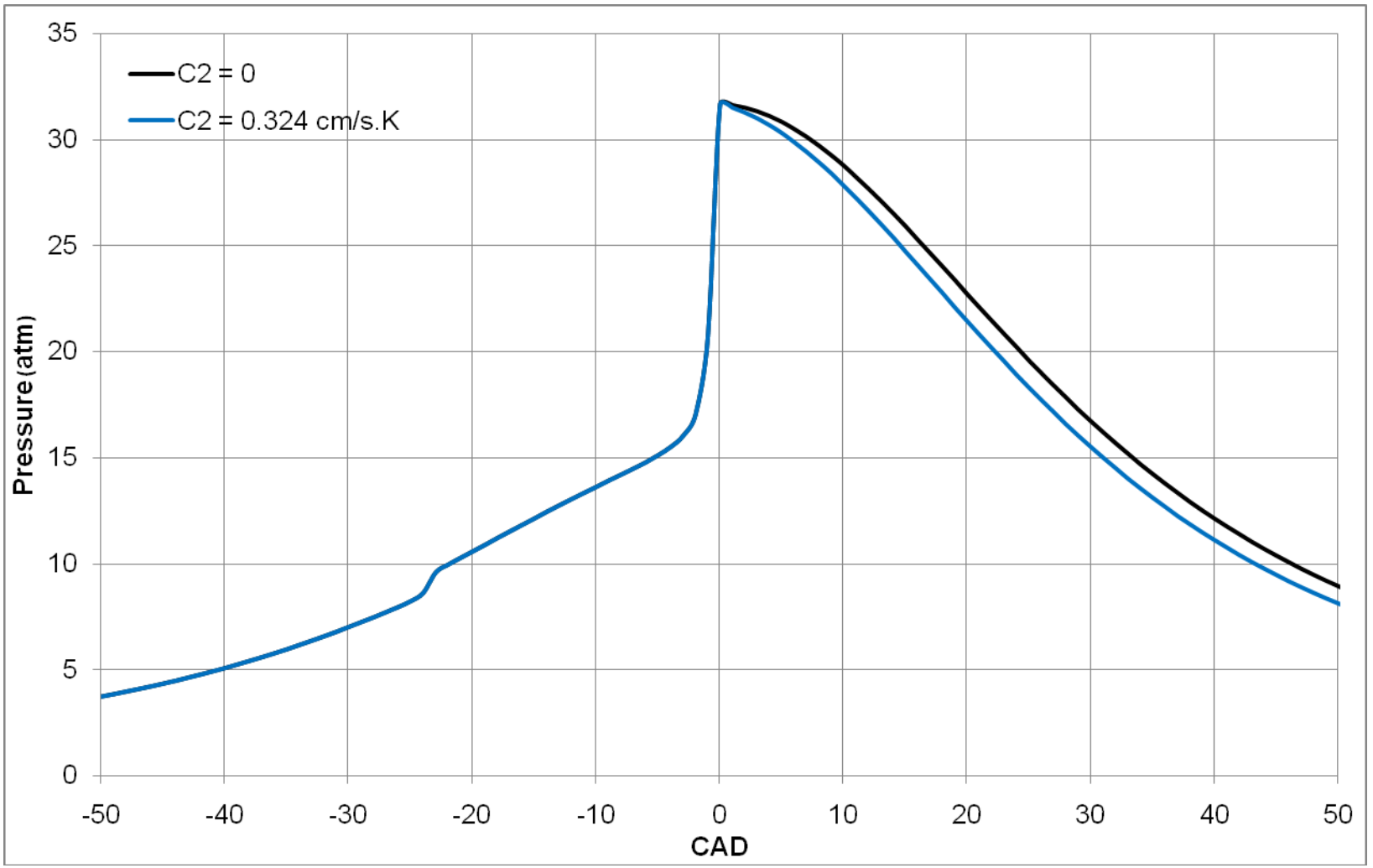

Figure 5.3: Pressure vs. CAD for Different Values of C_2, PRF 20, r_c = 8.17, 750 rpm, T_{in} = 363 K, P_{in} = 1 atm, ϕ = 0.4.

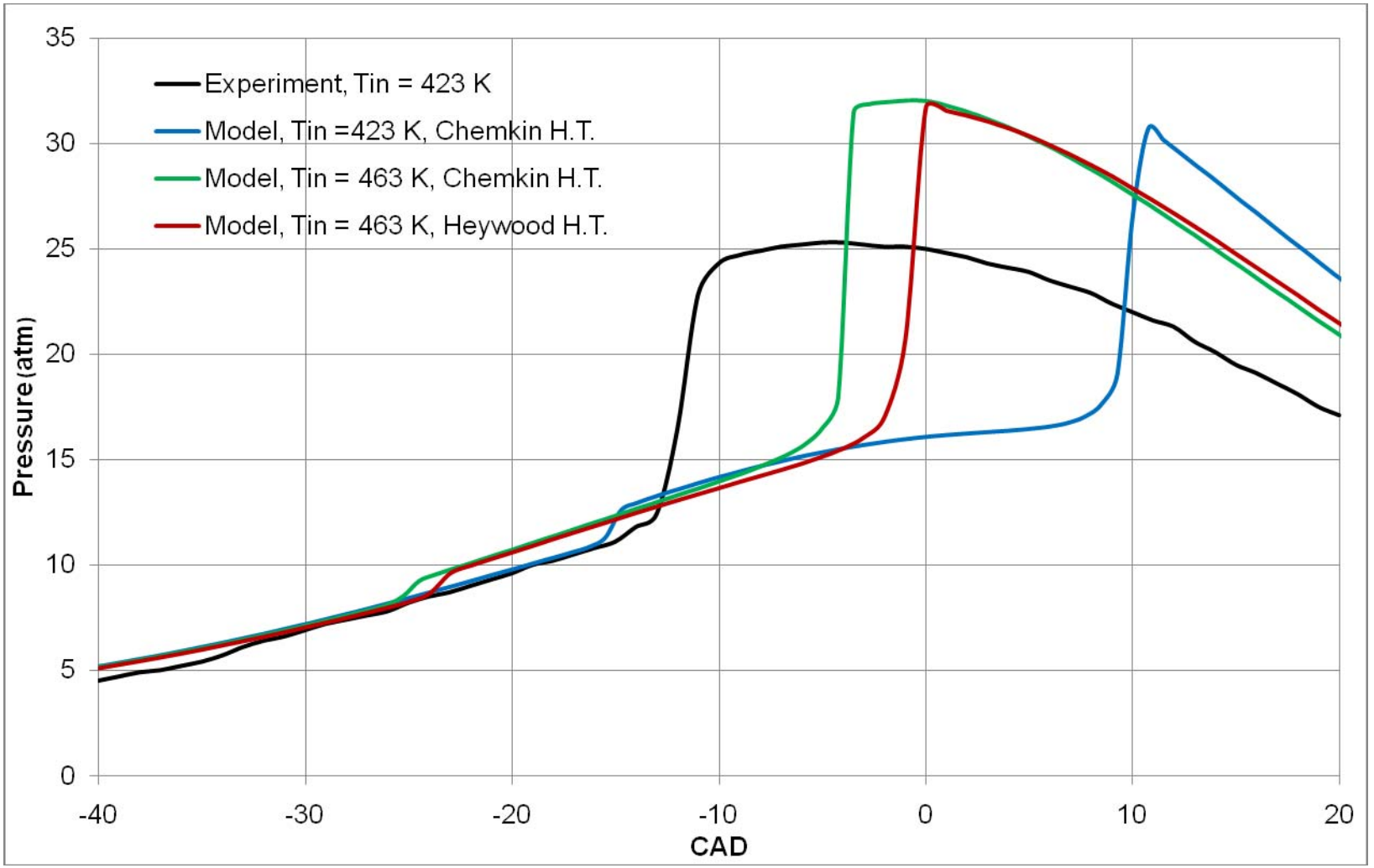

Figure 5.4: Pressure vs. CAD, Experimental and Curran Model, PRF 20, r_c = 8.17, 750 rpm, P_{in} = 1 atm, ϕ = 0.4.

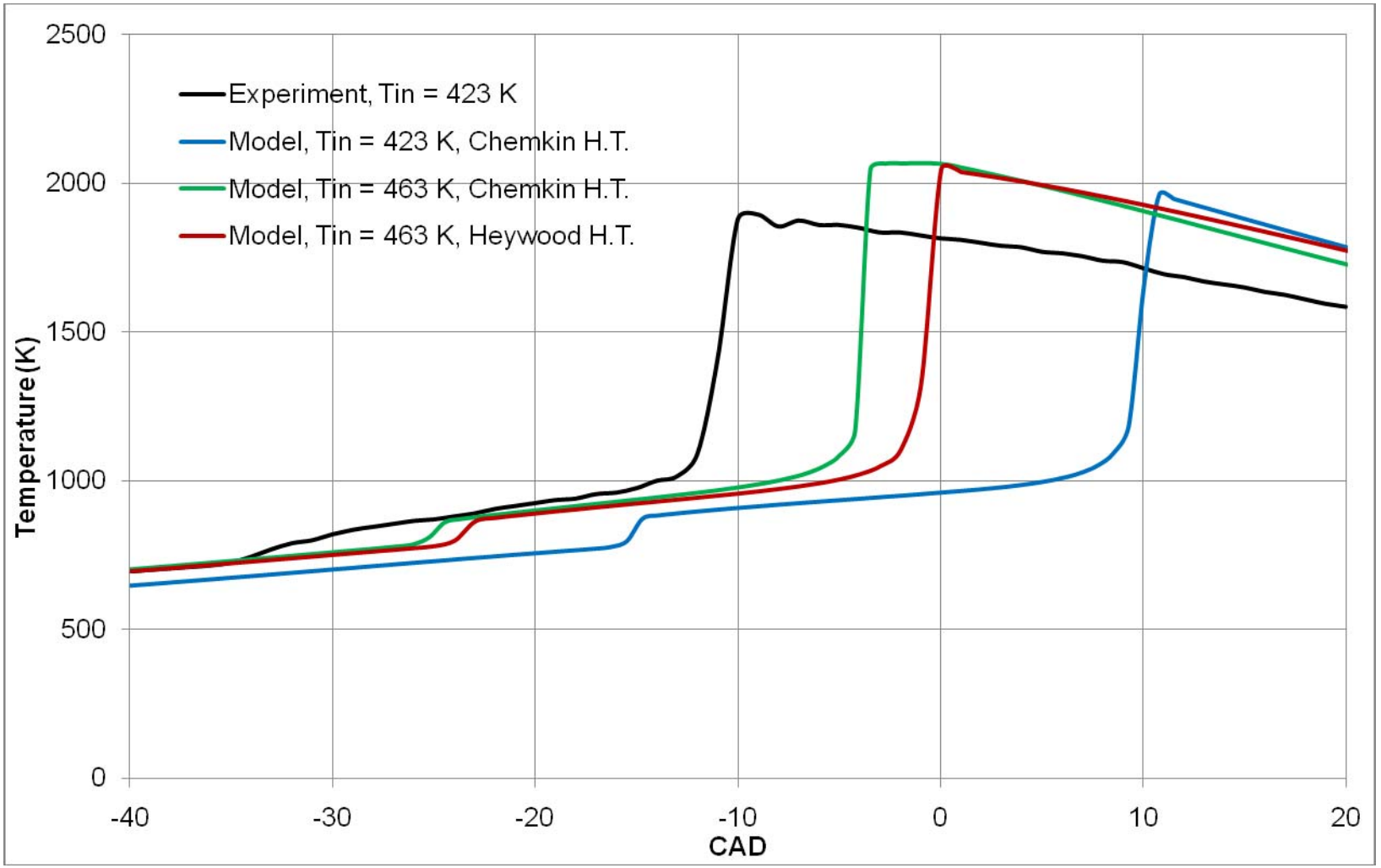

Figure 5.5: Temperature vs. CAD, Experimental and Curran Model, PRF 20, r_c = 8.17, 750 rpm, P_{in} = 1 atm, ϕ = 0.4.

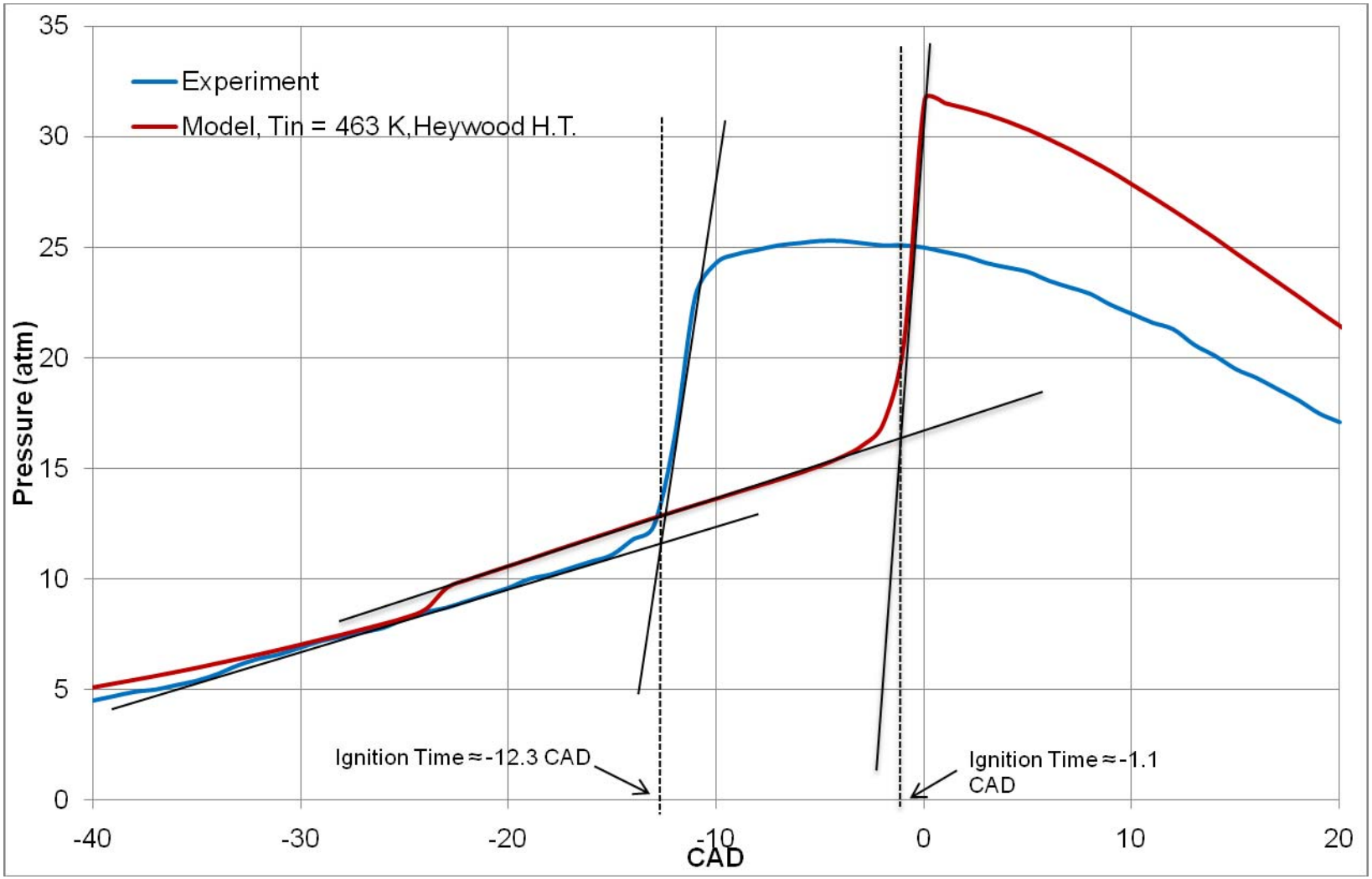

Figure 5.6: Determination of Ignition Time via Tangent Method, PRF 20, r_c = 8.17, 750 rpm, P_{in} = 1 atm, ϕ = 0.4.

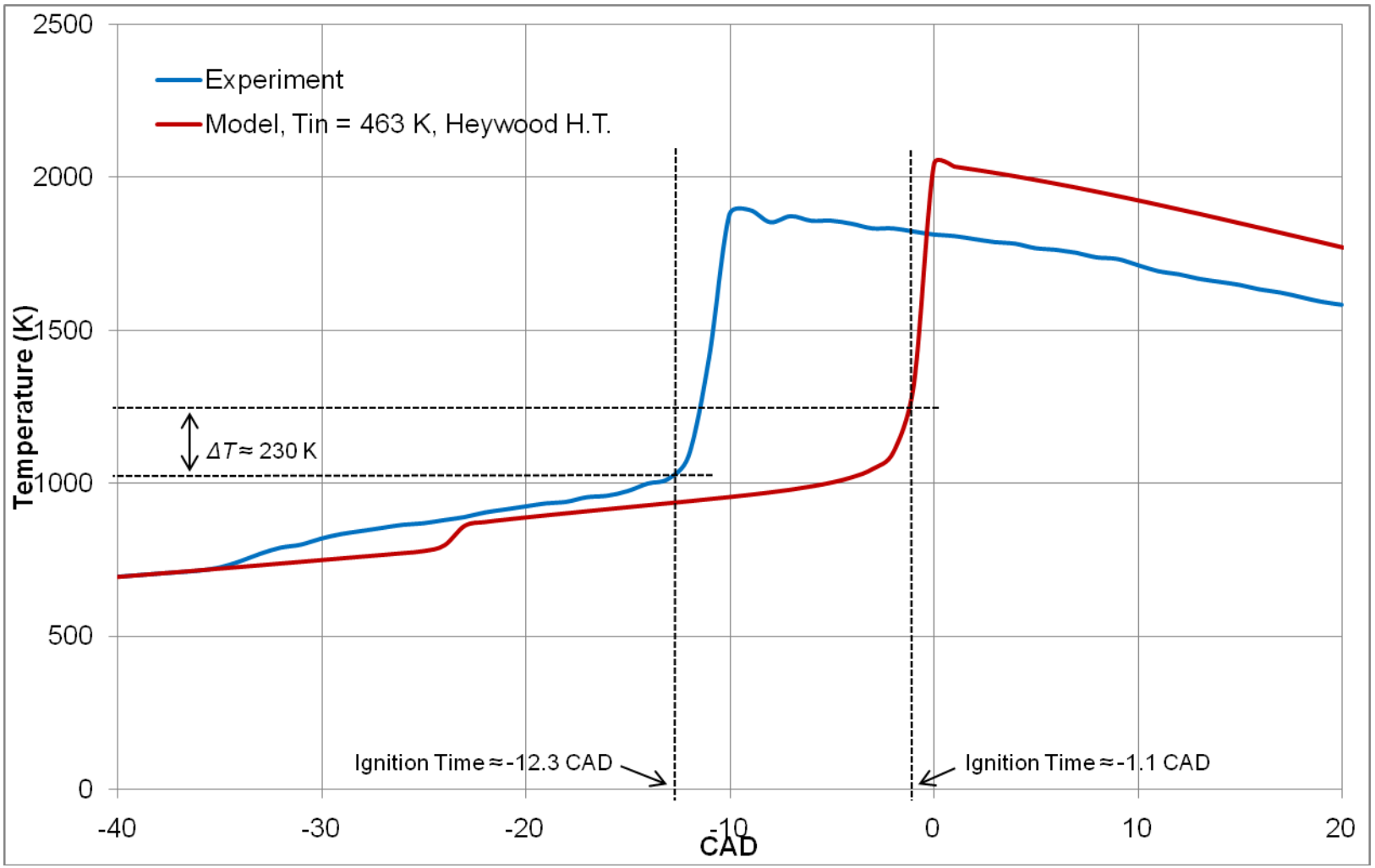

Figure 5.7: Determination of ΔT from Ignition Time via Tangent Method, PRF 20, r_c = 8.17, 750 rpm, P_{in} = 1 atm, ϕ = 0.4.

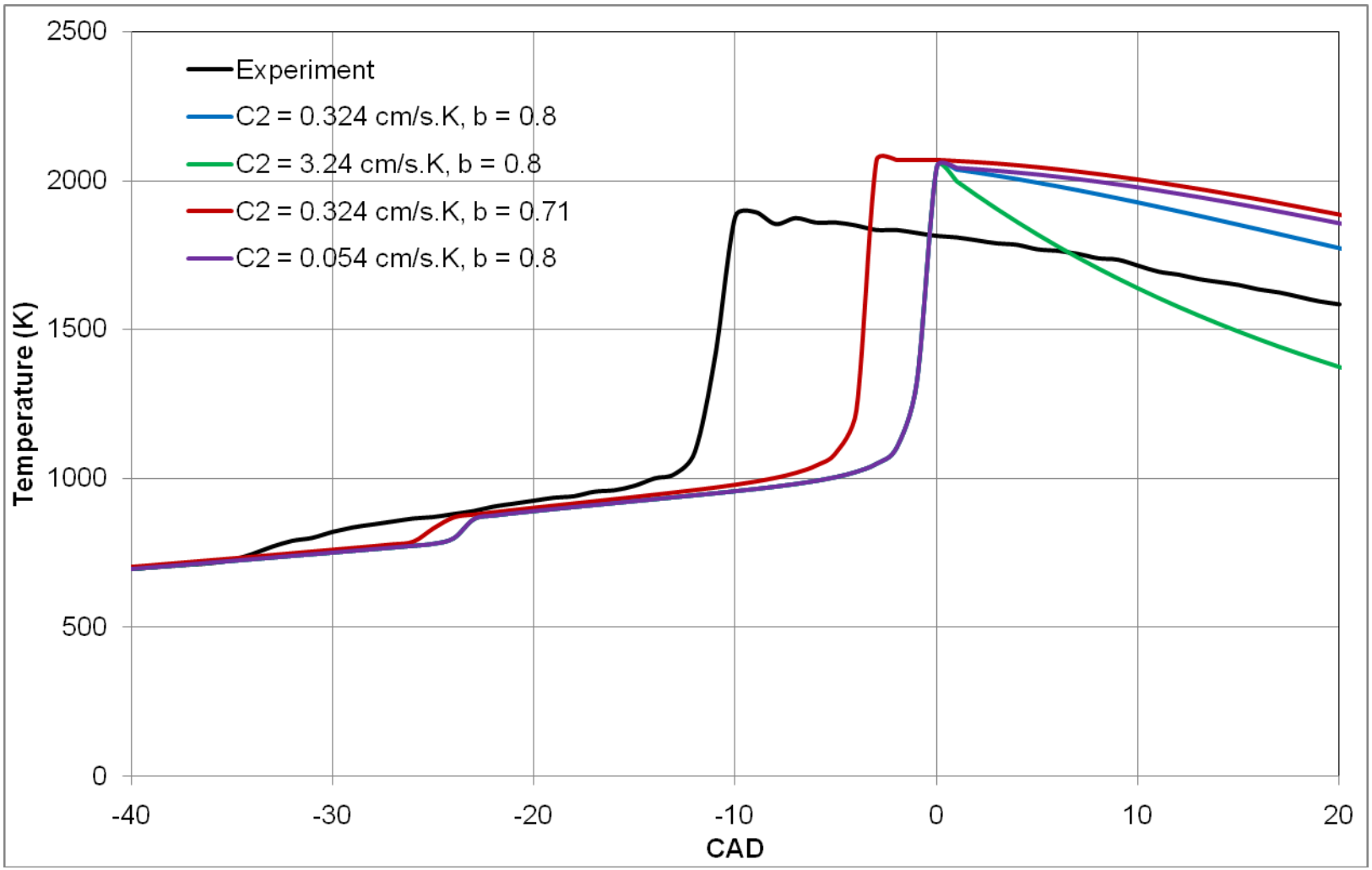

Figure 5.8: Temperature vs. CAD, Isolated H.T. Parameters, PRF 20, r_c = 8.17, 750 rpm, T_{in} = 463 K, P_{in} = 1 atm, ϕ = 0.4.

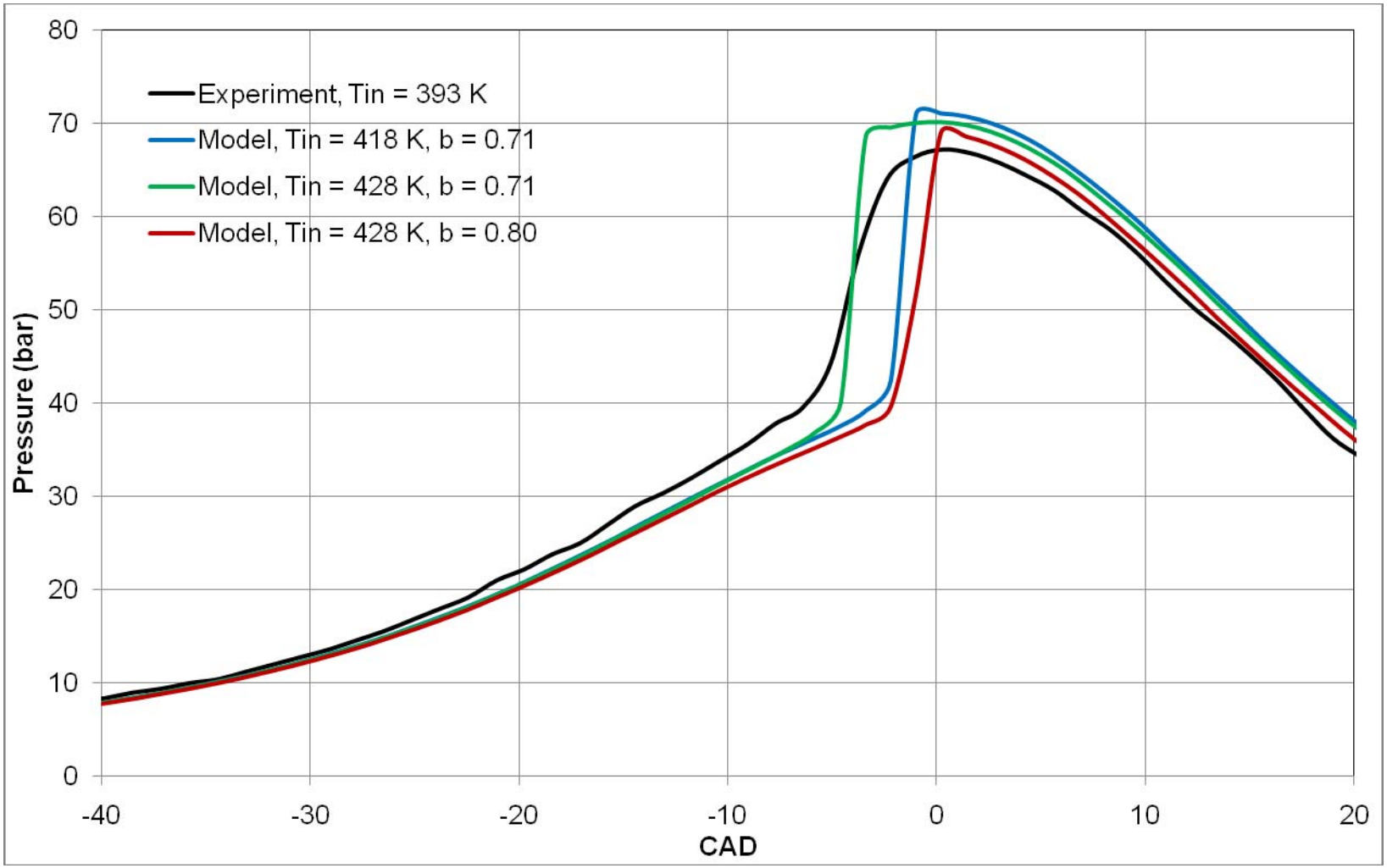

Figure 5.9: Pressure vs. CAD, Experimental and Curran Model, PRF84, r_c = 16.7, 900 rpm, P_{in} = 1 bar, ϕ = 1/3.5.

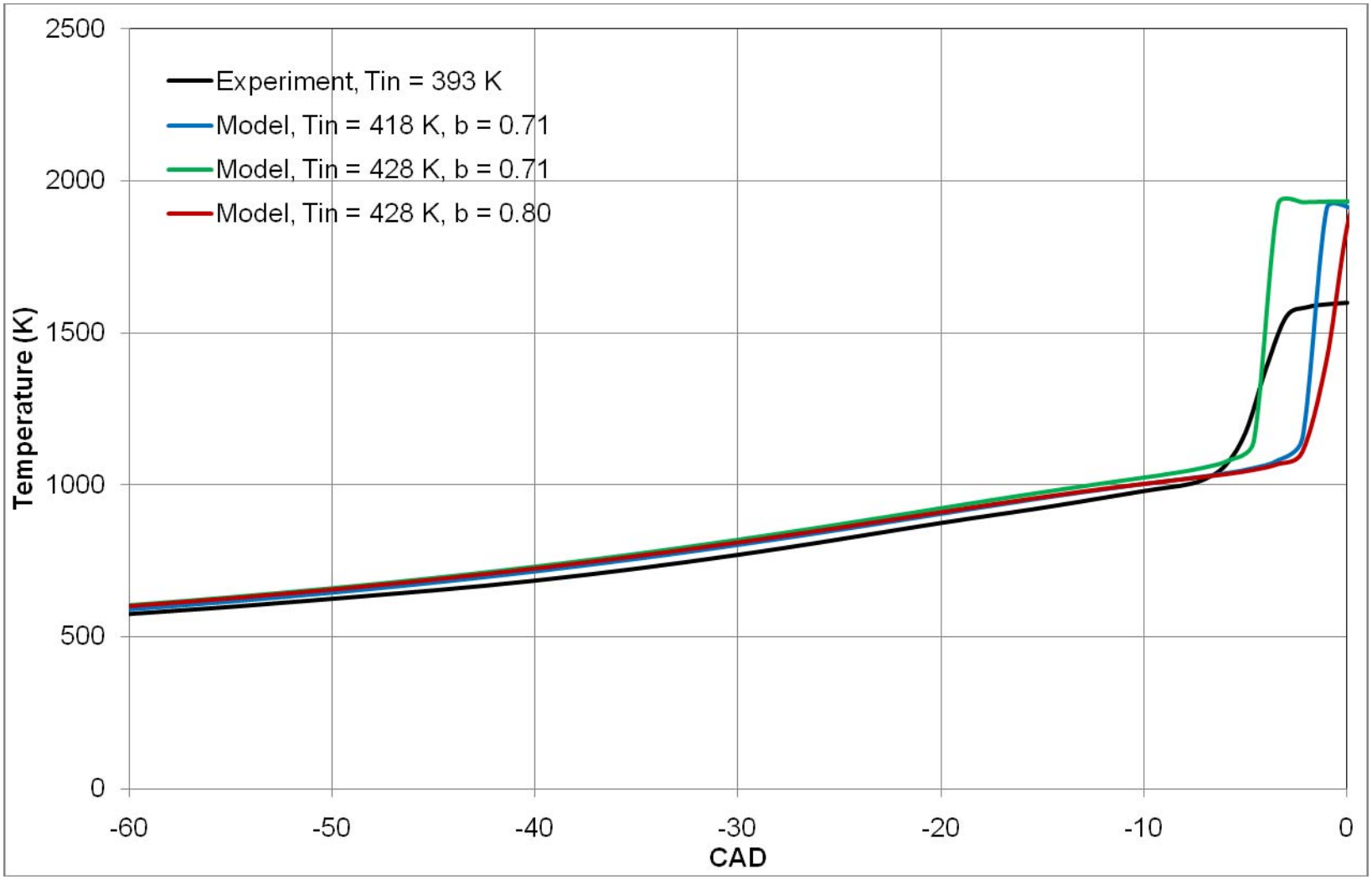

Figure 5.10: Temperature vs. CAD, Experimental and Curran Model, PRF84, r_c = 16.7, 900 rpm, P_{in} = 1 bar, ϕ = 1/3.5.

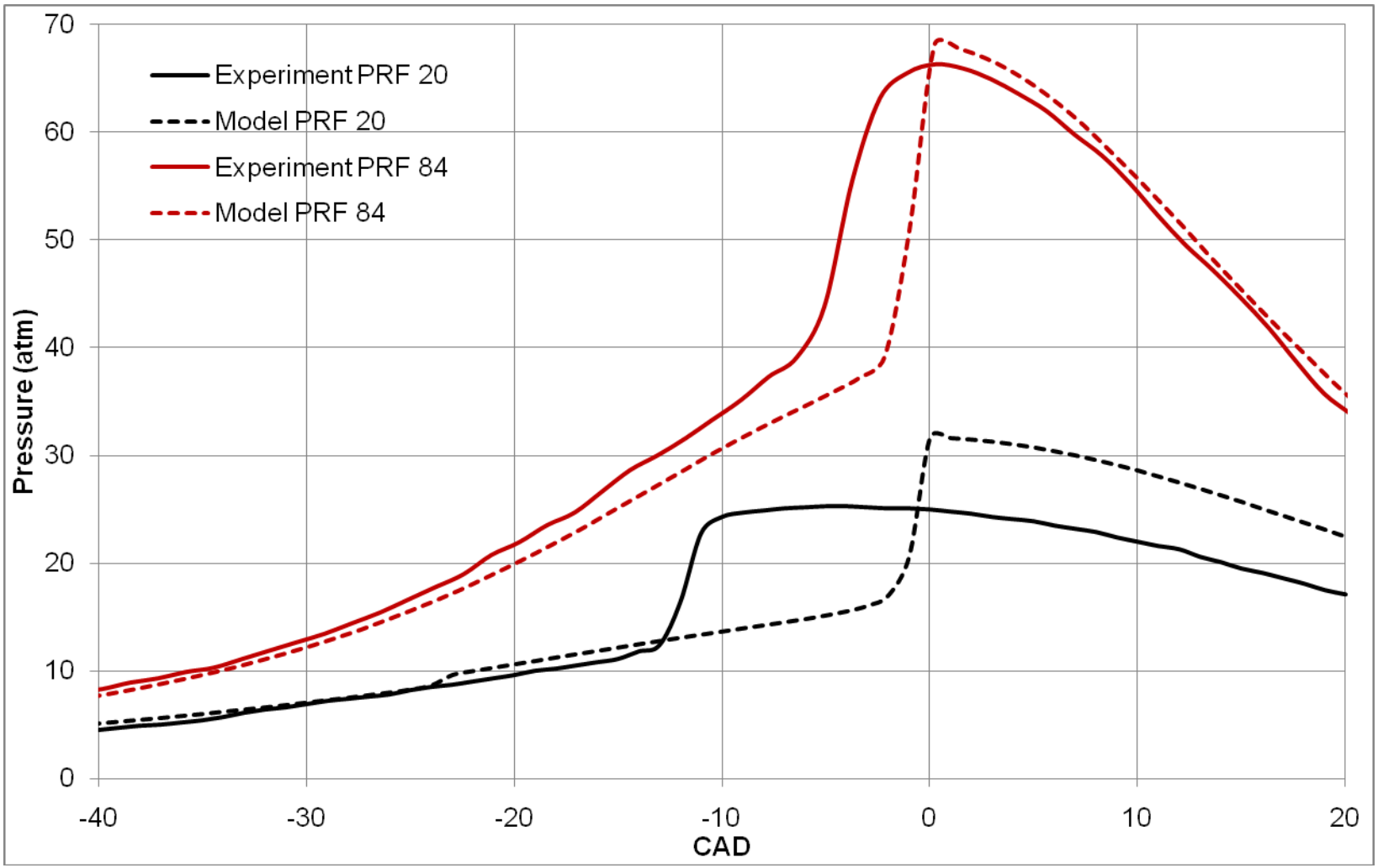

Figure 5.11: Pressure vs. CAD, Experimental and Baseline Curran Model for Both Fuels.

CHAPTER 6

PARAMETRIC STUDY

Model comparisons with data from shock tube experiments and homogeneous charge compression ignition (HCCI) engines using fuels exhibiting significantly different ignition tendencies have been made in Chap. 5. It was discovered that the kinetic model by Curran *et al*. (2002) predicted a delayed ignition time relative to the experiments for all fuels in both types of reactors. However, the model was capable of capturing many of the trends in the data. For example, simulations with each fuel in a constant volume reactor predicted shorter ignition delay at high temperatures, longer delays at low temperatures, and a nearly constant delay in the intermediate range from approximately 800 – 900 K as in the shock tube experiments (see Figs. 5.1 and 5.2). To model HCCI combustion, it was first necessary to determine the suitable parameters governing heat transfer and an appropriate inlet temperature to account for gas temperature inhomogeneities in a real engine. Once these were approximated, it was discovered that ignition time was delayed approximately 11° and 4° in the PRF 20 and PRF 84 engines, respectively (see Fig. 5.11). It is difficult to discern whether these discrepancies are due entirely to flaws of the kinetic model or if errors in the estimation of heat transfer parameters and inlet temperature also contribute significantly. Regardless, many of the trends observed in the simulated HCCI data are in accordance with the experimental

results. The two-stage ignition can be observed in the PRF 20 engine data, and the model captures this (although late) as well as predicts approximately the same induction time between the first and second stages. Peak pressures for the models are larger than experiments; however, this is also likely due to discrepancies in ignition time which is closer to top dead center (TDC) for the models and hence at a higher pressure. Additionally, the rate of pressure rise during the second stage ignition is slightly larger for the models. This may be the result of an imperfectly homogeneous experimental gas mixture in which a hot core would ignite first and result in a weaker ignition than the simultaneous ignition of the entire volume (CHEMKIN, 2006). Despite these difficulties in reproducing the exact experimental data, the agreement of trends allows a valuable parametric study to be conducted here using the IC engine model. Specifically, the effects of inlet pressure, temperature, octane number, equivalence ratio, and EGR rate on fuel autoignition and combustion are investigated.

6.1 Effect of Inlet Pressure

The practice of using a boosted inlet pressure via super- or turbo-charging an engine is becoming increasingly popular due to the increases in power density that can be achieved. However, as discussed in Sec. 2.2, a consequence of a high pressure hydrocarbon/air mixture is that the tendency toward autoignition increases and thus a boosted engine may result in knocking combustion. Turbo-charging is also frequently used in conjunction with exhaust gas recirculation (EGR) to combat the power losses associated replacing a portion of the intake air with diluent gases. There are therefore

many scenarios where engine intake pressure can deviate from that of natural aspiration (~ 1 atm).

Before extending to the complex IC engine model, it is instructive to observe the dependence of pressure on ignition in the adiabatic constant volume reactor. The transient pressure profiles for PRF 20 at T_{in} = 850 K, ϕ = 0.4, and three different inlet pressures are shown in Fig. 6.1 with the corresponding temperatures given in Fig. 6.2. The inlet temperature and pressures are similar to those that would be generated in an engine near the point of autoignition. A higher inlet pressure causes earlier ignition of both the first and second stages, with the most dramatic effect being on the timing of the hot second stage. Since temperature is the most important parameter governing the rate of branching reactions responsible for ignition (see Eq. 2.3), Tanaka *et al*. (2003) suggested that the induction time between the first and second stages is simply the time required for the energy released by the second stage reactions to raise the temperature from the value generated by the first stage reactions to the ignition (explosive) temperature. Utilizing the tangent method discussed in Sec. 5.2, the ignition temperature corresponding to each case is approximately 1220 K (superimposed in Fig. 6.2). Since this value is relatively consistent, the shorter second stage induction time at higher P_{in} is due to a larger energy release during the first stage which results in a higher temperature, though only slight, at the beginning of the second stage. The higher temperature accelerates the decomposition of H_2O_2 into 2OH (see R10 of Sec. 2.2) which more quickly overcomes degenerate branching leading to hot ignition. It is also worth noting that P_{in} has no bearing on the adiabatic flame temperature for a fixed T_{in} as shown in Fig.

6.2. This, however, does not imply that the total energy release due to combustion is constant over the range of inlet pressures. Figure 6.3 illustrates that the pressure rise ΔP due to combustion increases linearly with inlet pressure, which is a manifestation of conservation of energy since the system is adiabatic.

In view of the foregoing observations in a relatively simple constant volume, adiabatic reactor the effect of inlet pressure in an engine environment can now be discerned more clearly. Pressure profiles for two boosted inlet pressures and the baseline condition are shown in Fig. 6.4 for the modeled PRF 20 engine and the corresponding temperatures are given in Fig. 6.5. The second stage ignition is affected more significantly than the first stage, and the pressure rise due to combustion increases with P_{in}. Since ignition timing affects temperature increase, the maximum temperatures differ slightly due to differences in ignition timing. Figures 6.4 and 6.5 also give an indication of the importance of being able to control the ignition event in an HCCI engine. For example, the torque delivered by an engine is highly dependent upon the timing of ignition. If ignition is too early, the chemical energy released causing expansion of the gas can act against the compression stroke. If too late, a significant amount of energy can be lost due to higher exhaust gas temperatures transporting enthalpy out or some of the fuel energy can be lost by being carried out in the exhaust before combustion is complete.

PRF 84 is affected by inlet pressure in much the same manner as PRF 20, though higher P_{in} is required for PRF 84 to achieve similar ignition time scales due to octane number (ON) differences. Transient pressure and temperature profiles in the constant

volume adiabatic reactor for three different values of P_{in} at ϕ = 1/3.5 are shown in Figs. 6.6 and 6.7. The calculated ignition temperature was again relatively consistent at approximately 1060 K, and the pressure rise ΔP vs. P_{in} is linear as shown in Fig. 6.3. Two boosted pressures of 1.5 and 2.0 bar as well as the baseline are modeled in the PRF 84 engine and calculated pressures and temperatures are presented in Figs. 6.8 and 6.9, respectively. Two stage ignition is not easily seen in these profiles, which could be the result of fuel octane number and mixture strength making the first stage energy release undetectable. The isolated effects of octane number and equivalence ratio are investigated in Secs. 6.3 and 6.4, respectively. It is also possible that ignition is single stage. This possibility is examined next, while investigating the effect of inlet temperature.

6.2 Effect of Inlet Temperature

To some extent, the effect of inlet temperature has already been illustrated while attempting to suitably approximate ΔT to account for residual gas hot spots in HCCI engine modeling. For clarity, again first consider the constant volume adiabatic reactor. Figures 6.10 and 6.11 are transient pressure and temperature calculations, respectively, of PRF 20 at P_{in} = 40 atm, ϕ = 0.4, and varying T_{in}. A number of interesting observations can be made by considering the temperature profiles in Fig. 6.11. First, in agreement with the constant T_{in} calculations of Figs. 6.4 and 6.5, the induction time between the end of the first stage ignition and the second stage explosion decreases with increasing first stage energy release. Figure 6.11 also reveals that the temperature at the conclusion of the first stage reactions is independent of T_{in} with a value of approximately 926 K and

thus the first stage energy release increases as T_{in} decreases. This seems to indicate that at this critical temperature of 926 K, the reactions responsible for degenerate branching begin to dominate, or, in terms of the kinetic scheme presented in Sec. 2.2, R8 becomes faster than R2. The system remains in the negative temperature coefficient region until it reaches the hot ignition temperature, which is approximately constant at 1213 K as estimated by the tangent method. Note also that for T_{in} = 1000 K, ignition is single stage, and it can be inferred that such is the case for T_{in} > 926 K. To illustrate in the context of Chap. 2, consider again Fig. 2.1. Traversing the constant pressure line from point 1 to point 4, the system passes through the first stage explosion in region 2 until a critical temperature is reached separating regions 2 and 3. This corresponds to the end of the first stage ignition. In region 3, steady reaction again dominates until a second critical temperature is reached sending the system into the second stage explosion. Thus, a saturated hydrocarbon C_nH_{2n+2} for which n > 2 may exhibit a single or two-stage ignition depending on the initial conditions. In terms of the process described above, a system initially at point 1 of Fig. 2.1 will exhibit two-stage ignition, whereas one initially at point 3 will be single stage.

Now consider the effect of inlet temperature in the modeled HCCI engine. Pressure and temperature calculations are shown in Figs. 6.12 and 6.13, respectively, for the modeled PRF 20 engine at varying T_{in} including the baseline at 463 K. The temperature profiles show that even in the complex IC engine model where temperature and pressure are continually changing, an approximately constant critical temperature exists where the first stage ignition is concluded. Also note from the pressure trace that

the first stage energy release is slightly larger for lower T_{in}, which is in agreement with the constant volume reactor predictions of Figs. 6.10 and 6.11.

Constant volume reactor pressures and temperatures are provided in Figs. 6.14 and 6.15, respectively, for PRF 84 at ϕ = 1/3.5 while varying T_{in}. The critical temperature for single stage ignition appears to be slightly above 840 K, as degenerate branching (R8 of Sec. 2.2) takes over at this temperature and the first stage ignition is terminated. Hence, ignition becomes single stage for all T_{in} greater than this temperature. This suggests that ignition for the modeled PRF 84 engine is likely single stage from the inspection of pressures and temperatures near ignition in the constant T_{in} calculations of Figs. 6.8 and 6.9 and the constant P_{in} calculations of Figs. 6.16 and 6.17.

6.3 Effect of Octane Number

As discussed in Chap. 4, a fuel with high ON is more resistant to autoignition than one with low ON. Modeling fuels with wide range of ON is a simple matter when working with the PRF fuels *n*-heptane (*n*-C_7H_{16}) and *iso*-octane (*i*-C_8H_{18}) because, by definition, ON is the percentage of *i*-C_8H_{18} in a fuel mixture containing only *n*-C_7H_{16} and *i*-C_8H_{18}. To illustrate the effects of ON, consider the pressure and temperature profiles in the constant volume reactor for varying ON in Figs. 6.18 and 6.19, respectively. In these calculations, inlet pressure and temperature have been held constant at 40 atm and 800 K with ϕ = 0.4, which generates a two-stage ignition for each fuel mixture. Note that the fuels with lower ON have a larger first stage energy release resulting in shorter second stage induction times. Comparing the first stage ignition of the ON = 0 (100% *n*-C_7H_{16})

and ON = 100 (100% *i*-C_8H_{18}) profiles of Figs. 6.18 and 6.19 reveals that the first stage reactions of *n*-C_7H_{16} occur at a much faster rate and are more exothermic than those of *i*-C_8H_{18}. It can therefore be deduced that the first stage ignition commences earlier and releases more energy for lower ON due to a higher percentage of *n*-C_7H_{16} in the fuel composition. The temperature at the conclusion of the first stage reactions for each ON in Fig. 6.19 are used to generate Fig. 6.20, which shows the approximate critical temperature separating single and two stage ignition for each ON. Since the critical temperature for second stage explosion is approximately constant at 1150 K over the range of ON, as is the adiabatic flame temperature and the second stage explosion energy release rate, it appears that the reactions responsible for the first stage ignition are the most significant difference between the combustion of *n*-C_7H_{16} and *i*-C_8H_{18}.

6.4 Effect of Equivalence Ratio

Pressure and temperature in the constant volume reactor are provided for PRF 20 at varying fuel/air equivalence ratio ϕ, P_{in} = 40 atm, and T_{in} = 800 K in Figs. 6.21 and 6.22, respectively. The first stage as well as the overall energy release increases with increasing ϕ combined with a decrease in the second stage ignition delay. It is also observed that the rate of energy release during the second stage explosion, or burn rate, decreases significantly with decreasing ϕ particularly below ϕ = 0.4. The burn rate can be viewed as an indication of the severity of knock in uncontrolled autoignition since damaging knocking combustion is characterized by a very fast release of energy. Additionally, the burn rate, along with the ignition timing, is a critical parameter for control in HCCI combustion over a wide range of speeds and load conditions. The same

trends observed in the PRF 20 calculations of Figs. 6.21 and 6.22 can be seen in the profiles of pressure and temperature for PRF 84 with varying ϕ at P_{in} = 40 atm and T_{in} = 840 K shown in Figs. 6.23 and 6.24. These conditions generate two-stage ignition for each ϕ. HCCI engine modeling in the PRF 20 engine has predicted the pressure variation depicted in Fig. 6.25 for ϕ = 0.3, 0.4, and 0.5. It is curious that the first stage ignition timing is delayed (though slightly) as ϕ is increased, for constant volume predictions in Fig. 6.21 show the opposite. Nonetheless, second stage ignition delay decreases and the energy release due to combustion increases with ϕ as observed in the constant volume reactor predictions displayed in Figs. 6.21 and 6.22. Figure 6.26 shows the pressure variation for the modeled PRF 84 engine at ϕ = 0.286 (baseline), 0.4, and 0.5. The single stage ignition timing is not significantly affected by ϕ, however, combustion energy release and burn rates are influenced in a manner similar to the constant volume profiles of Fig. 6.23.

In their work with a rapid compression machine, Tanaka *et al*. (2003) found that ignition delay times for the second stage were much more strongly correlated with the *n*-C_7H_{16}/O_2 molar ratio than *i*-C_8H_{18}/O_2 and were independent of the ON and ϕ. To confirm this with the kinetic model, the second stage ignition delay times τ_{ig} (that is the time interval from the beginning of simulation to the second stage explosion) in the constant volume homogeneous reactor were calculated for multiple *n*-C_7H_{16}/O_2 and *i*-C_8H_{18}/O_2 ratios at P_{in} = 40 atm and T_{in} = 820 K to generate two-stage ignition for all fuel mixtures. The ignition delay is determined by CHEMKIN and corresponds to the time of the maximum temperature gradient. The test matrix for the present work is outlined in

Table 6.1 along with the results under the column "τ_{ig} 2-Stage (ms)". As can be seen from Fig. 6.27, a good correlation indeed exists for n-C_7H_{16}/O_2. Figure 6.28 shows pressure profiles for Runs 6-10 at n-$C_7H_{16}/O_2 = 0.0182$, which have varying ON and ϕ. With the exception of Run 6 (ON = 0, $\phi = 0.2$), τ_{ig} remains within a relatively narrow range of approximately 1.8 ms < τ_{ig} < 2.5 ms despite the significant differences in total energy release. This is not the case for constant i-C_8H_{18}/O_2 of Fig. 6.29, which provides pressure profiles from Runs 1-5. In Fig. 6.29, τ_{ig} varies from approximately 0.7 – 11.9 ms excluding Run 1 (ON = 100, $\phi = 0.2$). As a result, Fig. 6.30 for τ_{ig} vs. i-C_8H_{18}/O_2 shows no correlation.

It is interesting to examine whether a correlation exists between τ_{ig} and n-C_7H_{16}/O_2 when ignition is single stage. As suggested by Fig. 6.20, T_{in} was increased (from 820 K of Fig. 6.27) to 940 K to achieve single stage ignition for all the test conditions of Table 6.1 (excluding Run 6). Results are provided in Table 6.1 under column "τ_{ig} 1-Stage (ms)". Figure 6.31 reveals a correlation similar to that for two stage ignition shown in Fig. 6.27. Note that despite an increase of 120 K in T_{in}, τ_{ig} is approximately the same between both types of ignition for a given n-C_7H_{16}/O_2 except near n-$C_7H_{16}/O_2 = 0$. The constant ignition delay in this temperature range is reflected in Figs. 5.1 and 5.2 for each fuel mixture. This implies that, since the transition between single and two-stage ignition for each ON is approximately in the constant τ_{ig} temperature range of 800 – 950 K (see Figs. 5.1, 5.2, and 6.20), the type of ignition does not affect the delay time. To see this explicitly, calculations were made at an intermediate T_{in} = 900 K generating single and two-stage ignition depending on ON (see again Fig. 6.20). The

ignition delay corresponding to the hot ignition (that is from time = 0 to the time of the final gas explosion), whether single or two stage, is reported in the column heading "τ_{ig} Intermediate (ms)" of Table 6.1. Figure 6.32 demonstrates for T_{in} = 900 K that the correlation between τ_{ig} and *n*-C_7H_{16}/O_2 is preserved.

Run #	ON	ϕ	*n*-C_7H_{16}/O_2	*i*-C_8H_{18}/O_2	τ_{ig} 2-Stage (ms)	τ_{ig} 1-Stage (ms)	τ_{ig} Intermediate (ms)
1	100	0.200	0	0.0160	60.543	10.906	21.801
2	80	0.332	0.0040	0.0160	11.916	5.560	8.456
3	60	0.432	0.0107	0.0160	4.130	3.409	3.954
4	40	0.632	0.0240	0.0160	1.535	1.843	1.679
5	20	1.232	0.0640	0.0160	0.675	0.721	0.585
6	0	0.200	0.0182	0	5.027	--	3.911
7	20	0.350	0.0182	0.0046	2.523	2.747	2.496
8	40	0.479	0.0182	0.0121	2.187	2.450	2.332
9	60	0.736	0.0182	0.0273	2.041	1.976	2.112
10	80	1.509	0.0182	0.0727	1.840	1.150	1.419
11	30	1.114	0.0500	0.0214	0.824	0.916	0.743
12	50	1.280	0.0400	0.0400	1.018	0.954	0.916
13	90	0.336	0.0020	0.0180	17.441	6.159	10.584

Table 6.1: Ignition Delay Test Matrix and Results for Varying Fuel/O_2 Ratios.

6.5 Effect of Exhaust Gas Recirculation

EGR in an engine can have both thermodynamic and chemical effects on the autoignition and combustion of fuel/air mixtures. The thermodynamic effects are due to an increase in the specific heat capacity c_p of the gas mixture with introduction of combustion products, primarily CO_2, H_2O, and N_2, to the intake charge. A mixture with higher c_p requires the addition of more energy via physical compression and/or chemical reaction to raise its temperature. Since the reactions leading to ignition are temperature

dependent (see Eq. 2.3), ignition timing will be delayed until the gas has been compressed by the piston to its ignition temperature. The term "thermodynamic cooling" is often used to refer to the thermodynamic effect of EGR addition because the mixture c_p usually increases with increasing EGR thereby inhibiting the temperature rise. The chemical effects of EGR vary depending on the constituent. In this section, the thermodynamic effects are first investigated by observing the effect of EGR on compressed gas temperatures. The chemical effects are then studied in the constant volume reactor to eliminate the thermodynamic cooling effects associated with compression by the piston. Finally, different EGR rates are used in the HCCI engine models to show the overall effects.

The primary constituents of EGR are the products of complete combustion of a fuel/air mixture, CO_2, H_2O, and N_2. Figure 6.33 demonstrates the effect of each constituent on the adiabatic compressed gas temperature of the motored PRF 20 engine. Motored operation indicates no heat release due to chemical reaction and therefore temperature changes are due only to differences in c_p. A baseline condition of 100% O_2 is shown with mixtures of 20% O_2 and 80% diluent. The highest temperatures are achieved for 80% N_2, which is close to the composition of air (21% O_2 and 79% N_2). CO_2 as the diluent generates the most modest temperature rise. These effects are easily understood by observing the differences in c_p of each species, shown as a function of temperature in Fig. 6.34 (Moran and Shapiro, 2004). The range of 300 – 1000 K in this figure is typical of the temperatures achieved due to compression by a piston in IC engines. CO_2 has the highest c_p and therefore requires more energy input to raise the

temperature than the other gases. It should be expected, then, that ignition will commence later with addition of CO_2 than with equivalent additions of H_2O or N_2. It is also interesting to note that N_2 has a slightly lower c_p than air and thus dilution of air with additional N_2 will actually raise the compressed gas temperature.

Sjöberg *et al*. (2007) has shown that the reduction of mole fraction of O_2, y_{O2}, in the reactant mixture with introduction of EGR has the chemical effect of retarding ignition in an HCCI engine. The influence of y_{O2}, or volume percentage O_2, in the constant volume reactor can be observed in Fig. 6.35. In these calculations, PRF 20 with a fuel/O_2 equivalence ratio of 0.4, providing $y_{O2} = 0.975$, was used as the base reactant mixture at $P_{in} = 40$ atm and $T_{in} = 900$ K. To generate a similar volume percentage of O_2 as found in air, each diluent was added in increments of 1% from 78% to 85% of the total reactant mixture. The test matrix and ignition delay τ_{ig} corresponding to the maximum temperature gradient for each diluent is given in Table 6.2. It should be noted that all cases exhibited two-stage ignition and τ_{ig} in Table 6.2 corresponds to the hot second stage ignition. Figure 6.35 clearly shows an increase in ignition delay as y_{O2} decreases. It is expected that the delay is largest for CO_2 as the diluent based on its high thermodynamic cooling as seen in Figs. 6.33 and 6.34. Although the constant volume reactor eliminates temperature increases due to compression, the thermodynamic effect of inhibiting the gas temperature rise as a result of the chemical reactions remains. The first stage ignition delay, however, is nearly independent of the type of diluent as depicted in Fig. 6.36 due to limited exothermic reactions that increase the temperature preceding the first stage

ignition. This is not the case for the second stage ignition, though, as the temperature will be affected by the energy released from the first stage.

Mole Fraction Diluent	Mole Fraction O_2	τ_{ig} (ms) with CO_2	τ_{ig} (ms) with H_2O	τ_{ig} (ms) with N_2
0.78	0.214	2.404	1.636	2.010
0.79	0.205	2.650	1.813	2.232
0.80	0.195	2.932	2.021	2.491
0.81	0.185	3.259	2.267	2.796
0.82	0.175	3.637	2.561	3.158
0.83	0.166	4.080	2.916	3.592
0.84	0.156	4.600	3.352	4.120
0.85	0.146	5.218	3.890	4.693

Table 6.2: Test Matrix and Results for PRF 20 Second Stage τ_{ig} with Varying y_{O2}.

It is observed from Fig. 6.33 that thermodynamic cooling is greater for H_2O as the diluent than N_2, yet as Fig. 6.35 shows, the total ignition delay is shorter with H_2O than N_2. Since the kinetic model by Curran and co-workers (2002) considers N_2 to be an inert species (that is not involved in any chemical reaction in the model), only thermodynamic effects of N_2 exist. This suggests a chemical effect of H_2O that enhances ignition relative to the addition of inert N_2. Sjöberg *et al*. (2007) discovered similar ignition enhancement with H_2O in their experiments with an HCCI engine. To further illustrate this effect, consider Figs. 6.37 – 6.41 which show the variation in the species H, O, OH, HO_2, and H_2O_2, respectively, for each diluent at 79% of the total mixture corresponding to y_{O2} = 0.205 in the constant volume reactor for PRF 20 at P_{in} = 40 atm, T_{in} = 900 K, and fuel/O_2 equivalence ratio = 0.4. Though not explicitly shown in the kinetic scheme presented in Sec. 2.2, the radicals H and O are involved in the chain reaction mechanisms that

characterize explosive gas mixtures. The first stage ignition, occurring at approximately the same instant for each diluent, is readily seen in the profiles of y_H and y_O in Figs. 6.37 and 6.38. It is interesting that the peak for both radicals during the first stage ignition is smallest for H_2O as the diluent. Following the first stage, however, the mole fractions of H, O, OH, and HO_2 increase faster for mixtures diluted with H_2O than with CO_2 or N_2. Note the relationship between OH, HO_2, and H_2O_2 (HOOH) in reactions R8 – R10 of Sec. 2.2. R8, producing HO_2, is responsible for degenerate branching, and as Fig. 6.40 shows, a peak in HO_2 occurs just after the first stage ignition. The mole fraction of HO_2 then decreases as a sharp increase in H_2O_2 is observed following ignition in Fig. 6.41 as R9 predicts. HO_2 begins to accumulate again as degenerate branching (R8) continues, faster now for H_2O as the diluent, and H_2O_2 continues to increase though at a slower rate. It is also during this time that OH begins to accumulate (see Fig. 6.39) as predicted by the branching reaction R10. Soon HO_2 and H_2O_2 peak and then rapidly decrease while OH increases exponentially. The second stage ignition, as indicated by the occurrence of the maximum temperature gradient, follows. Though not shown as a reactant in the Hu and Keck (1987) mechanism presented in Sec. 2.2, it is reasonable to suggest that the presence of H_2O contributes to the production of the species shown in Figs. 6.37 – 6.41 after the first stage ignition. This is intuitive considering that, of the three diluents considered, only H_2O contains the hydrogen atoms that are present in these species (with the obvious exception of the oxygen radical O).

Sjöberg *et al*. (2007) also found that the chemical effect of H_2O ignition enhancement is stronger for two-stage ignition fuels than single stage. Since it has been

shown previously in Fig. 6.20 that a PRF can exhibit single or two-stage ignition, calculations were made for PRF 20 at fuel/O_2 equivalence ratio = 0.4, P_{in} = 40 atm, and T_{in} = 960 K in the constant volume reactor to generate single stage ignition. The test matrix is the same as that given in Table 6.2. Figure 6.42 provides the percent difference between the ignition delay using N_2 and H_2O as the diluents, calculated as

$$\% \text{ Difference} = \left[\frac{\left(\tau_{ig}\right)_{N_2} - \left(\tau_{ig}\right)_{H_2O}}{\left(\tau_{ig}\right)_{N_2}} \right] \times 100, \tag{6.1}$$

for both single and two-stage ignition. The delay times for single stage ignition differ somewhat more than those for two-stage. The kinetic model therefore predicts that the chemical effect of H_2O ignition enhancement relative to N_2 addition is stronger for single stage than two-stage ignition, which is in contrast with that observed by Sjöberg and coworkers. Further investigation is required to determine the reasons for such a discrepancy. However, since single stage ignition is manifested at higher temperatures and the H_2O ignition enhancement has not been observed at the lower temperatures of the first stage ignition, it seems possible that this chemical effect of H_2O is temperature dependent. If such is the case, then the stronger effect for single stage ignition predicted by the kinetic model is supported. Calculations with PRF 84 are consistent with the trends observed for PRF 20. Both single and two-stage ignition was generated for PRF 84 with fuel/O_2 equivalence ratio = 0.4, P_{in} = 40 atm, and T_{in} = 880 and 820 K, respectively. The chemical effect of ignition enhancement with H_2O was again observed, and as Fig. 6.43 illustrates, the effect is stronger for single stage ignition.

To illustrate the combined effect of the complete combustion products as EGR in an engine, pressures and temperatures were calculated in the modeled PRF 20 and PRF 84 engines at varying EGR rates. To employ EGR, a fraction of the exhaust gas from a calculation (run) without EGR is included as added species in the $\phi = 0.4$ inlet fuel/air mixture. This process is iterated until visible convergence of a steady state is achieved. For example, the inlet gas mixture for run 1 at 10% EGR includes 10% of the exhaust gas on a molar basis from a run with 0% EGR included as added species to the $\phi = 0.4$ mixture of fuel and air. The overall composition of such a mixture is then 90% $\phi = 0.4$ fuel + air and 10% exhaust gas from the run without EGR. Run 2 would contain 10% of the exhaust from run 1 added to a $\phi = 0.4$ fuel/air mixture and so on with subsequent runs. Pressure and temperature profiles are provided in Figs. 6.44 and 6.45 for the modeled PRF 20 engine at the baseline conditions of Table 5.3 with varying EGR rates composed of the complete combustion products (CCP). Table 6.3 lists the composition of each fuel/air/EGR mixture. Figures 6.44 and 6.45 demonstrate that the second stage ignition time is delayed significantly with increasing % EGR. Since y_{O2} decreases with increasing CCP EGR, this suggests that y_{O2} reduction and thermodynamic cooling due to increased CO_2 and H_2O overcome the chemical H_2O ignition enhancement and thermodynamic "warming" of increased N_2 (see Fig. 6.34). It is also observed from Figs. 6.44 and 6.45 that the first stage ignition time is approximately constant. This can be explained at least in part with another inspection of Fig. 6.36, which reveals that the first stage ignition delay changes only slightly (< 0.15 ms) in the range of y_{O2} corresponding to 0 – 20% CCP EGR. Additionally, Fig. 6.45 shows that the compressed gas temperature

prior to first stage ignition is approximately constant regardless of % EGR and therefore suggests that the impact of thermodynamic cooling on first stage ignition time is minimal.

PRF 20 Engine						
% CCP EGR	O_2	N_2	*n*-C_7H_{16}	*i*-C_8H_{18}	CO_2	H_2O
0	0.208	0.784	0.00590	0.00148	0	0
10	0.188	0.793	0.00531	0.00133	0.00591	0.00674
15	0.177	0.798	0.00502	0.00125	0.00887	0.01010
20	0.167	0.802	0.00472	0.00118	0.01180	0.01350
PRF 84 Engine						
% CCP EGR	O_2	N_2	*n*-C_7H_{16}	*i*-C_8H_{18}	CO_2	H_2O
0	0.209	0.786	0.000779	0.00409	0	0
10	0.188	0.798	0.000701	0.00368	0.00440	0.00496
15	0.178	0.804	0.000662	0.00348	0.00660	0.00744
20	0.167	0.810	0.000623	0.00327	0.00880	0.00992

Table 6.3: Intake Charge Composition (Mole Fraction) for Varying CCP EGR Rates.

Varying EGR rates were used in the PRF 84 engine and the resulting pressure and temperature profiles are provided in Figs. 6.46 and 6.47. Note that ignition is single stage for all intake compositions. The change in ignition time with EGR addition is substantially less than that observed for the second stage of the two-stage ignition in the PRF 20 engine shown in Figs. 6.44 and 6.45, which is consistent with the observation that ignition enhancement due to H_2O addition is stronger for single stage ignition as seen in Figs. 6.42 and 6.43. Since the y_{O_2} reduction with increasing EGR rate is approximately the same as the PRF 20 engine as shown in Table 6.3 and thermodynamic cooling does not appear to affect the temperature significantly prior to ignition, it is reasonable to suggest that the chemical effect of H_2O addition on the single stage ignition is primarily responsible for the enhancement compared to the two-stage PRF 20 engine ignition.

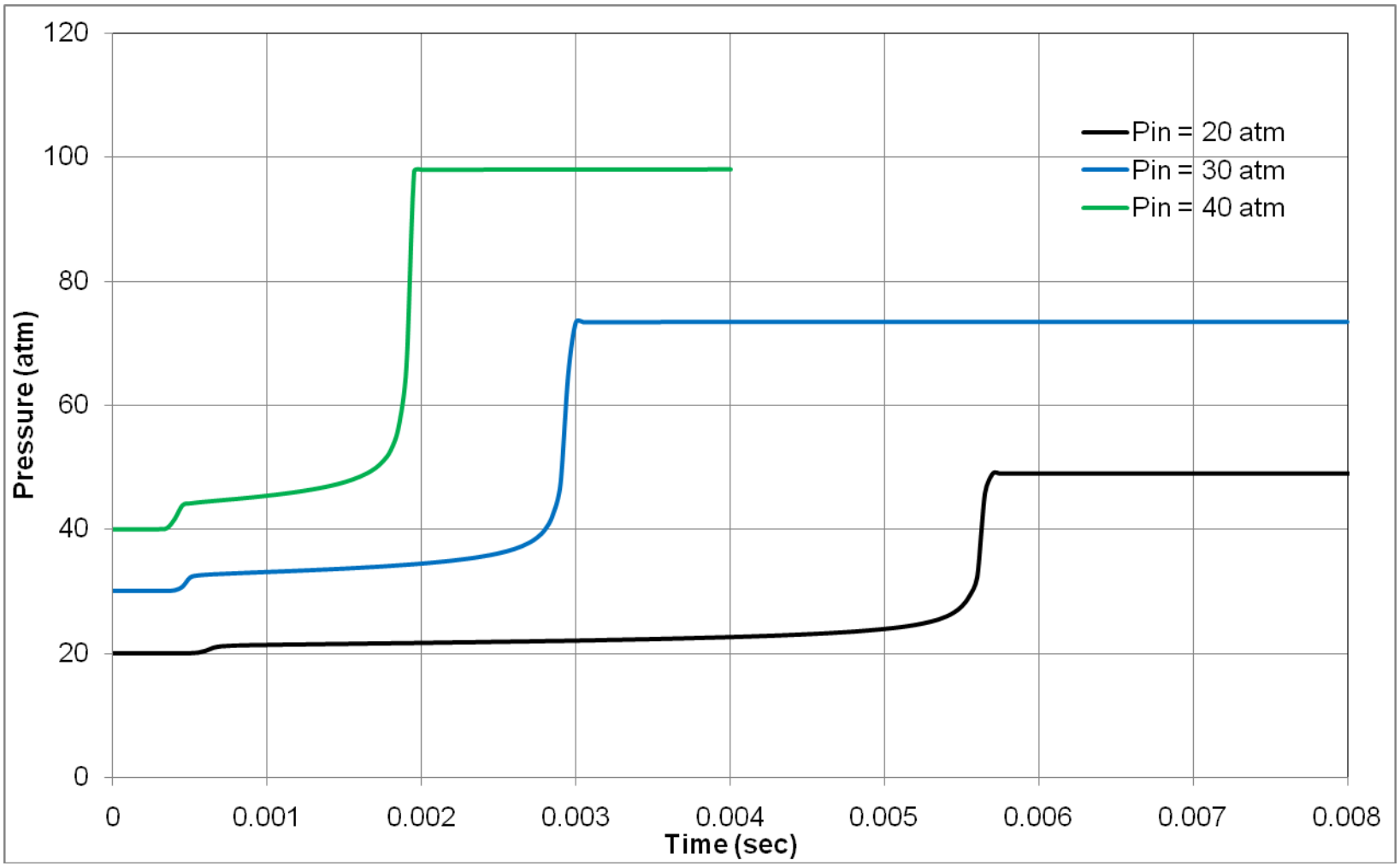

Figure 6.1: Pressure vs. Time, Constant Volume Reactor, PRF 20, T_{in} = 850 K, ϕ = 0.4.

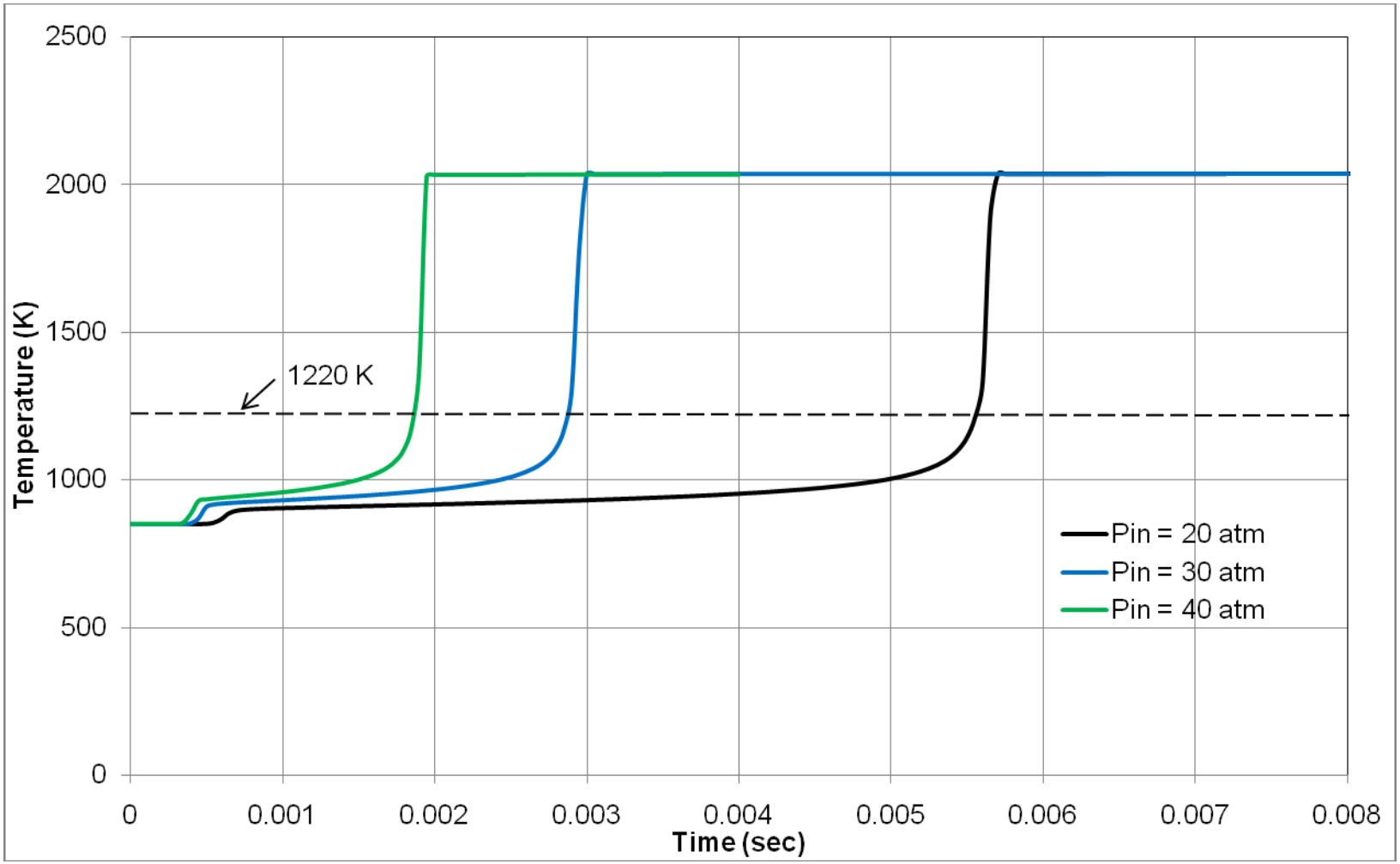

Figure 6.2: Temperature vs. Time, Constant Volume Reactor, PRF 20, T_{in} = 850 K, ϕ = 0.4.

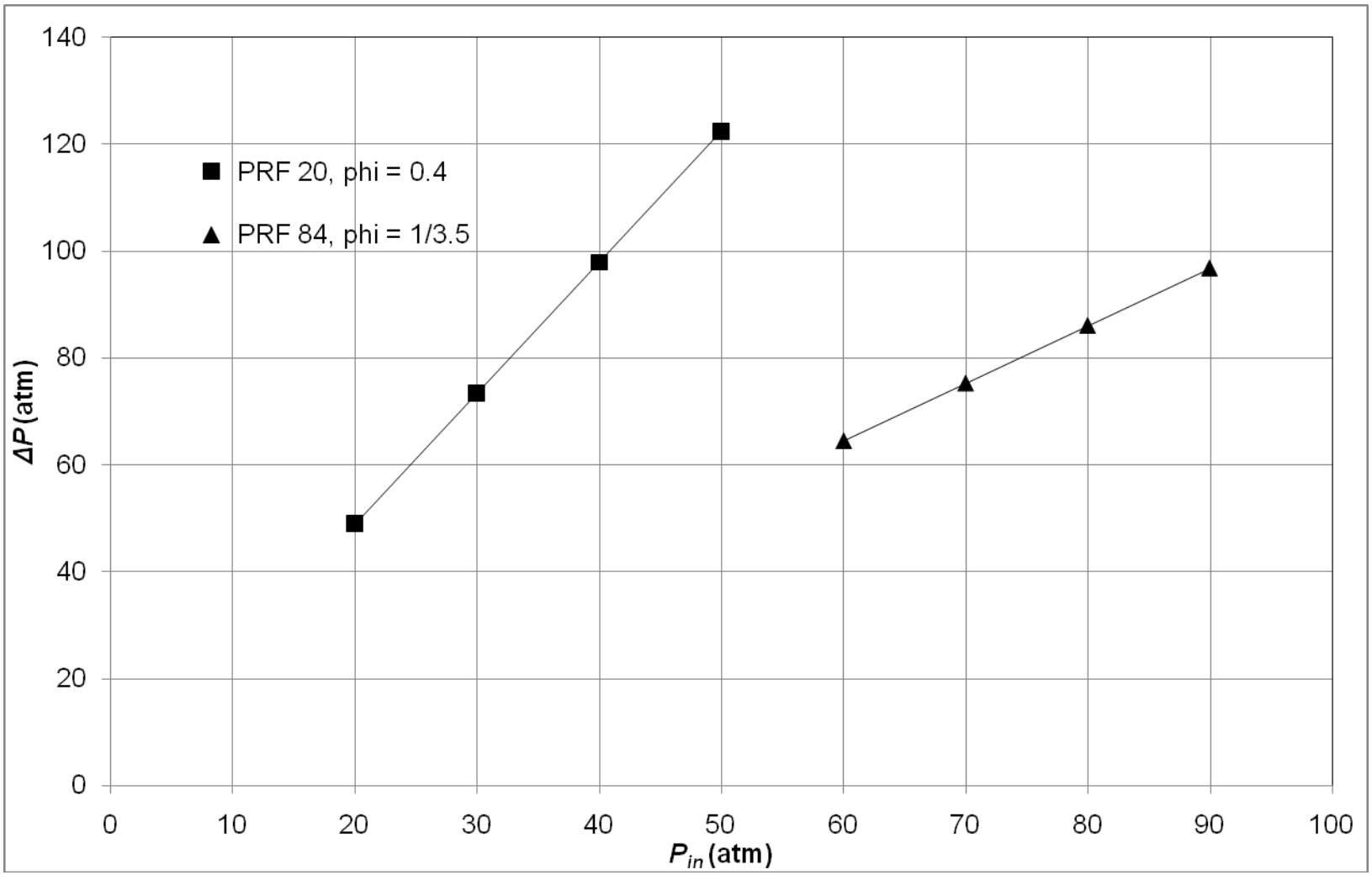

Figure 6.3: Pressure Rise vs. Inlet Pressure, Constant Volume Reactor, T_{in} = 850 K.

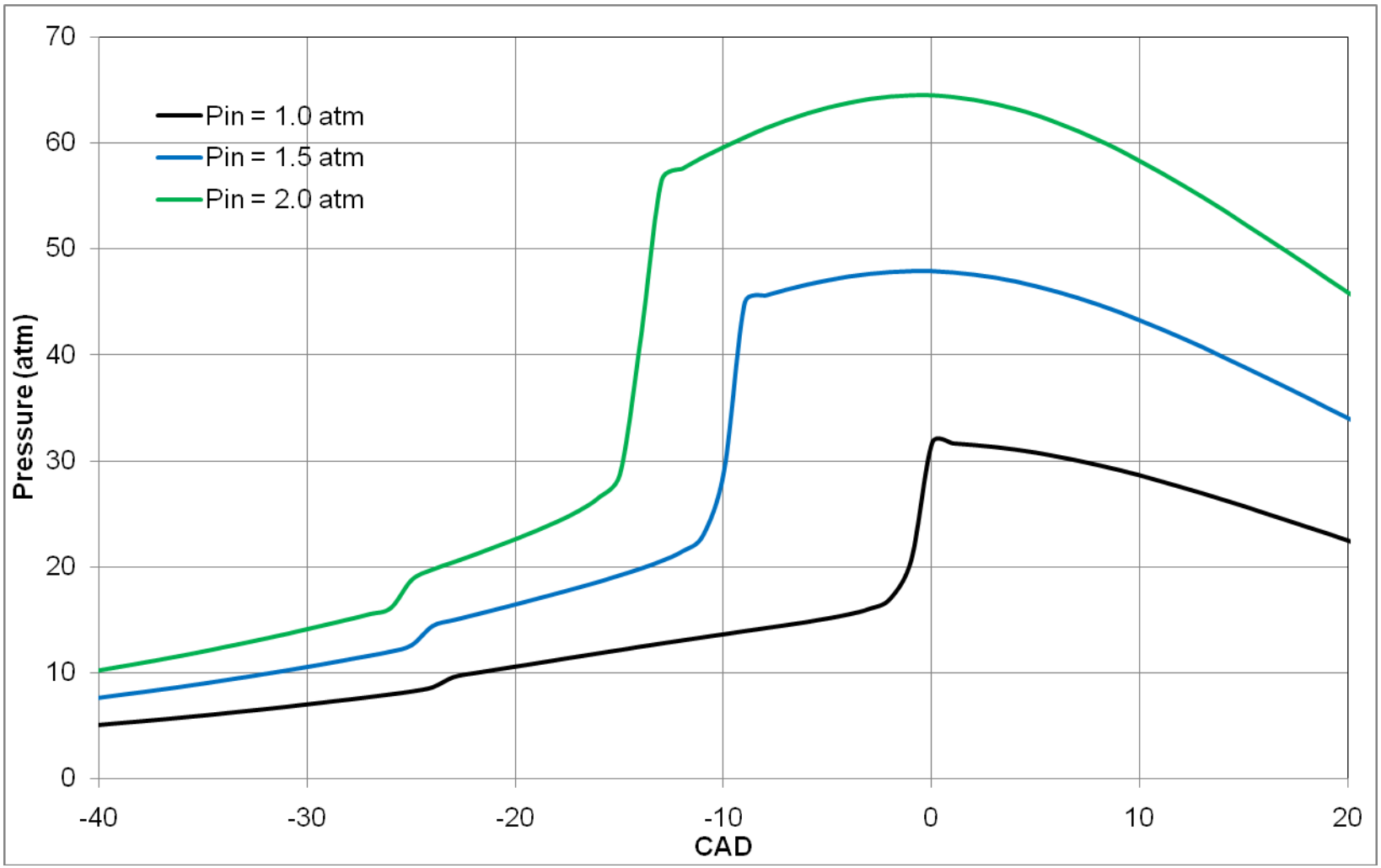

Figure 6.4: Pressure vs. CAD for Three Different Inlet Pressures Modeling the PRF 20 Engine.

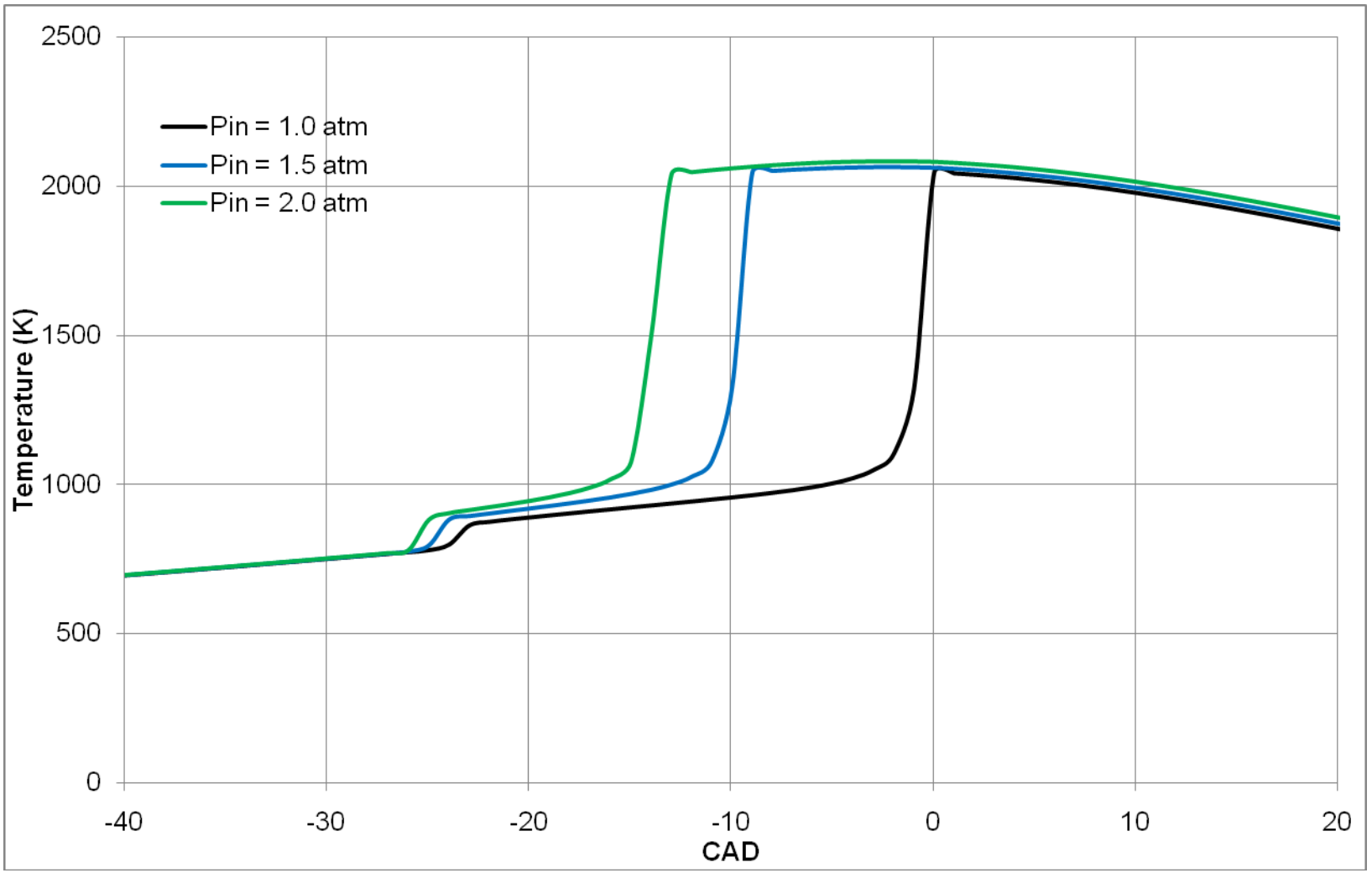

Figure 6.5: Temperature vs. CAD for Three Different Inlet Pressures Modeling the PRF 20 Engine.

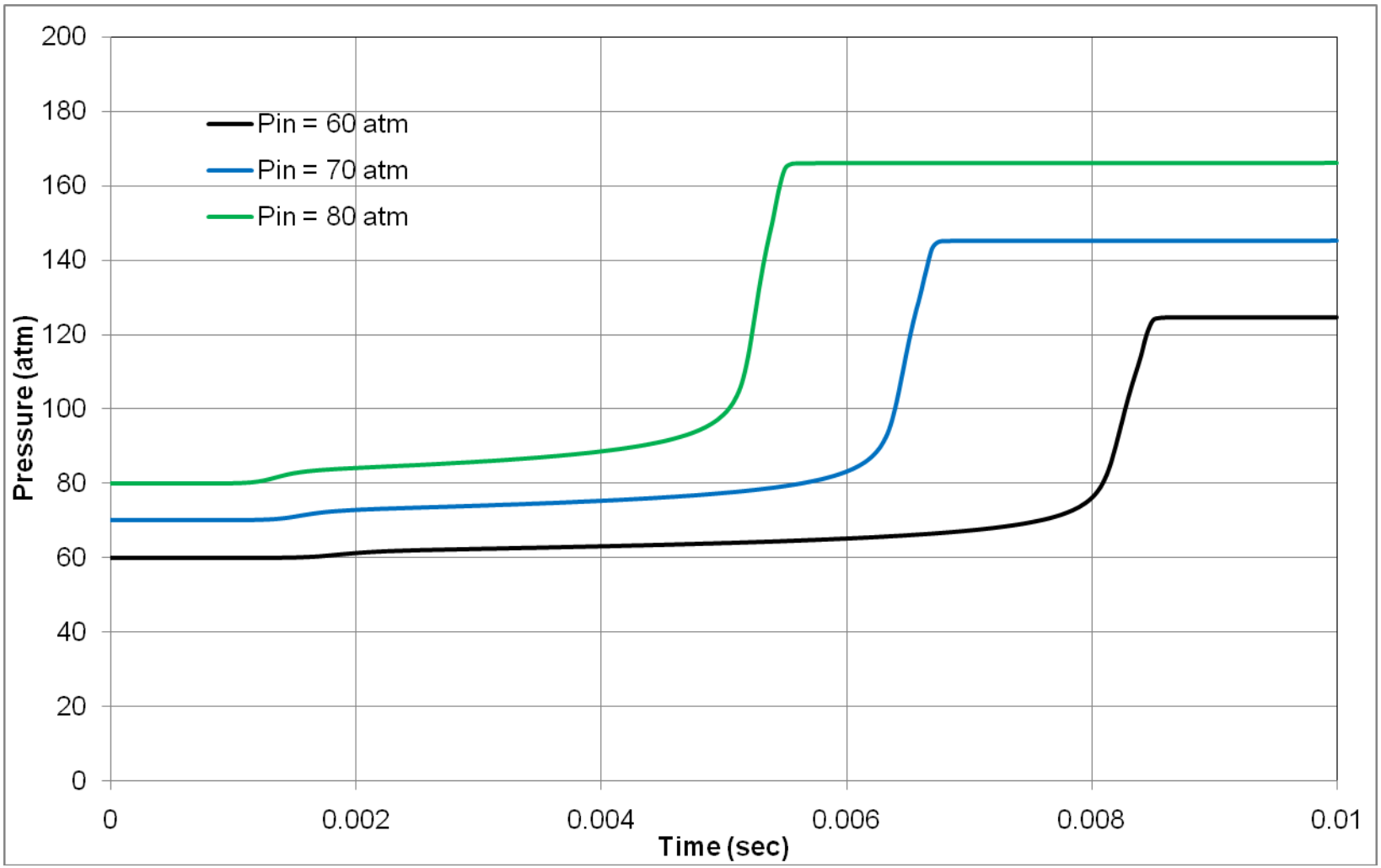

Figure 6.6: Pressure vs. Time, Constant Volume Reactor, PRF 84, T_{in} = 850 K, ϕ = 1/3.5.

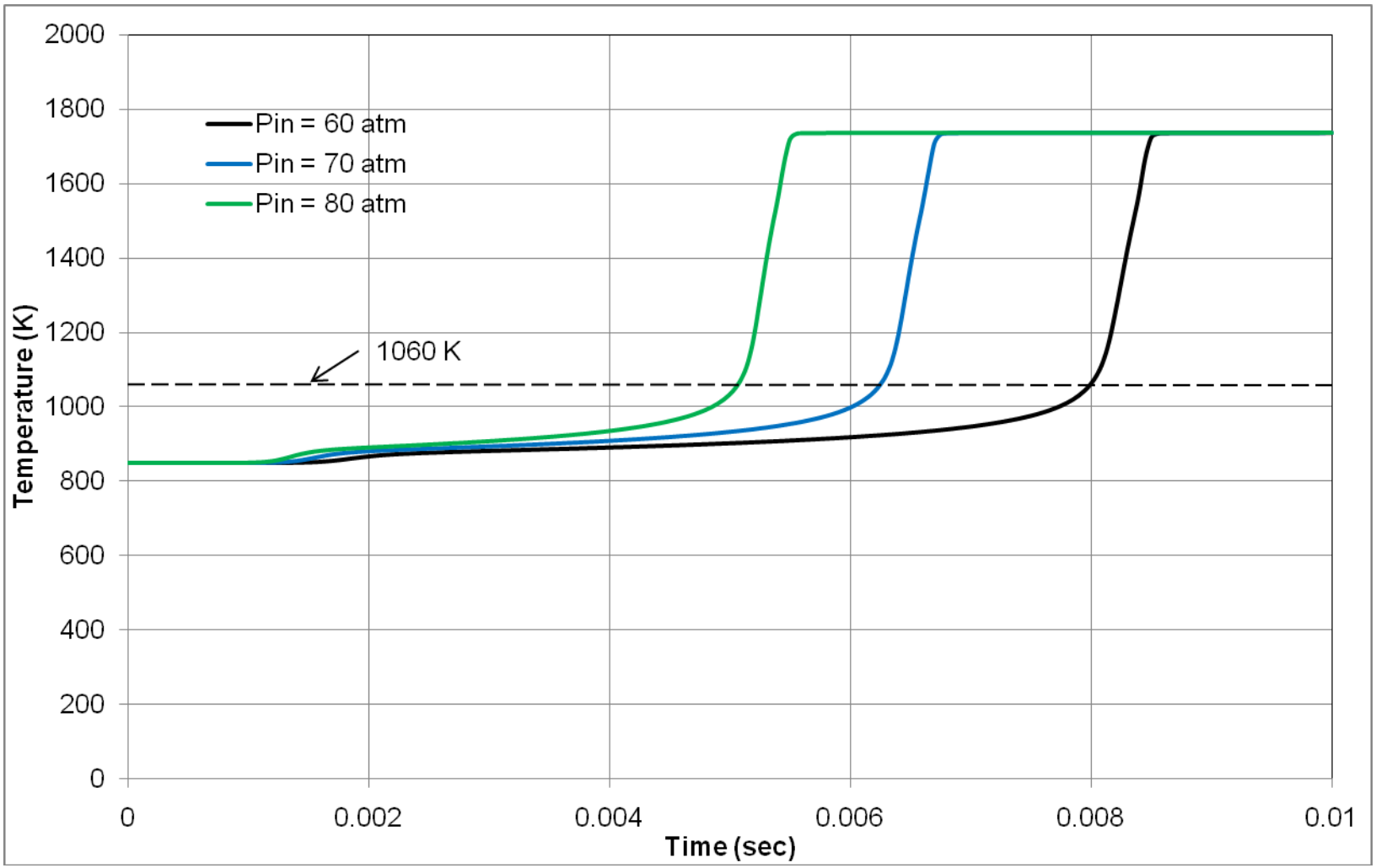

Figure 6.7: Temperature vs. Time, Constant Volume Reactor, PRF 84, T_{in} = 850 K, ϕ = 1/3.5.

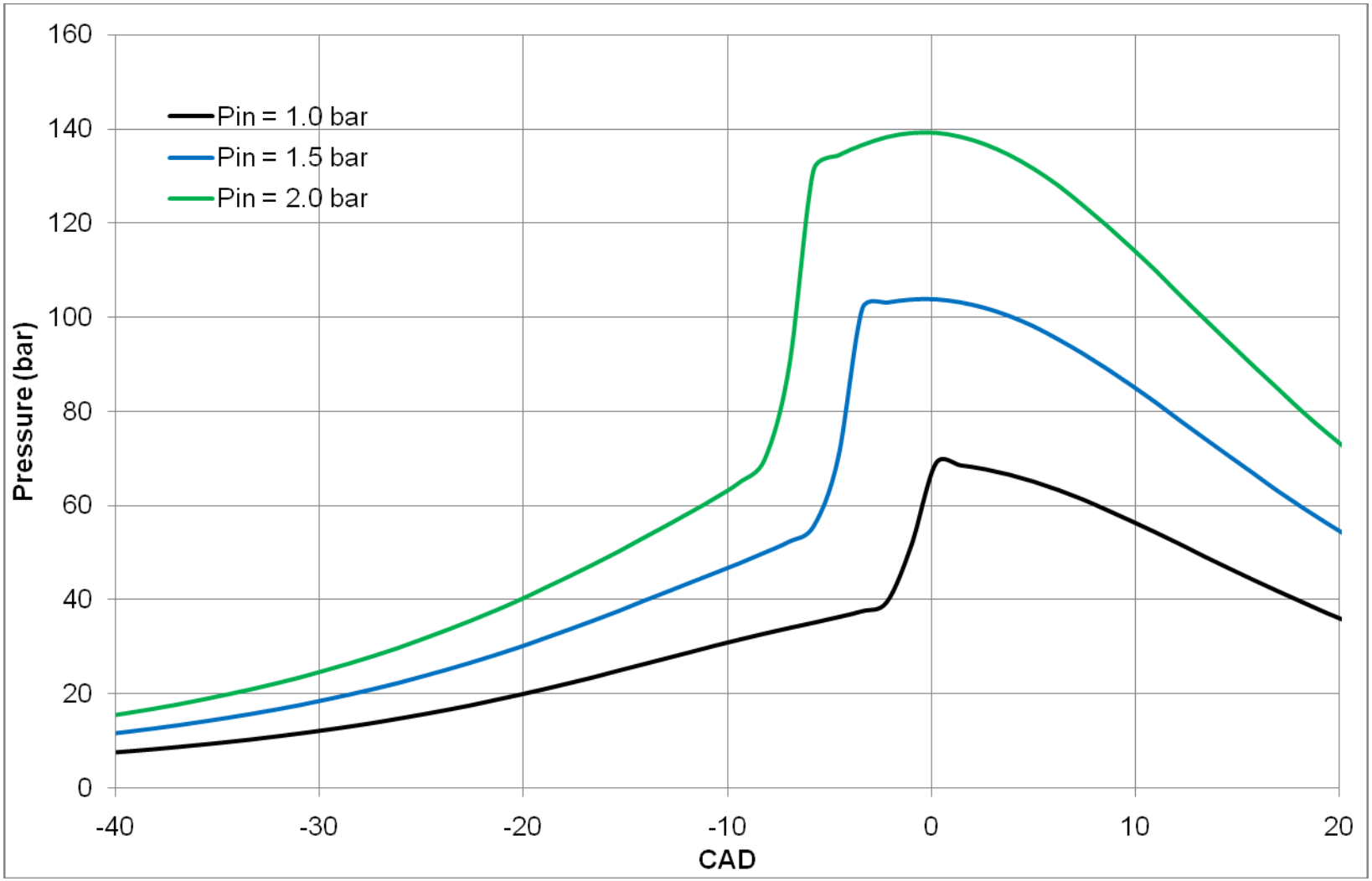

Figure 6.8: Pressure vs. CAD for Three Different Inlet Pressures Modeling the PRF 84 Engine.

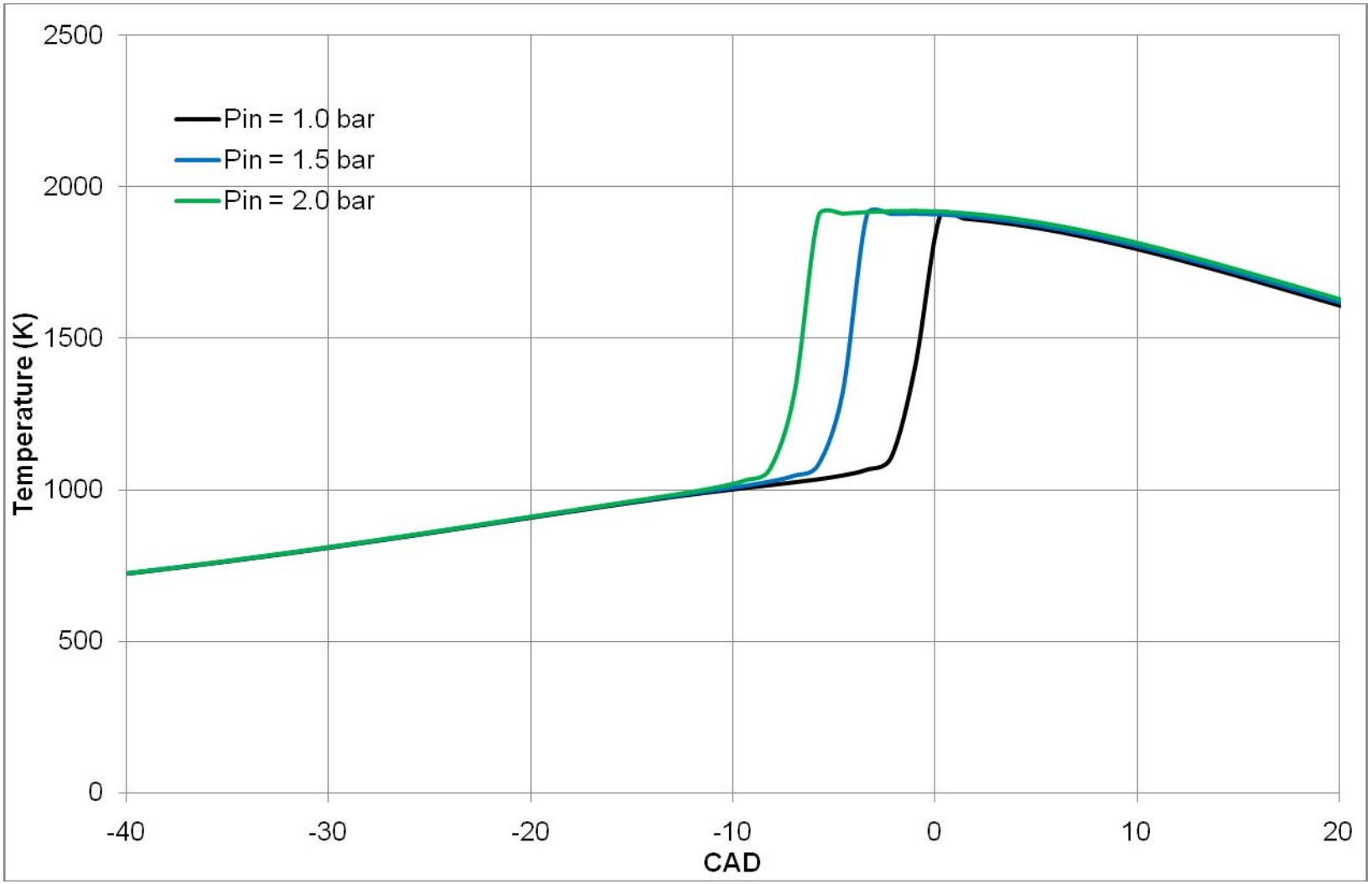

Figure 6.9: Temperature vs. CAD for Three Different Inlet Pressures Modeling the PRF 84 Engine.

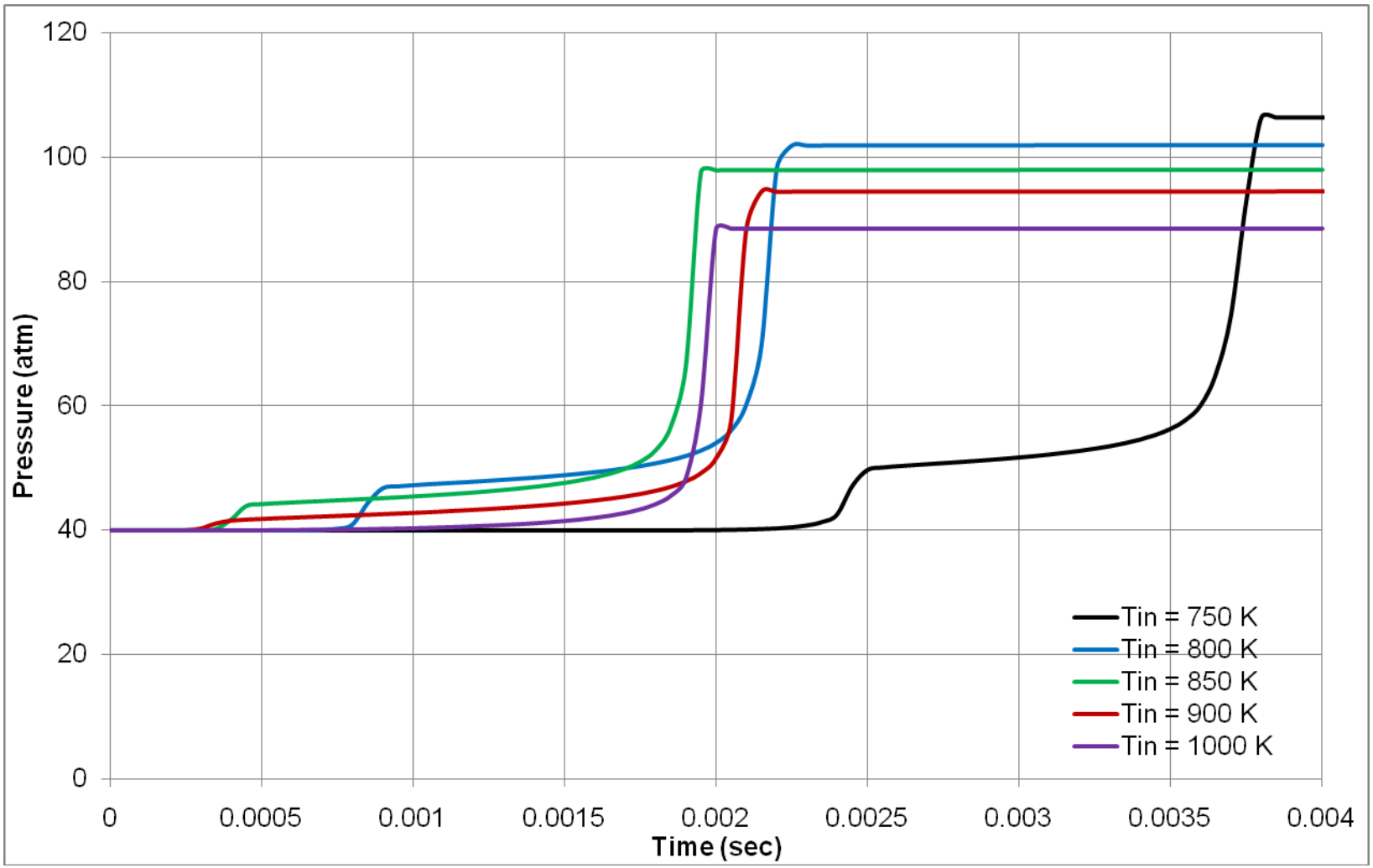

Figure 6.10: Pressure vs. Time, Constant Volume Reactor, PRF 20, P_{in} = 40 atm, ϕ = 0.4.

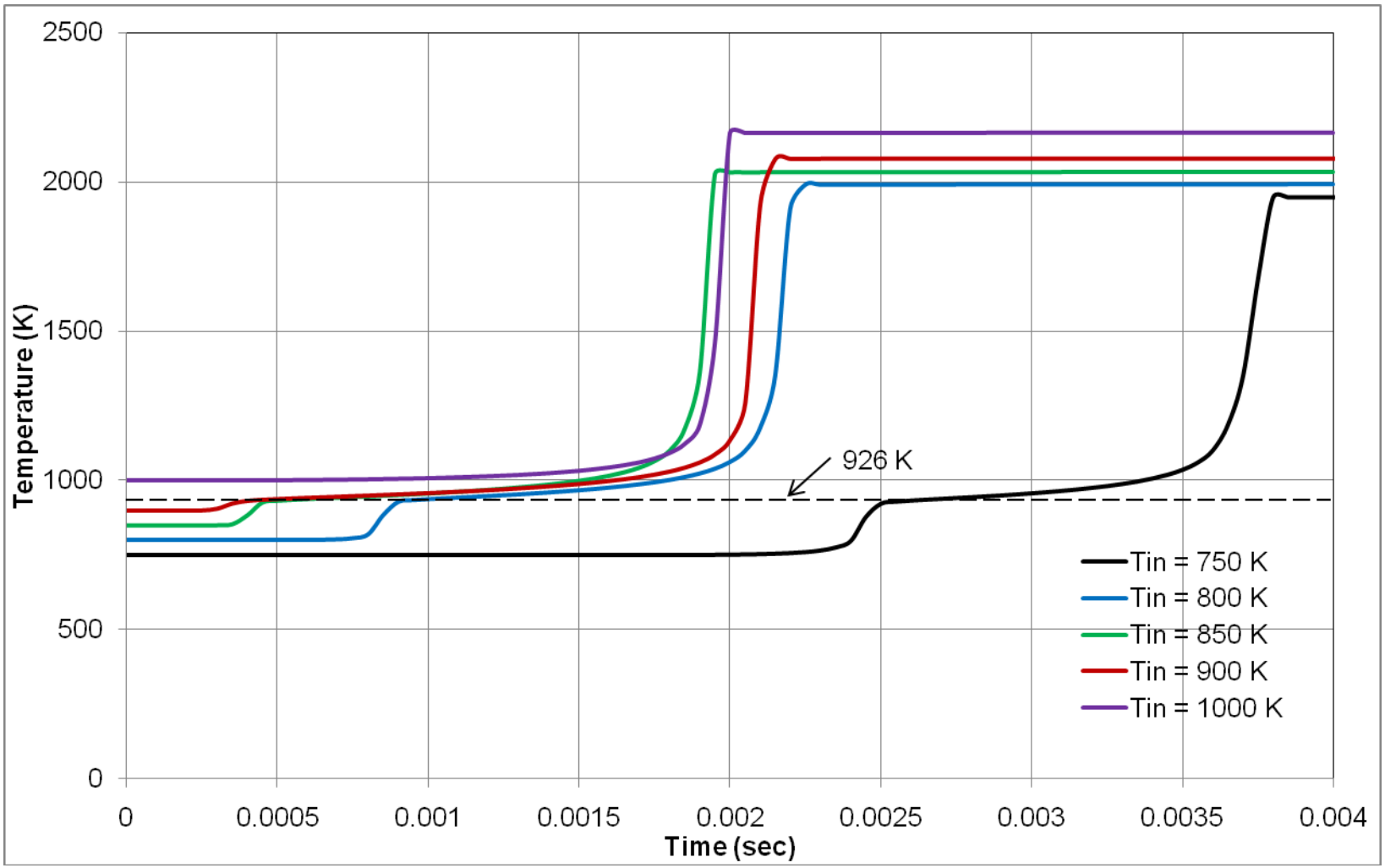

Figure 6.11: Temperature vs. Time, Constant Volume Reactor, PRF 20, P_{in} = 40 atm, ϕ = 0.4.

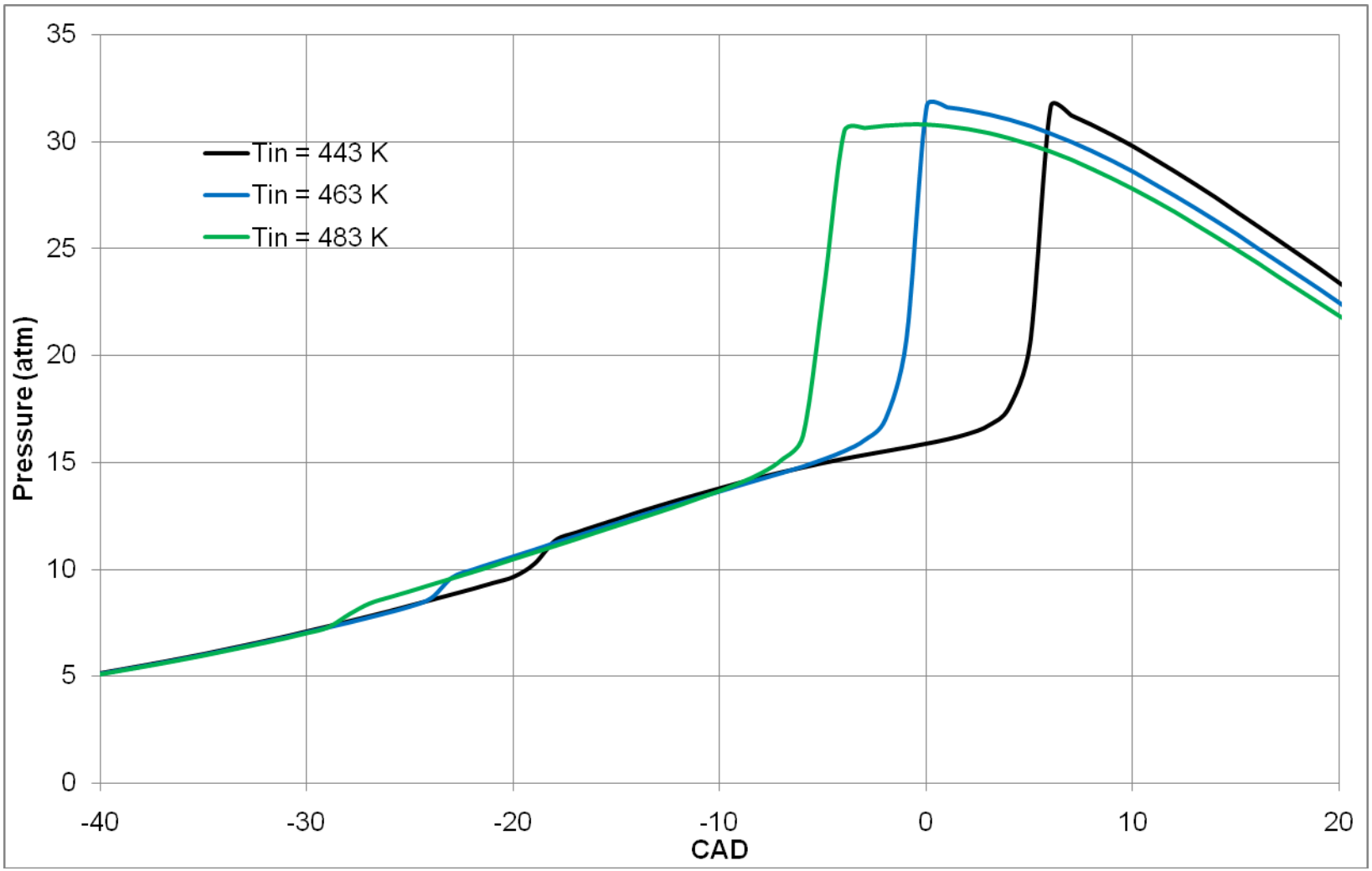

Figure 6.12: Pressure vs. CAD for Three Different Inlet Temperatures Modeling the PRF 20 Engine.

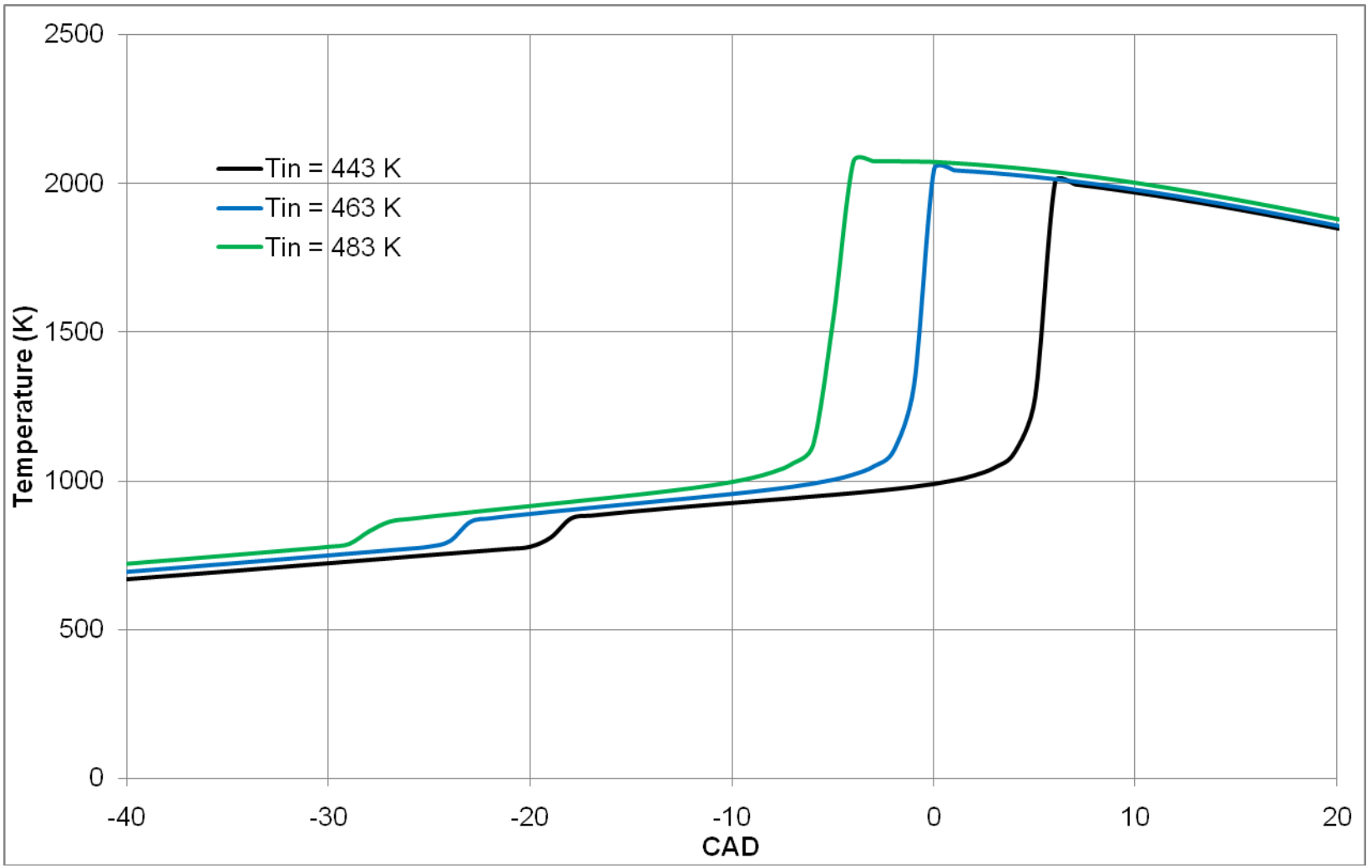

Figure 6.13: Temperature vs. CAD for Three Different Inlet Temperatures Modeling the PRF 20 Engine.

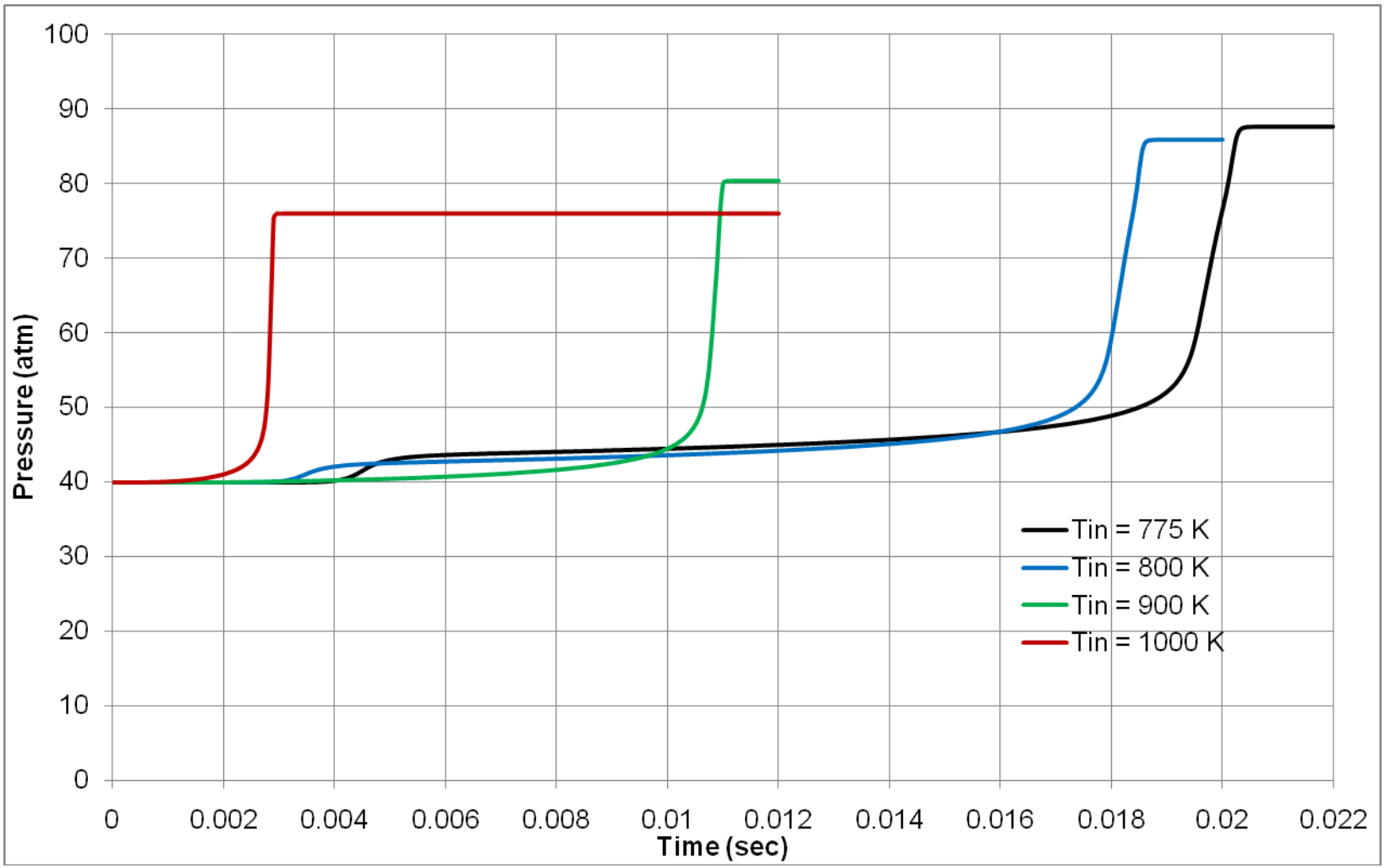

Figure 6.14: Pressure vs. Time, Constant Volume Reactor, PRF 84, P_{in} = 40 atm, ϕ = 1/3.5.

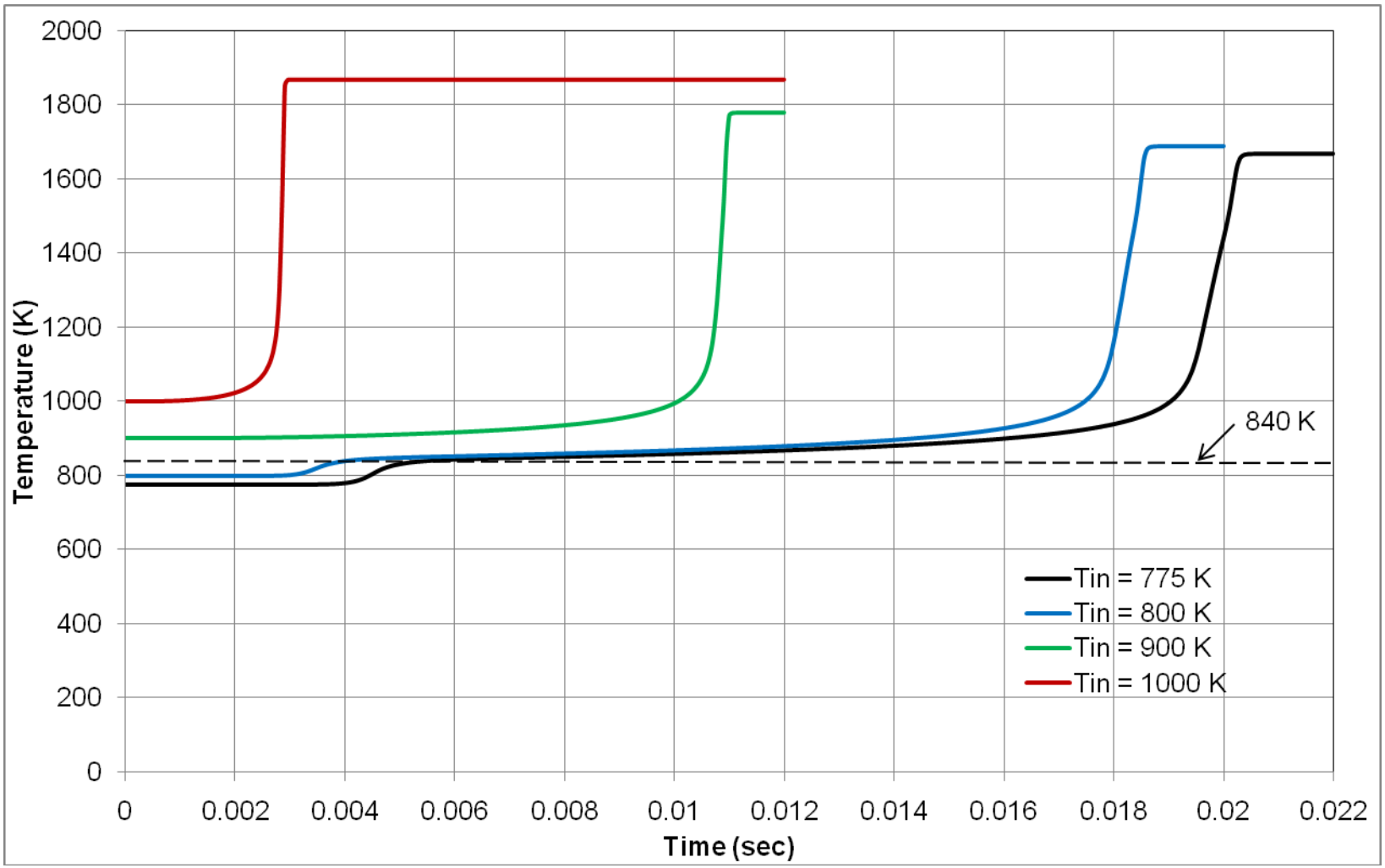

Figure 6.15: Temperature vs. Time, Constant Volume Reactor, PRF 84, P_{in} = 40 atm, ϕ = 1/3.5.

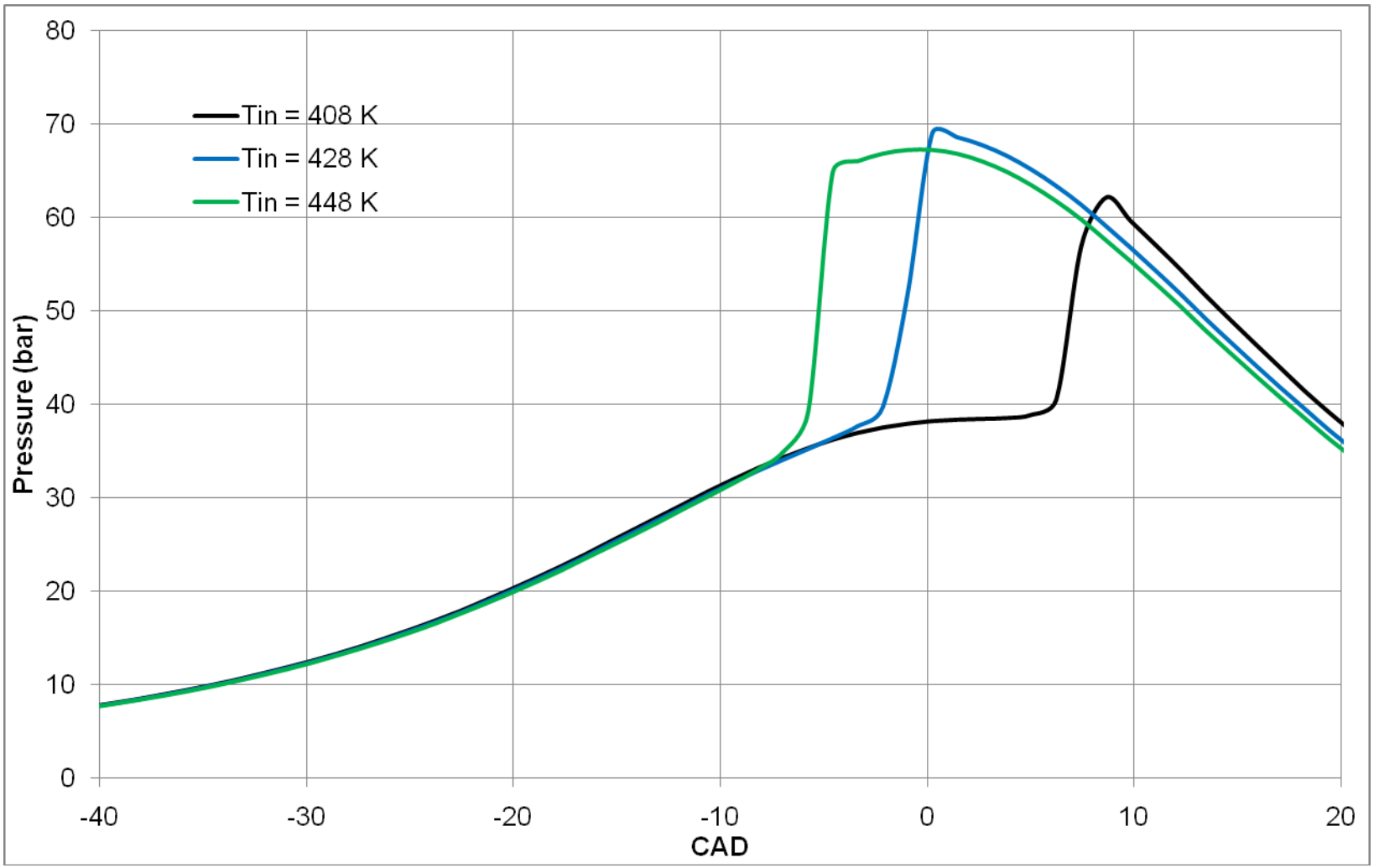

Figure 6.16: Pressure vs. CAD for Three Different Inlet Temperatures Modeling the PRF 84 Engine.

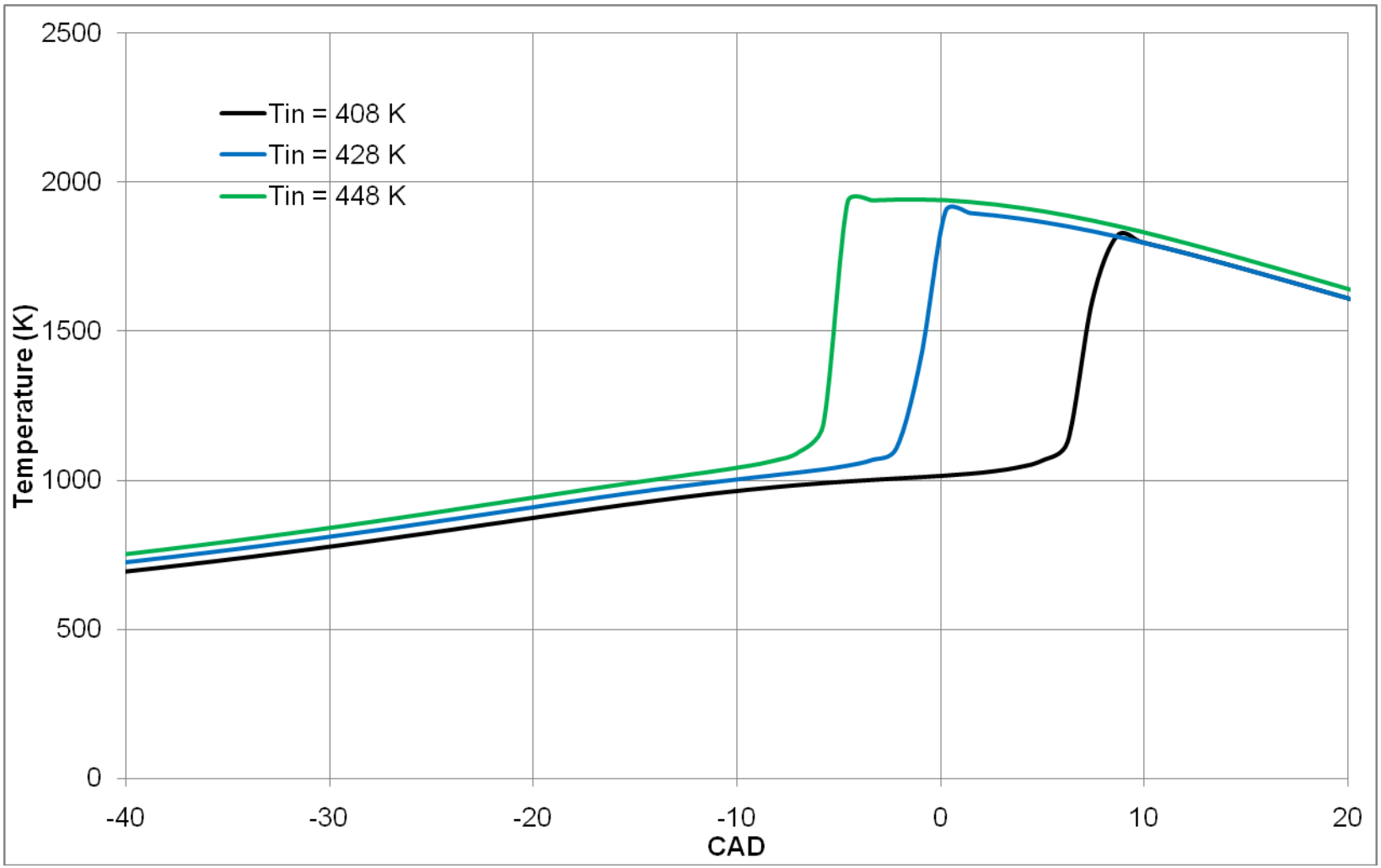

Figure 6.17: Temperature vs. CAD for Three Different Inlet Temperatures Modeling the PRF 84 Engine.

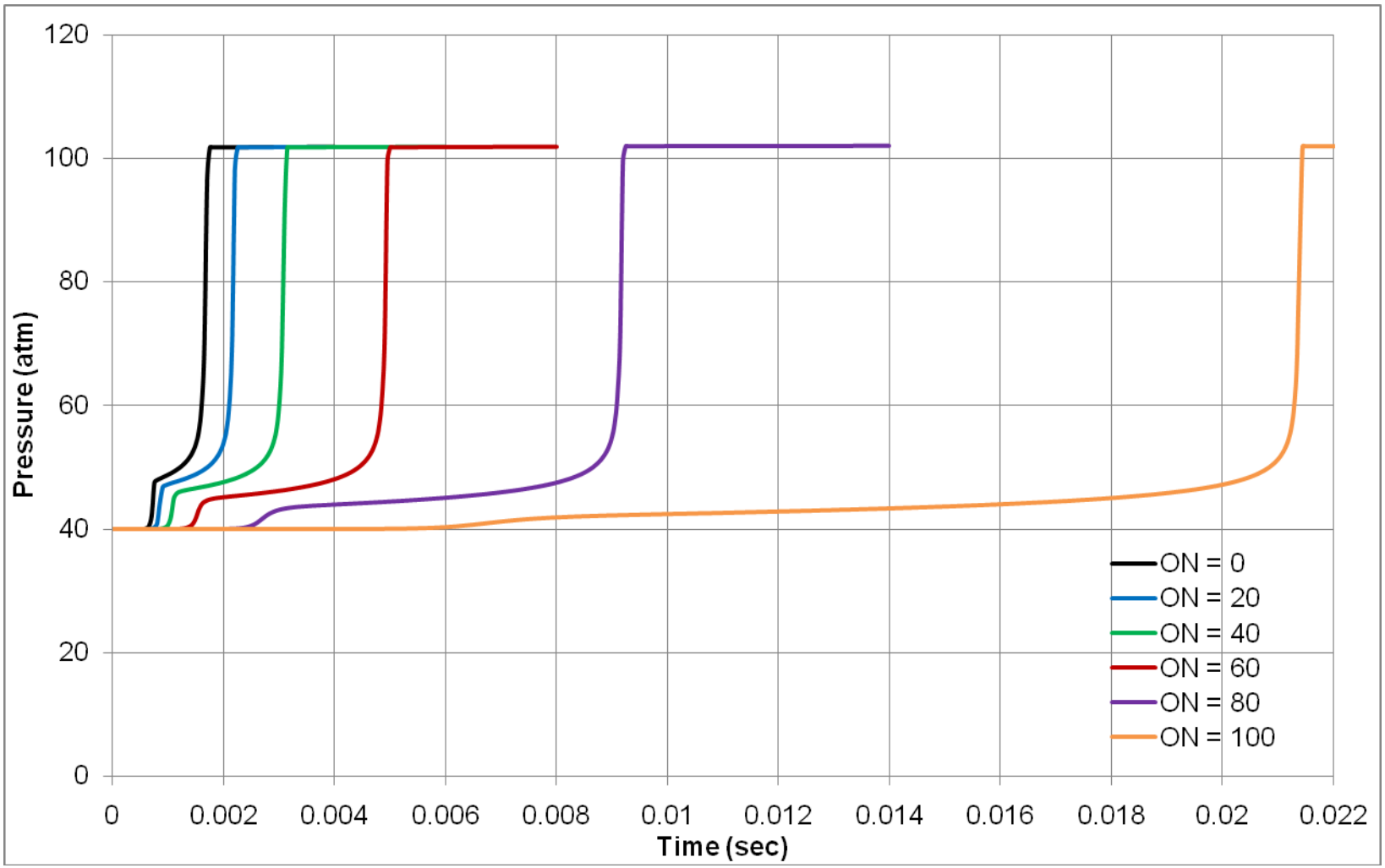

Figure 6.18: Pressure vs. Time, Constant Volume Reactor, Varying ON, P_{in} = 40 atm, T_{in} = 800 K, ϕ = 0.4.

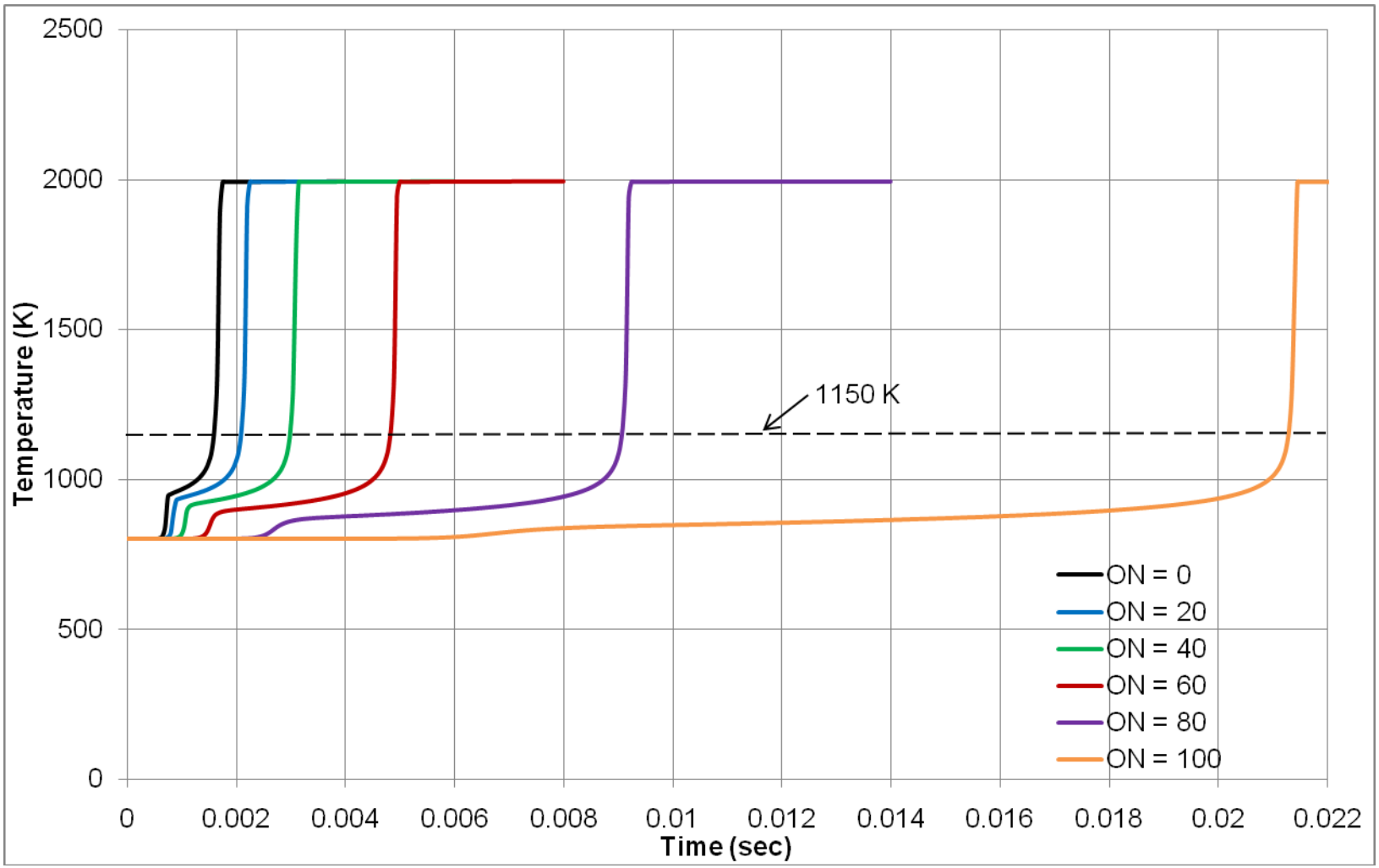

Figure 6.19: Temperature vs. Time, Constant Volume Reactor, Varying ON, P_{in} = 40 atm, T_{in} = 800 K, ϕ = 0.4.

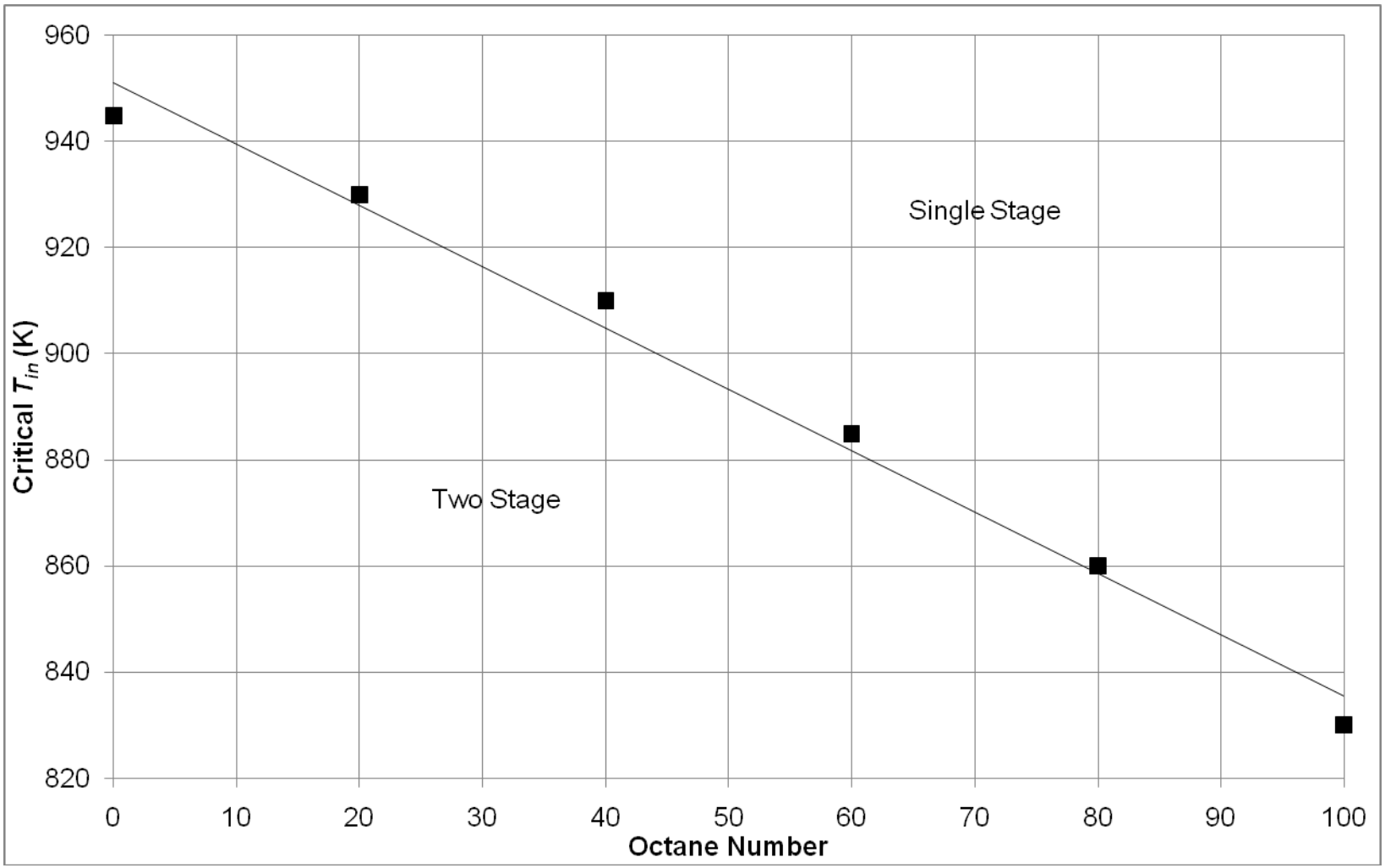

Figure 6.20: Critical T_{in} Separating Single and Two Stage Ignition vs. ON for P_{in} = 40 atm, ϕ = 0.4.

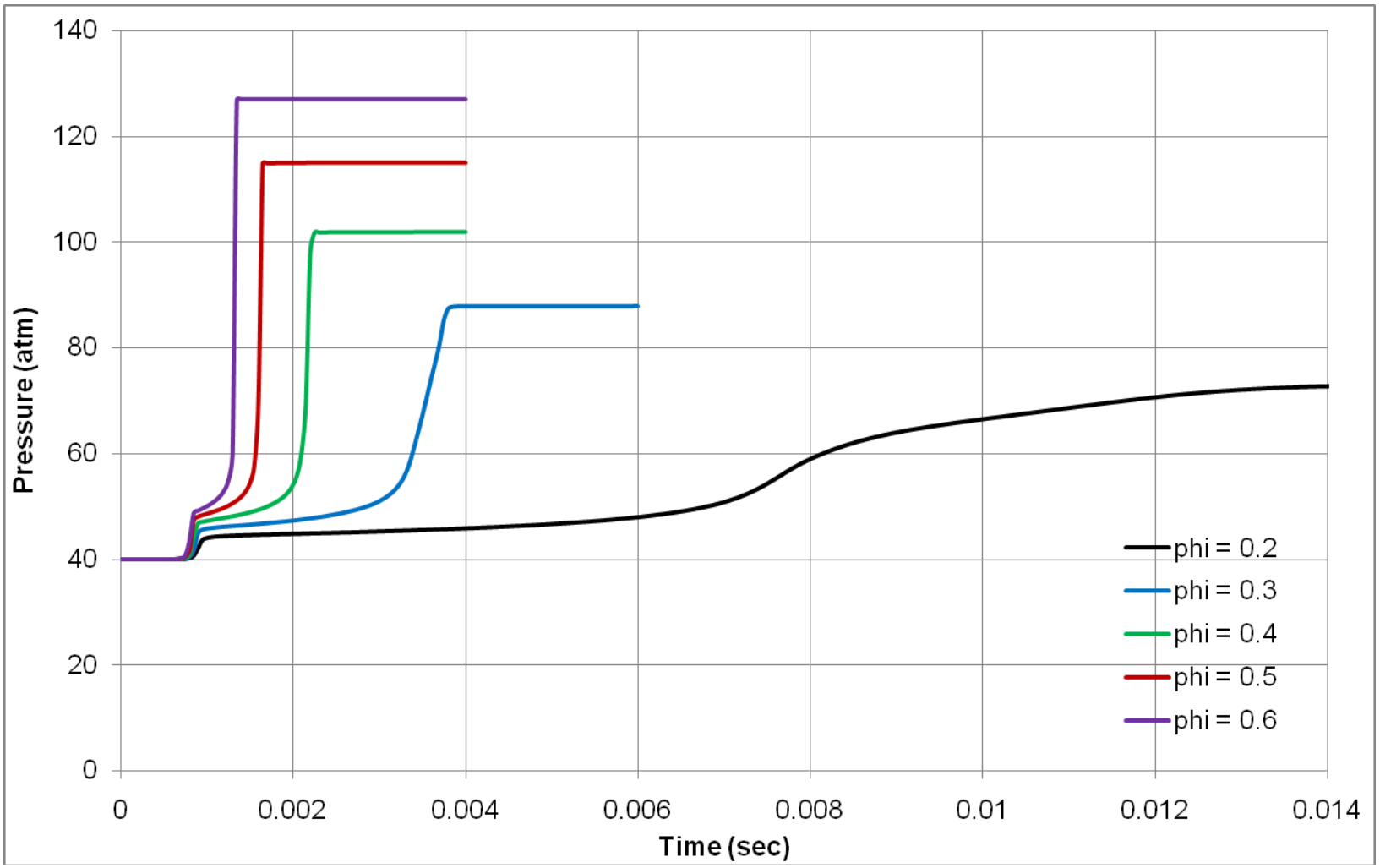

Figure 6.21: Pressure vs. Time, Constant Volume Reactor, PRF 20, Varying ϕ (phi), P_{in} = 40 atm, T_{in} = 800 K.

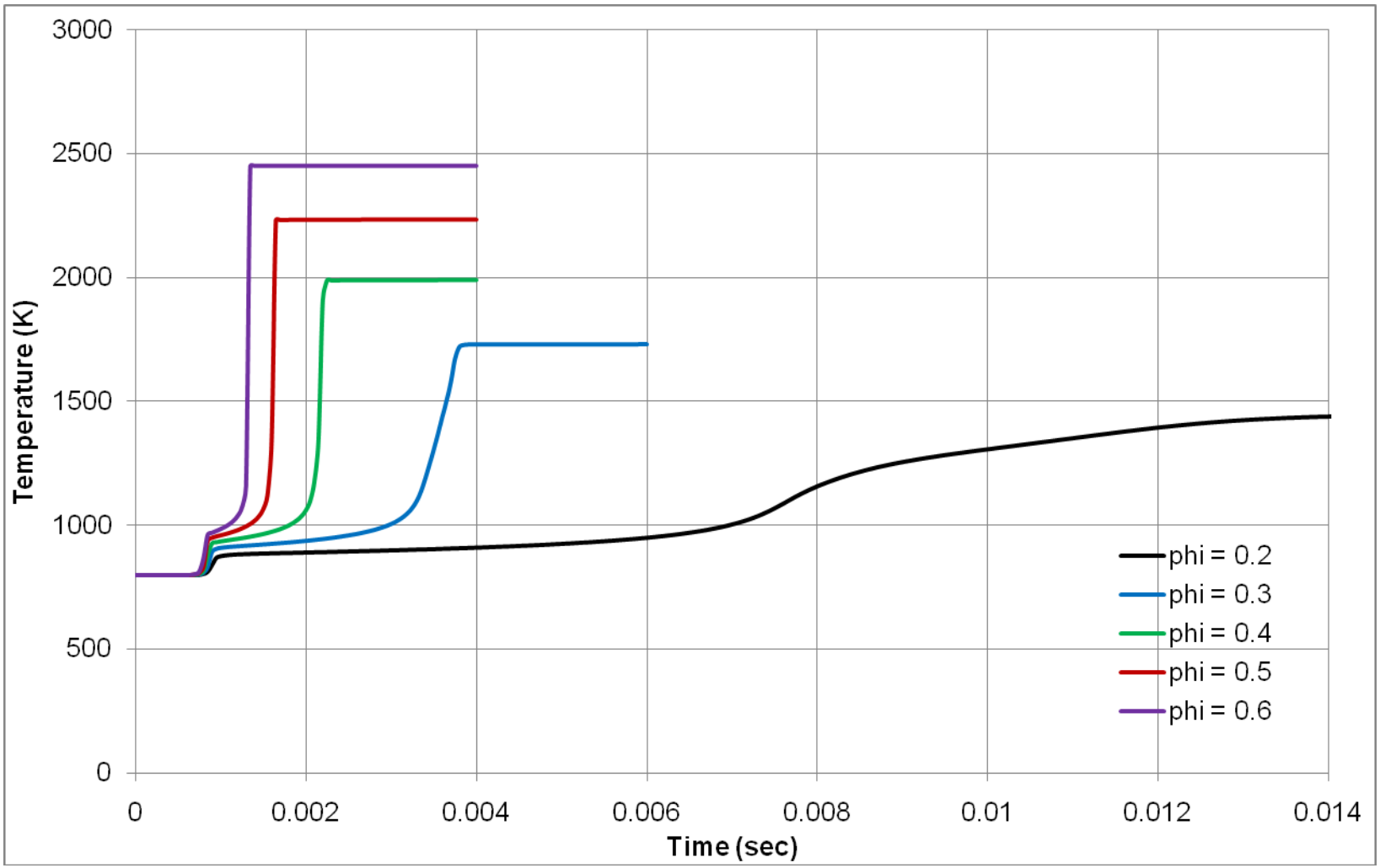

Figure 6.22: Temperature vs. Time, Constant Volume Reactor, PRF 20, Varying ϕ (phi), P_{in} = 40 atm, T_{in} = 800 K.

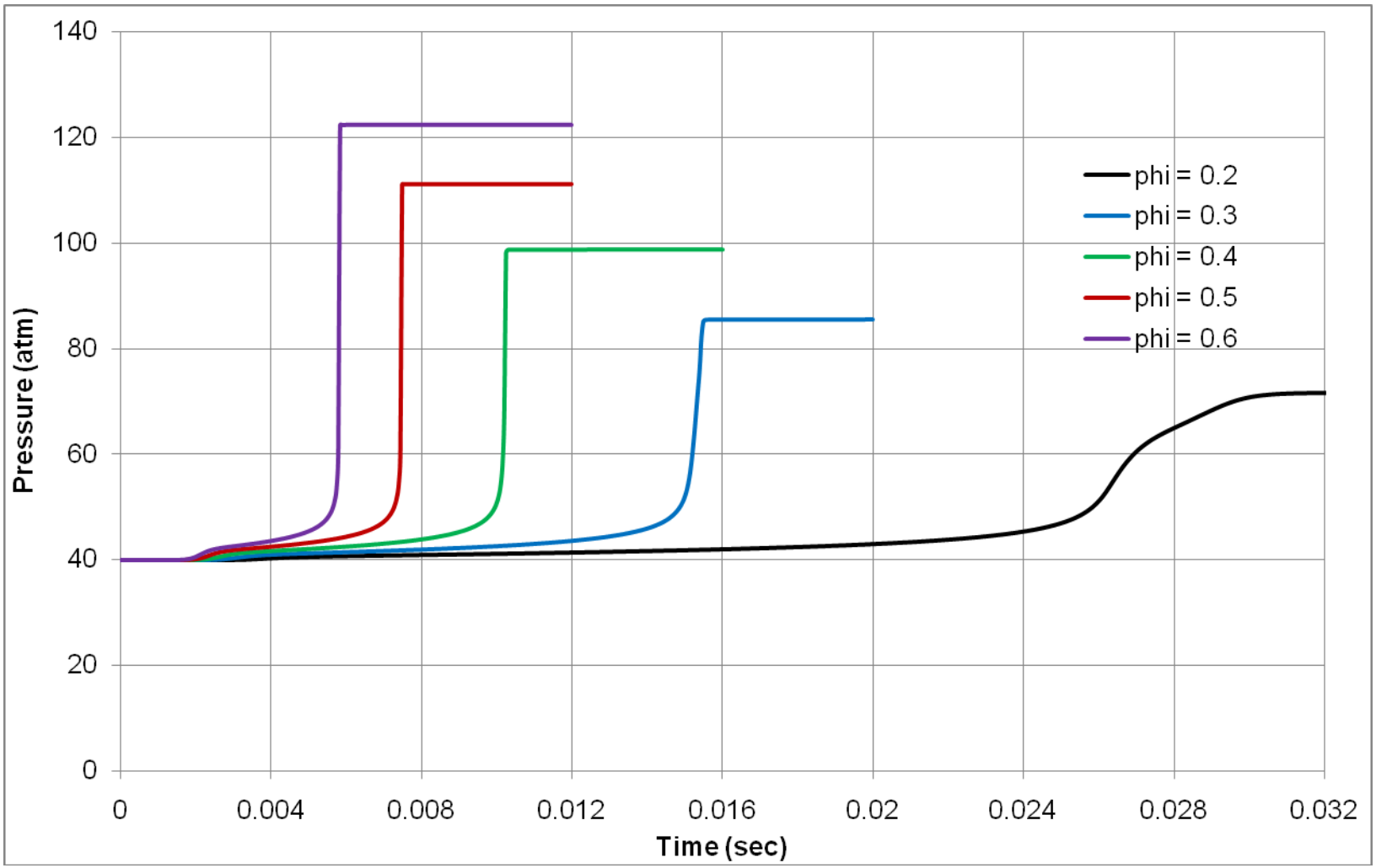

Figure 6.23: Pressure vs. Time, Constant Volume Reactor, PRF 84, Varying ϕ (phi), P_{in} = 40 atm, T_{in} = 840 K.

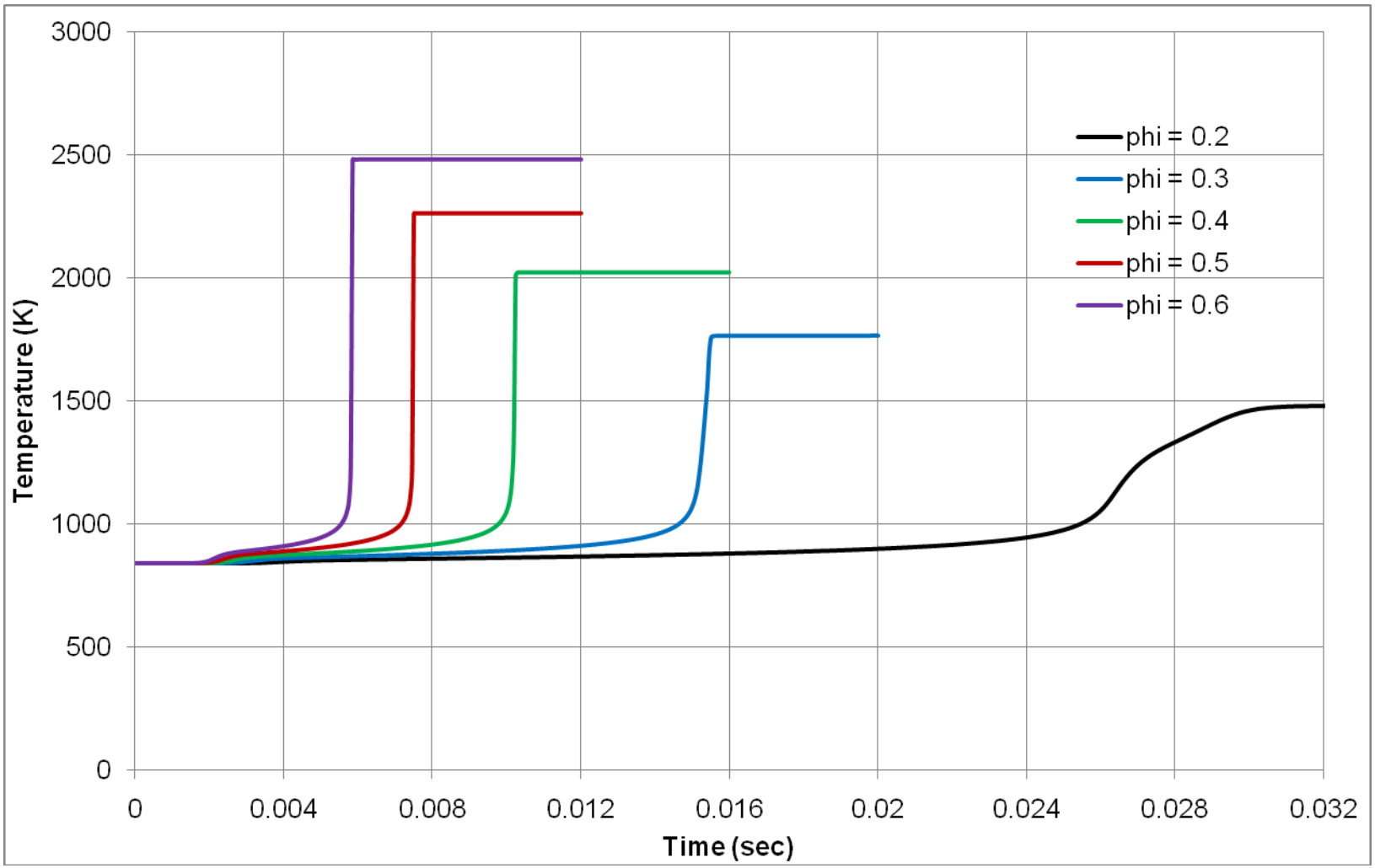

Figure 6.24: Temperature vs. Time, Constant Volume Reactor, PRF 84, Varying ϕ (phi), P_{in} = 40 atm, T_{in} = 840 K.

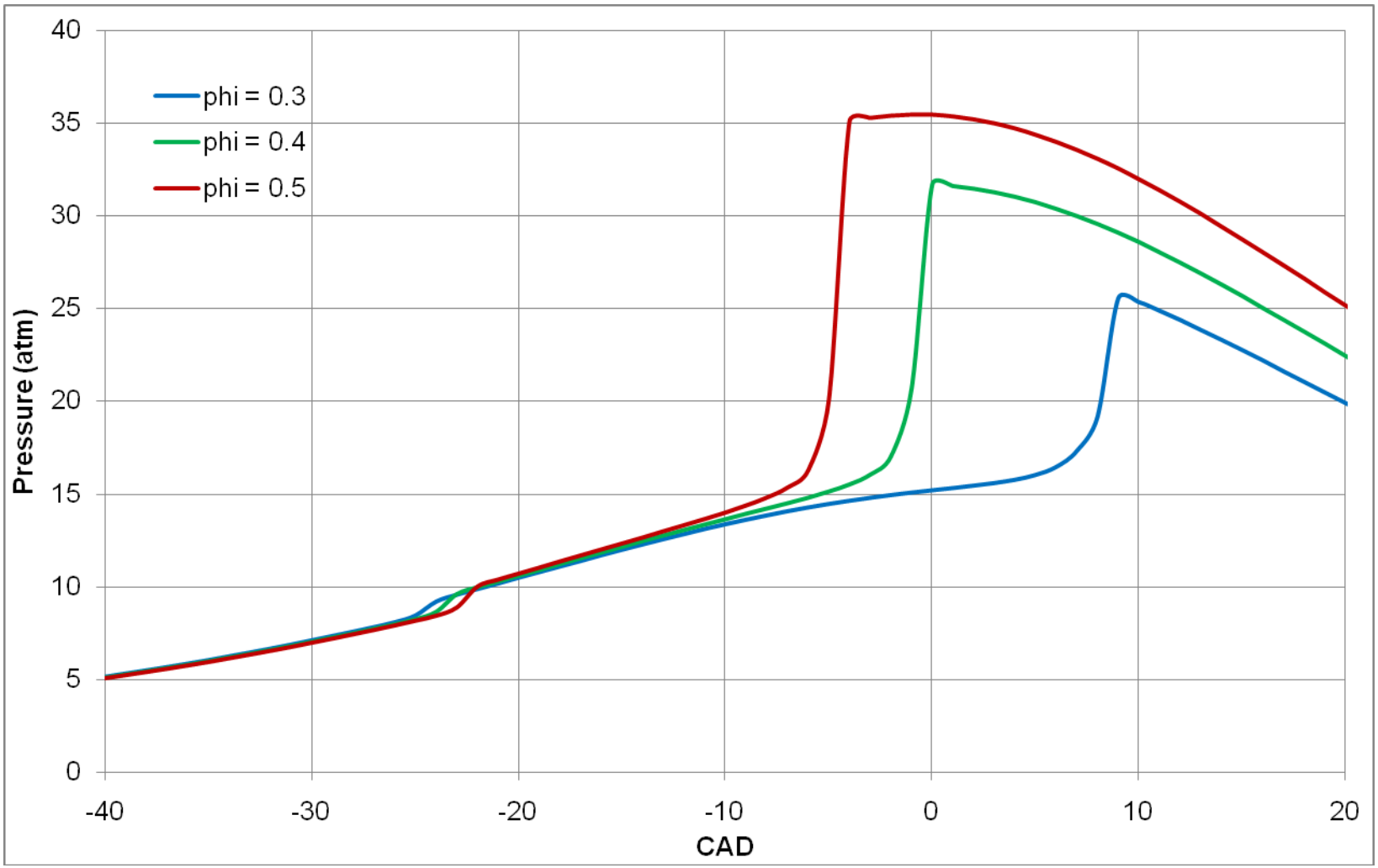

Figure 6.25: Pressure vs. CAD for Three Different Equivalence Ratios (phi) Modeling the PRF 20 Engine.

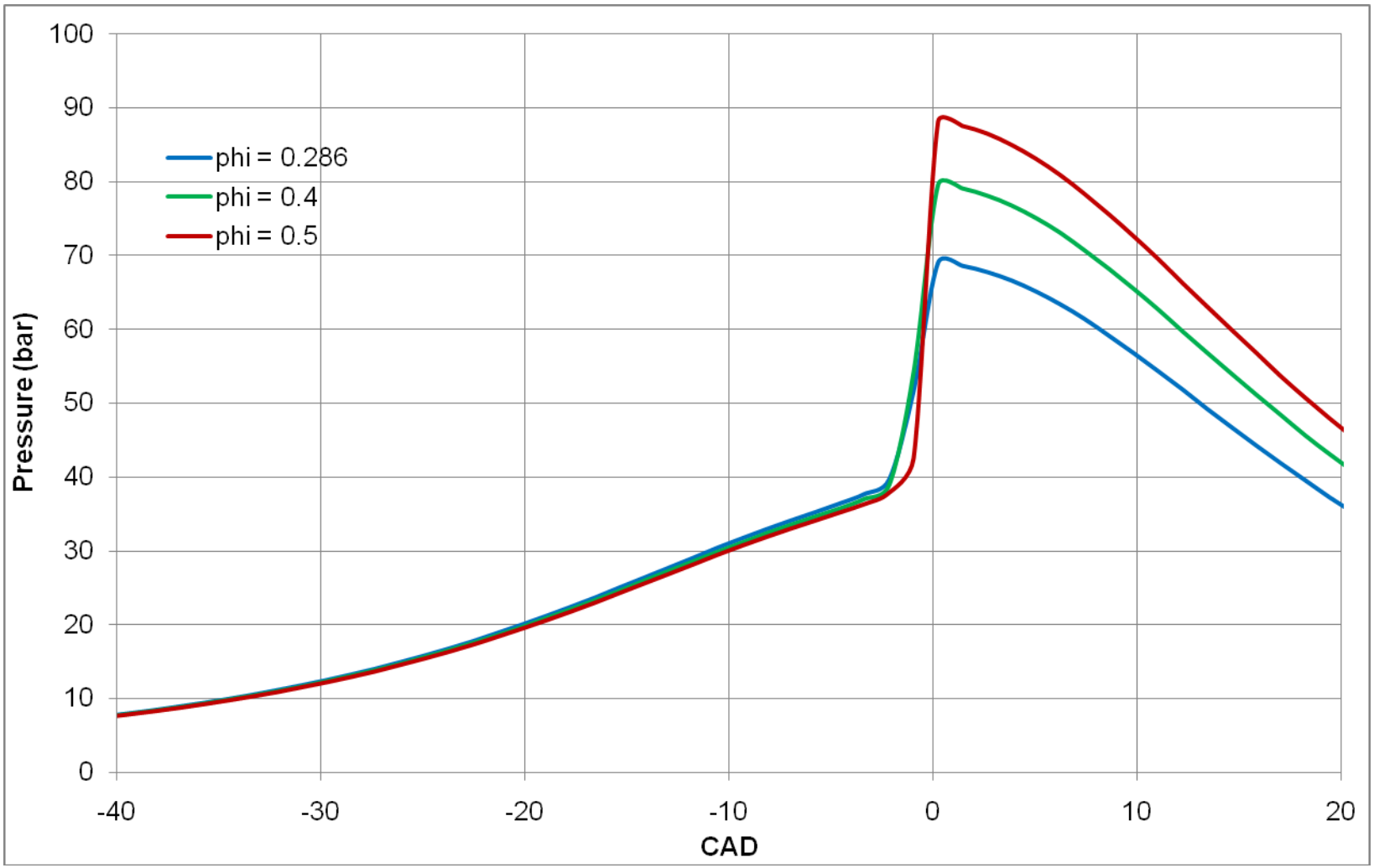

Figure 6.26: Pressure vs. CAD for Three Different Equivalence Ratios (phi) Modeling the PRF 84 Engine.

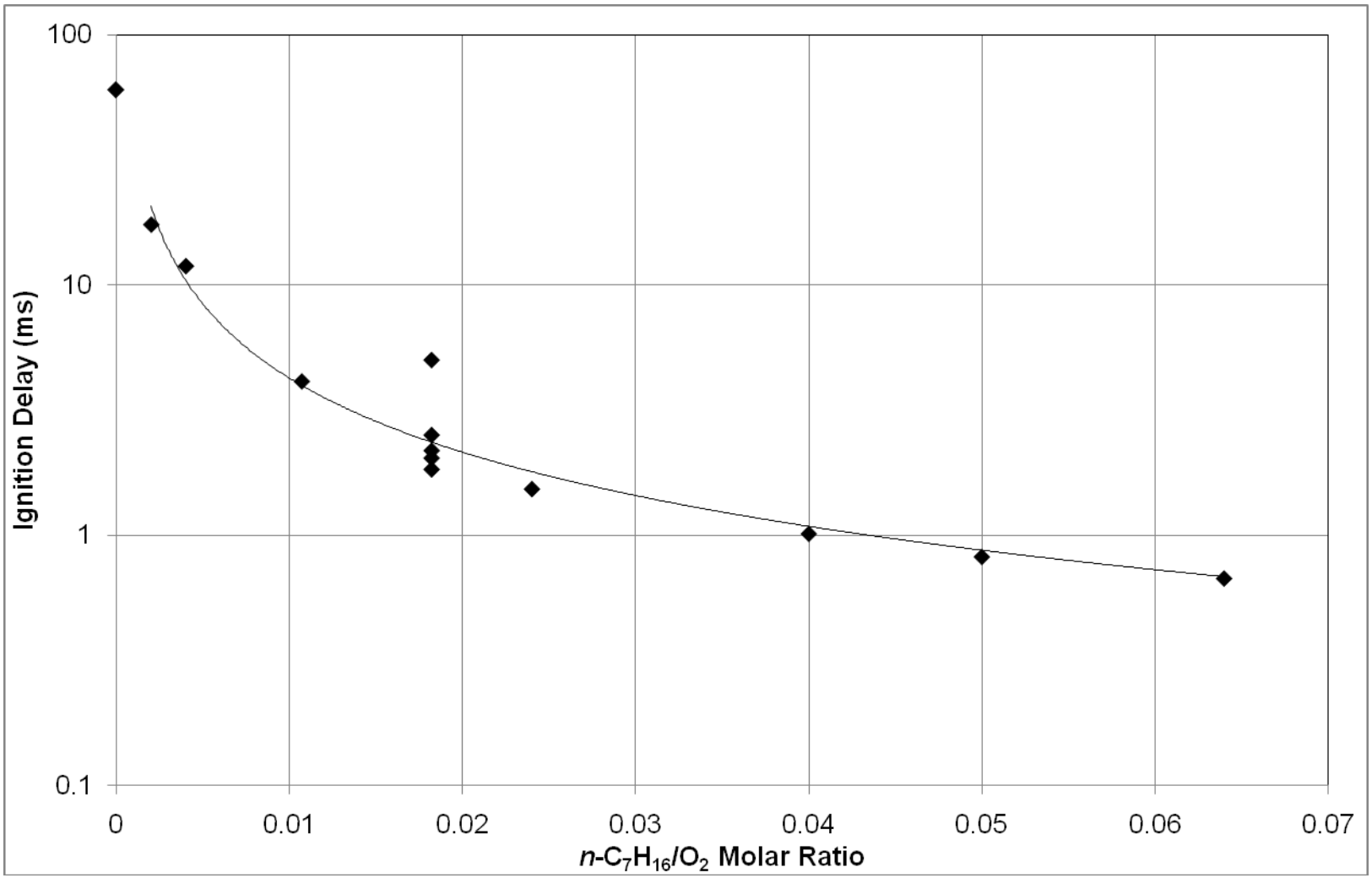

Figure 6.27: Second Stage Ignition Delay vs. n-C_7H_{16}/O_2, Constant Volume Reactor, P_{in} = 40 atm, T_{in} = 820 K.

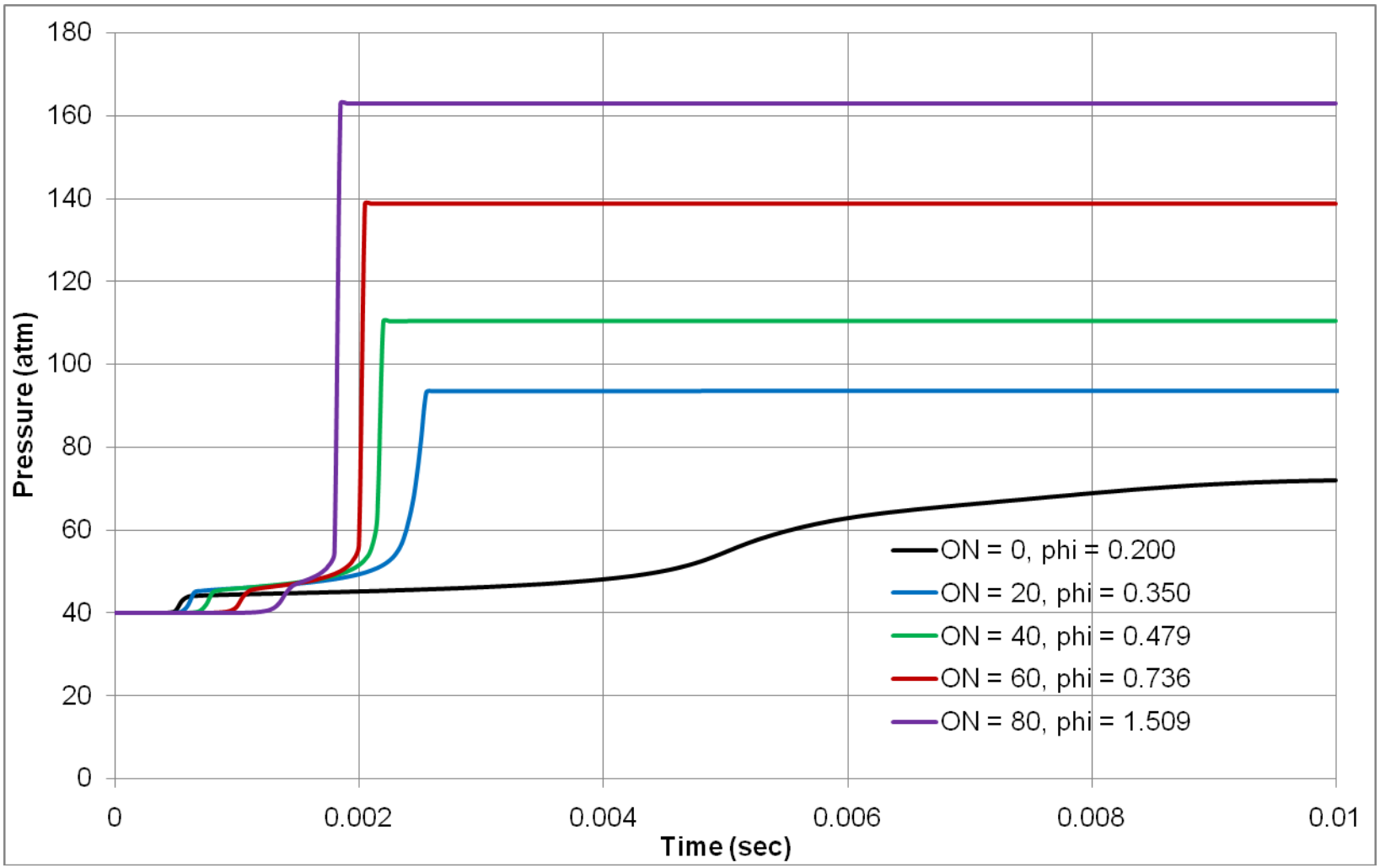

Figure 6.28: Pressure vs. Time, Constant Volume Reactor, n-$C_7H_{16}/O_2 = 0.0182$, $P_{in} = 40$ atm, $T_{in} = 820$ K.

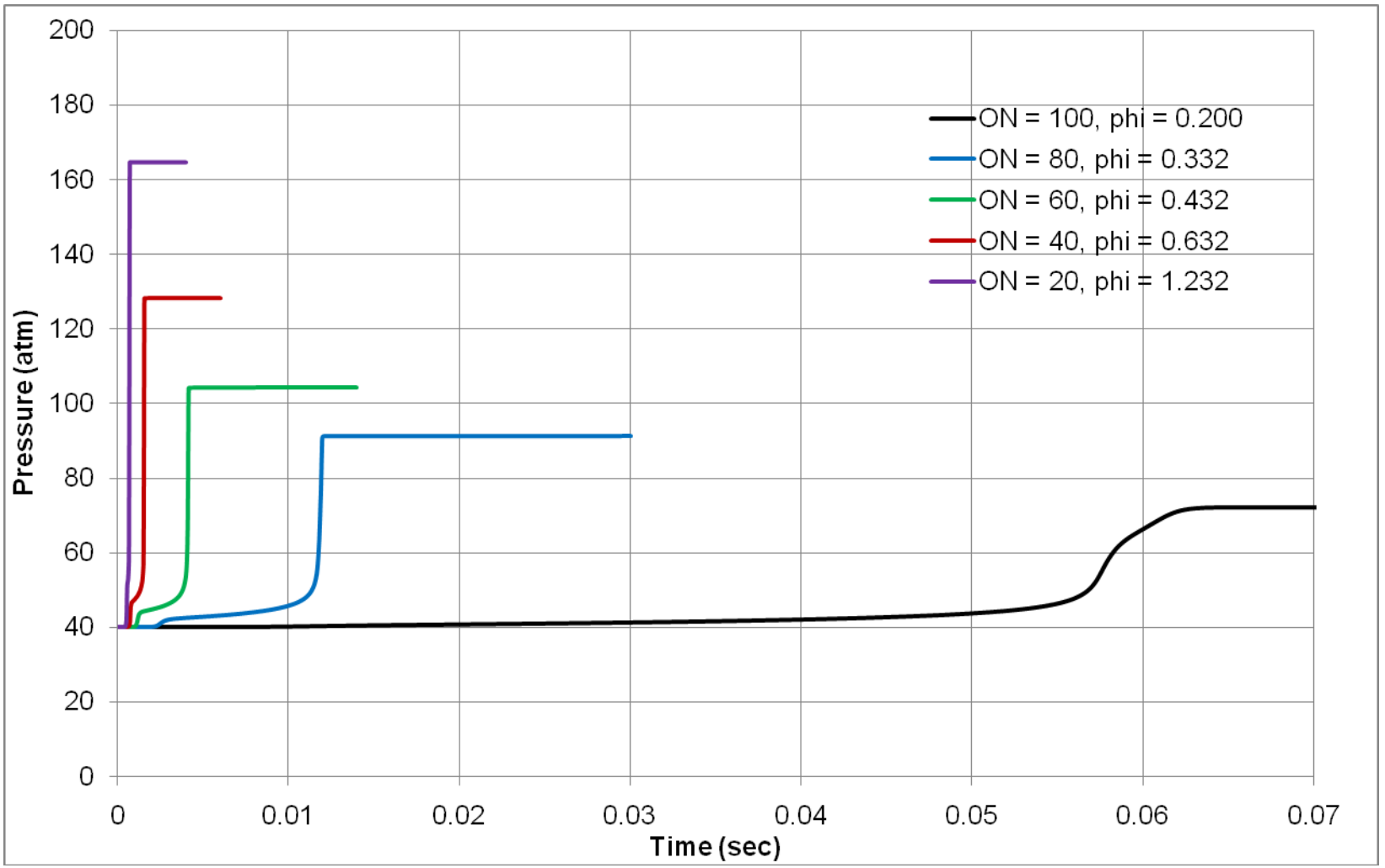

Figure 6.29: Pressure vs. Time, Constant Volume Reactor, i-$C_8H_{18}/O_2 = 0.0160$, $P_{in} = 40$ atm, $T_{in} = 820$ K.

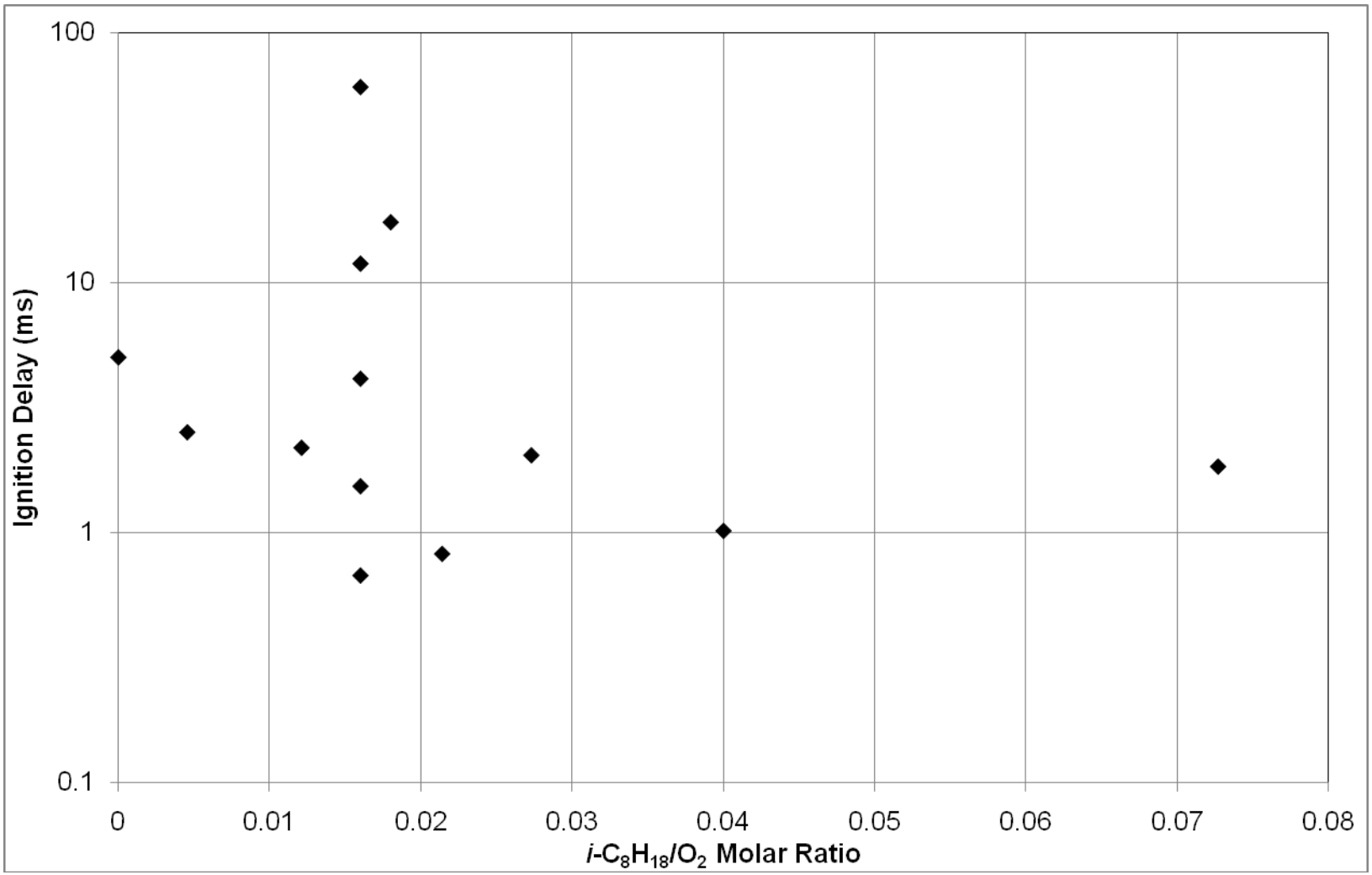

Figure 6.30: Second Stage Ignition Delay vs. i-C_8H_{18}/O_2, Constant Volume Reactor, P_{in} = 40 atm, T_{in} = 820 K.

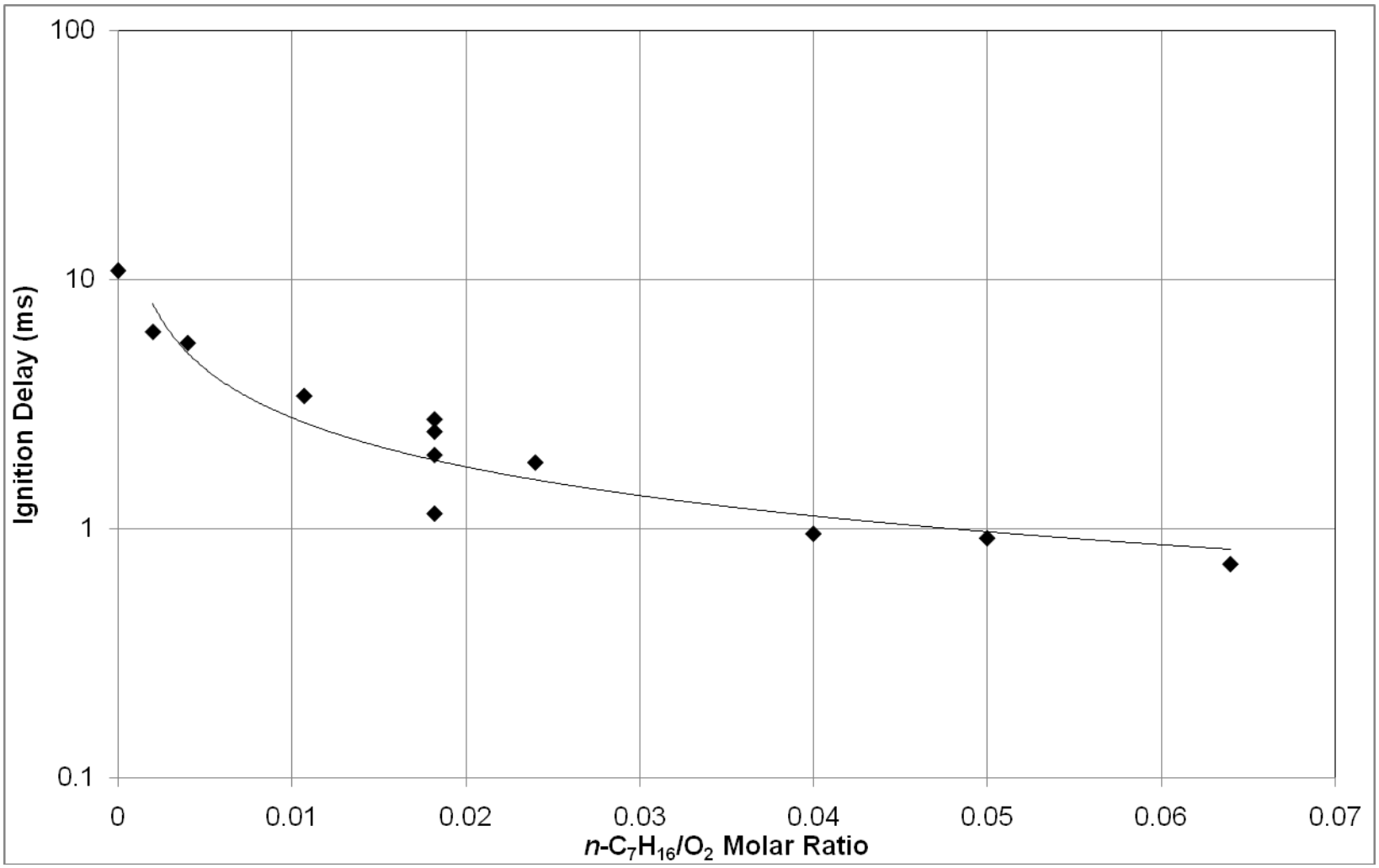

Figure 6.31: Single Stage Ignition Delay vs. n-C_7H_{16}/O_2, Constant Volume Reactor, P_{in} = 40 atm, T_{in} = 940 K.

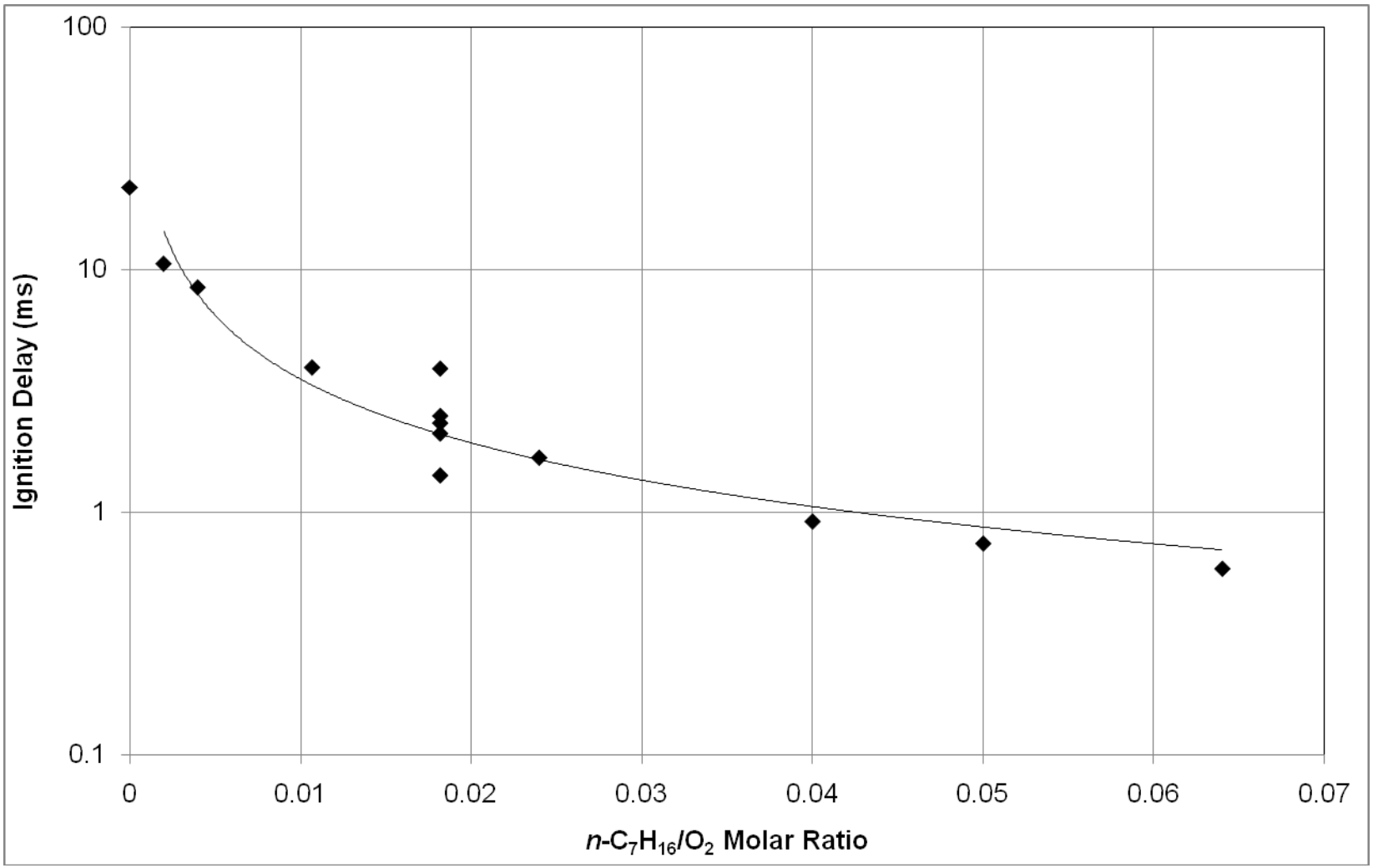

Figure 6.32: Single and Two Stage Ignition Delay vs. n-C_7H_{16}/O_2, Constant Volume Reactor, P_{in} = 40 atm, T_{in} = 900 K.

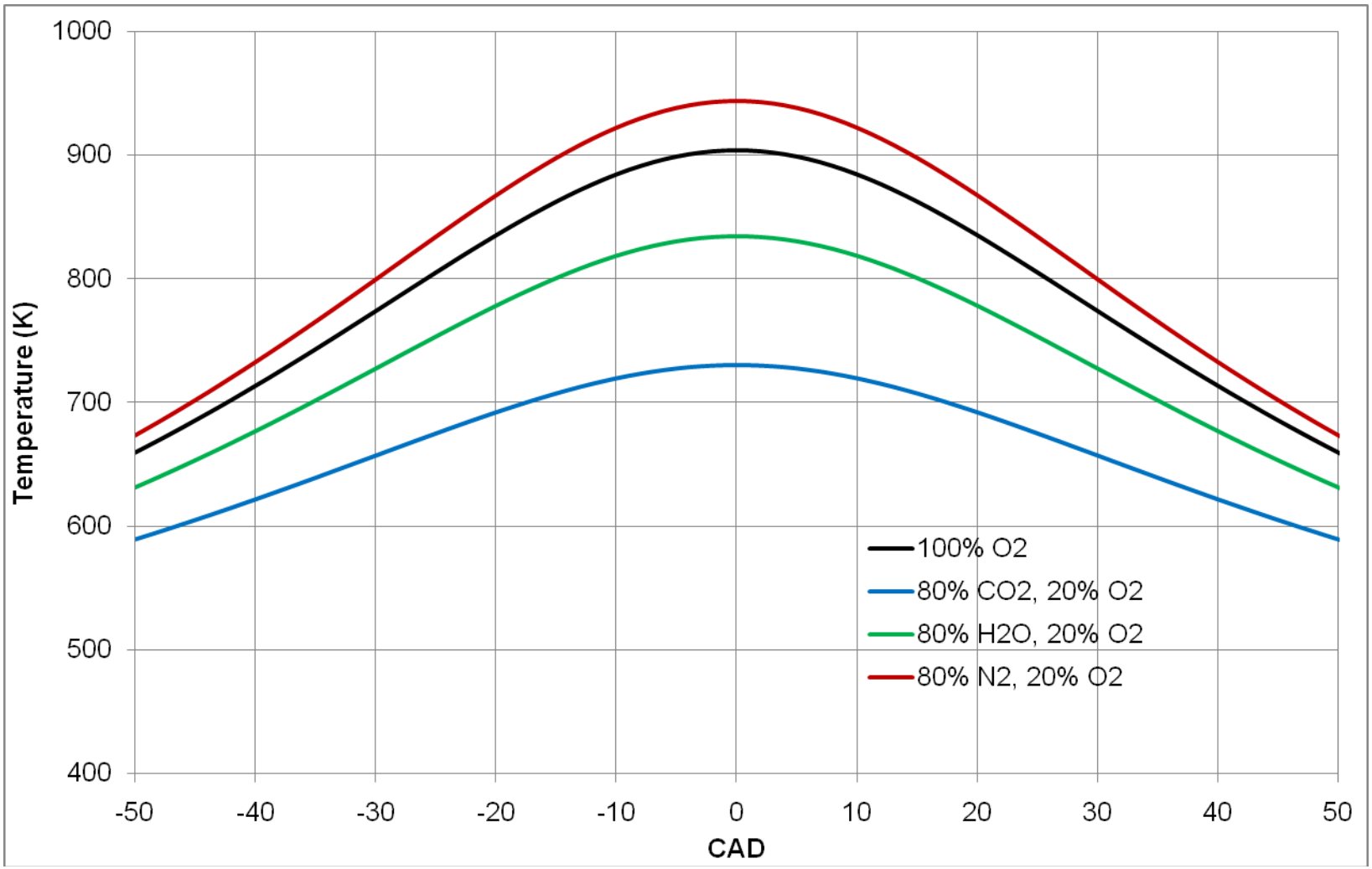

Figure 6.33: Compressed Gas Temperature vs. CAD in the Modeled PRF 20 Engine, P_{in} = 1 atm, T_{in} = 463 K.

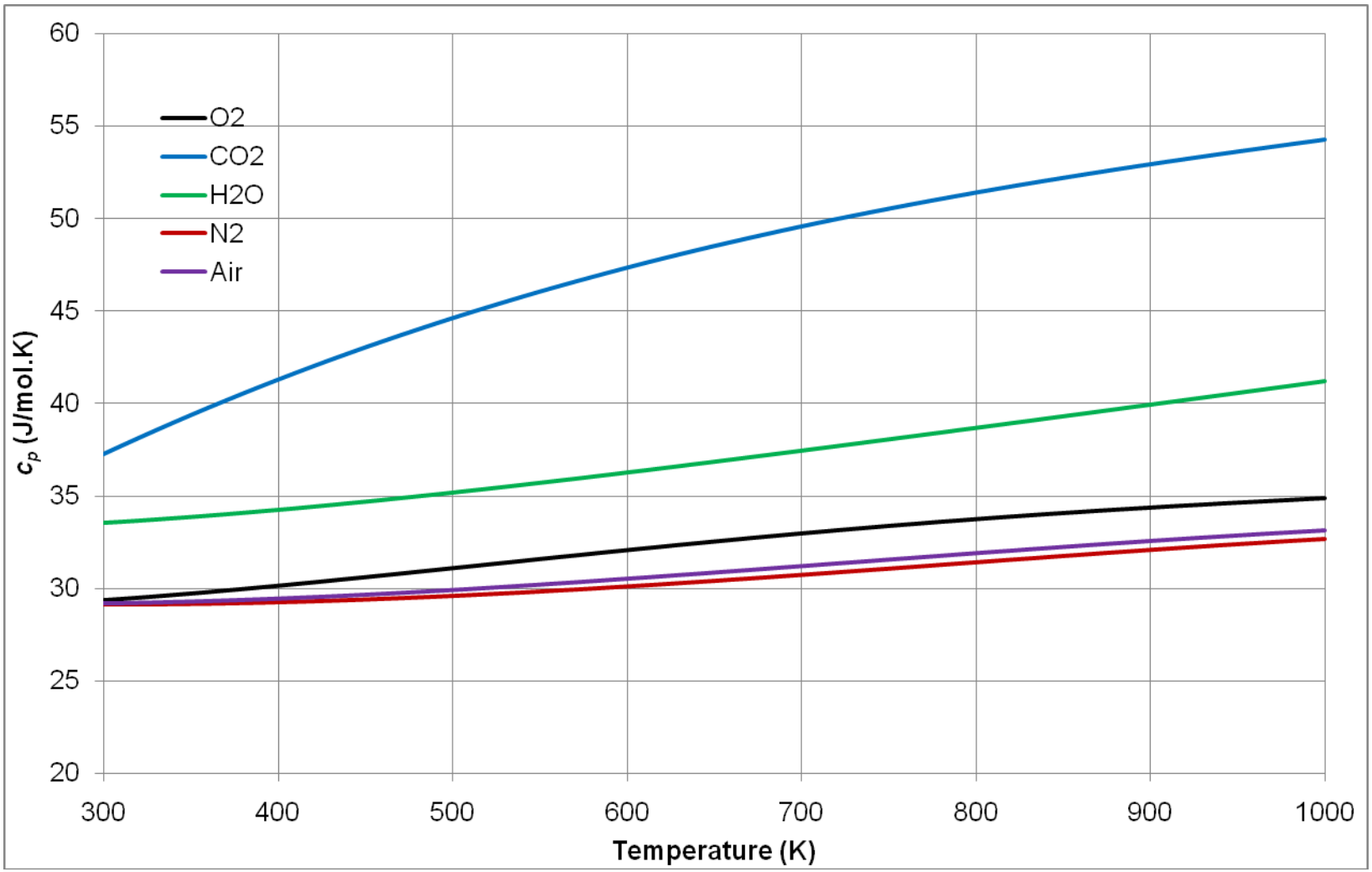

Figure 6.34: c_p vs. Temperature for Multiple Gases.

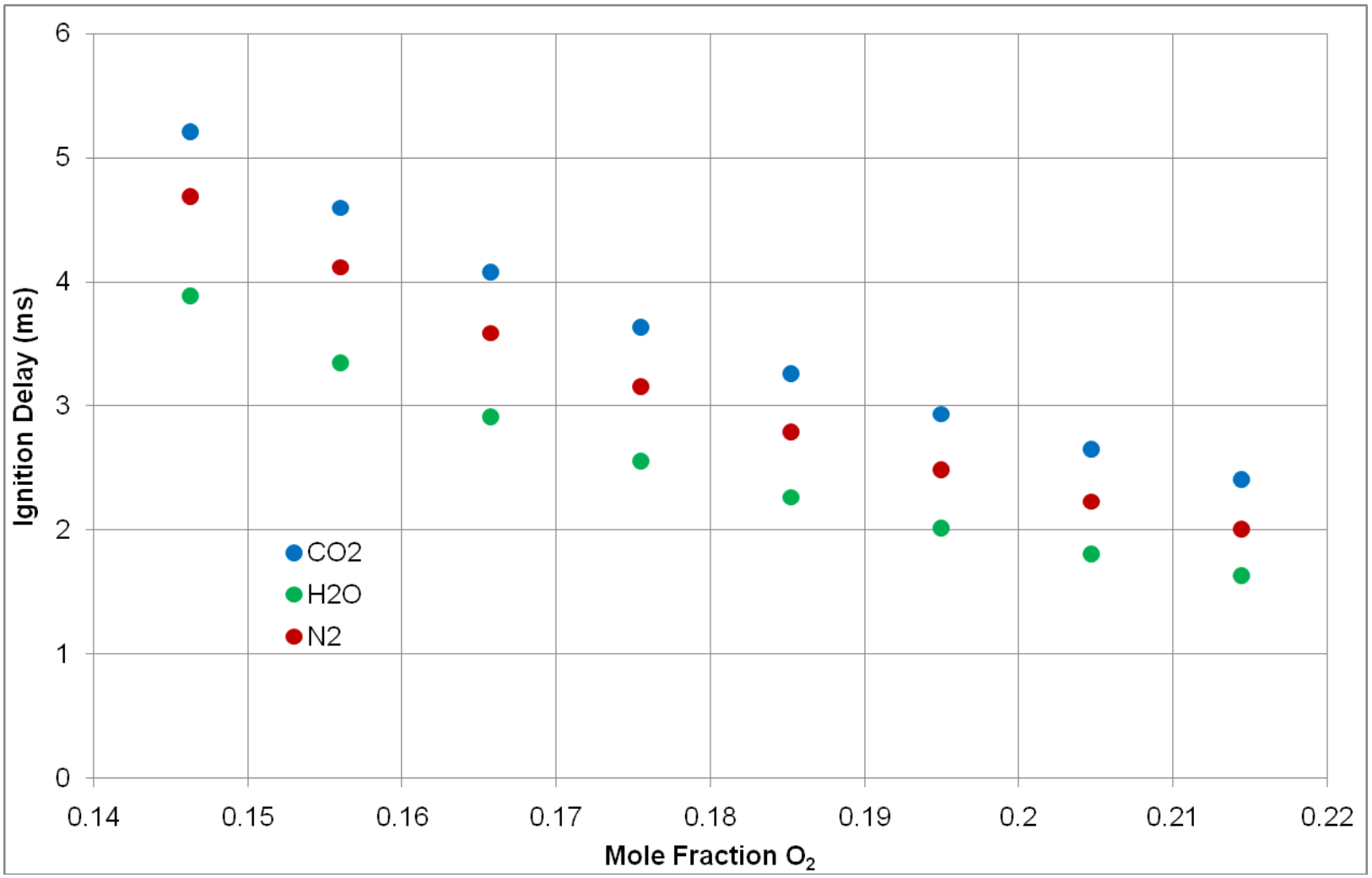

Figure 6.35: τ_{ig} vs. y_{O2}, Constant Volume Reactor, PRF 20, P_{in} = 40 atm, T_{in} = 900 K, Fuel/O_2 Equivalence Ratio = 0.4.

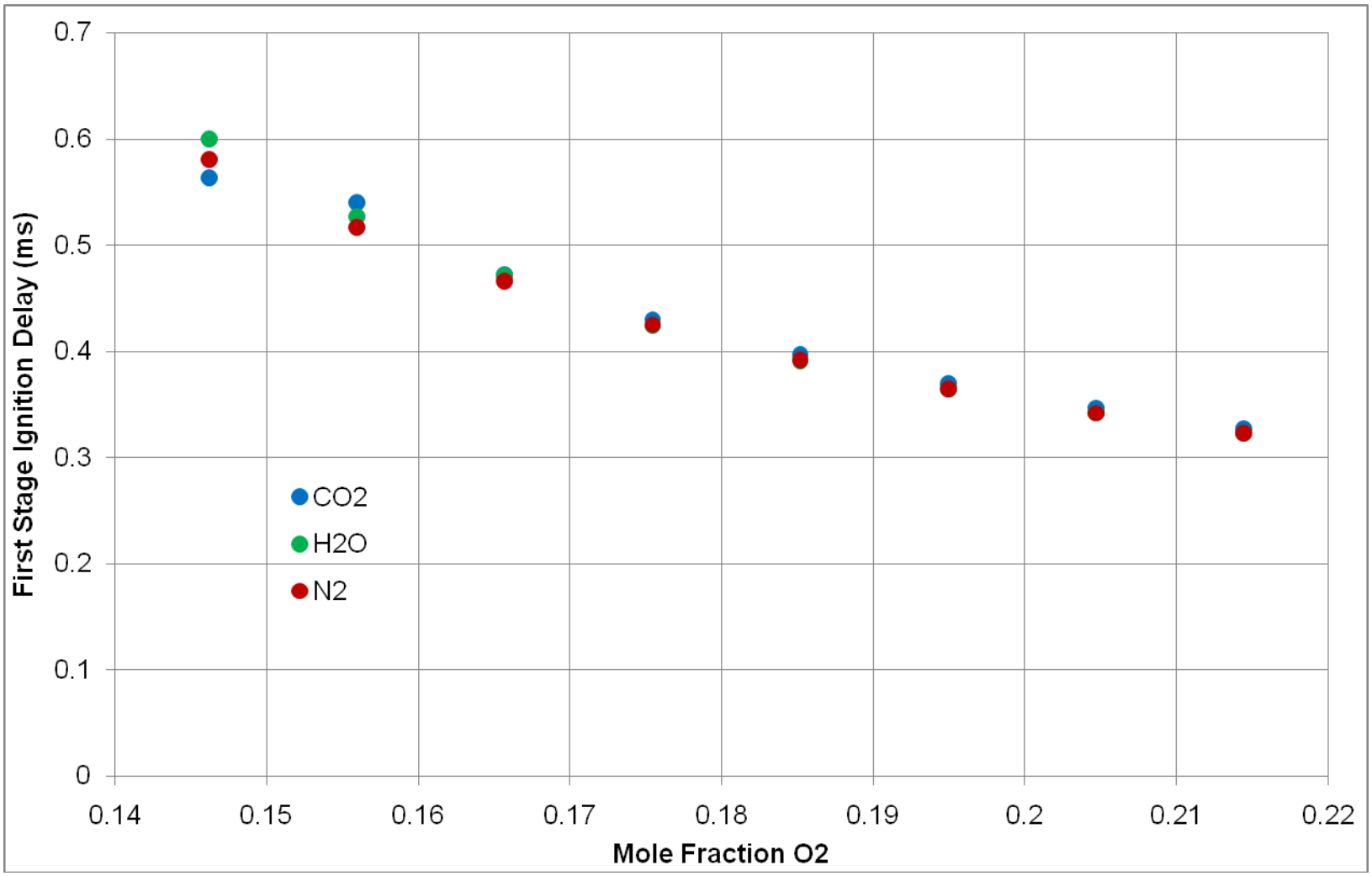

Figure 6.36: First Stage Ignition Delay vs. y_{O2}, PRF 20, P_{in} = 40 atm, T_{in} = 900 K, Fuel/O_2 Equivalence Ratio = 0.4.

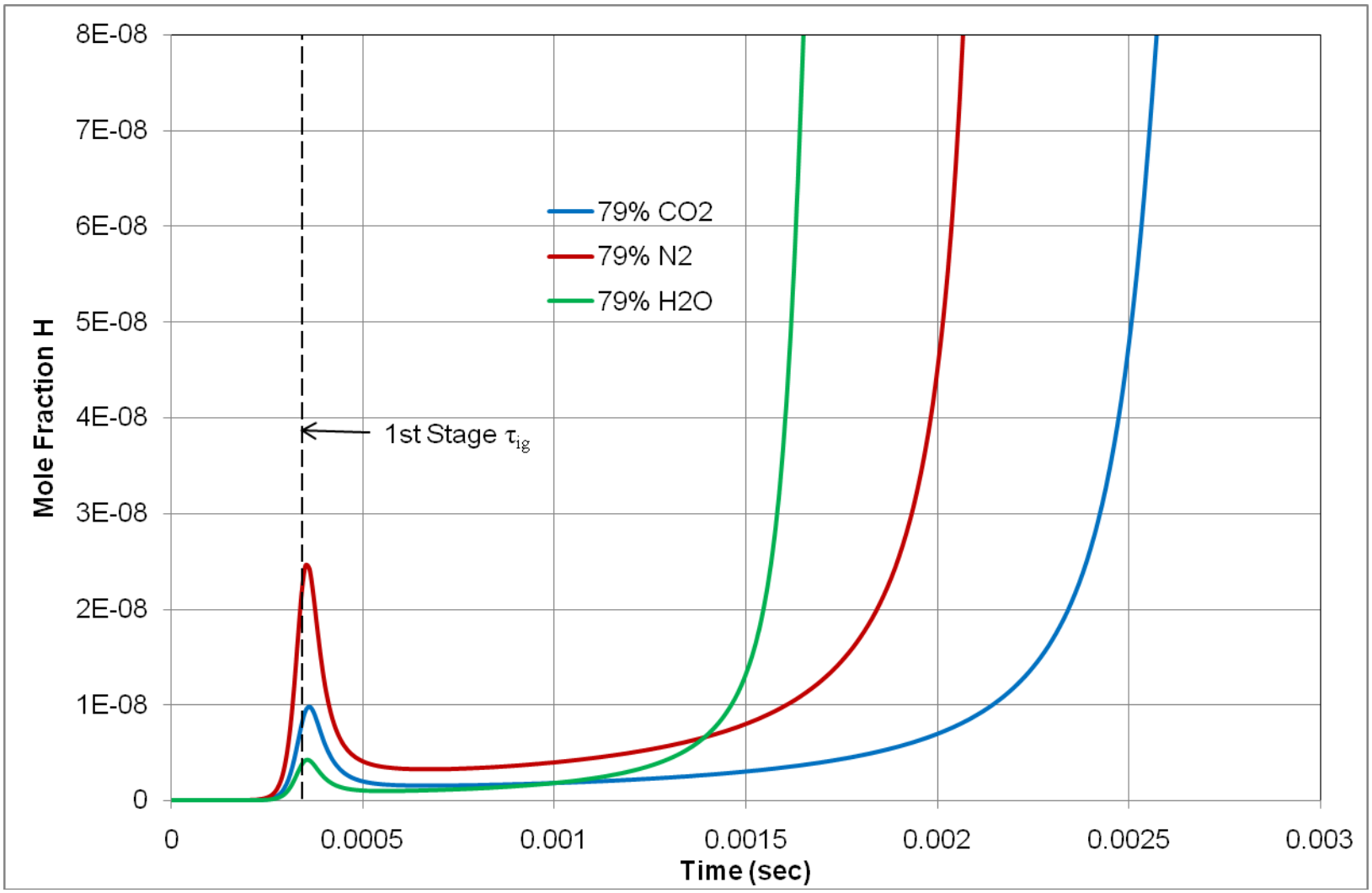

Figure 6.37: Mole Fraction H vs. Time, PRF 20, $y_{O_2} = 0.205$, $P_{in} = 40$ atm, $T_{in} = 900$ K, Fuel/O_2 Equivalence Ratio = 0.4.

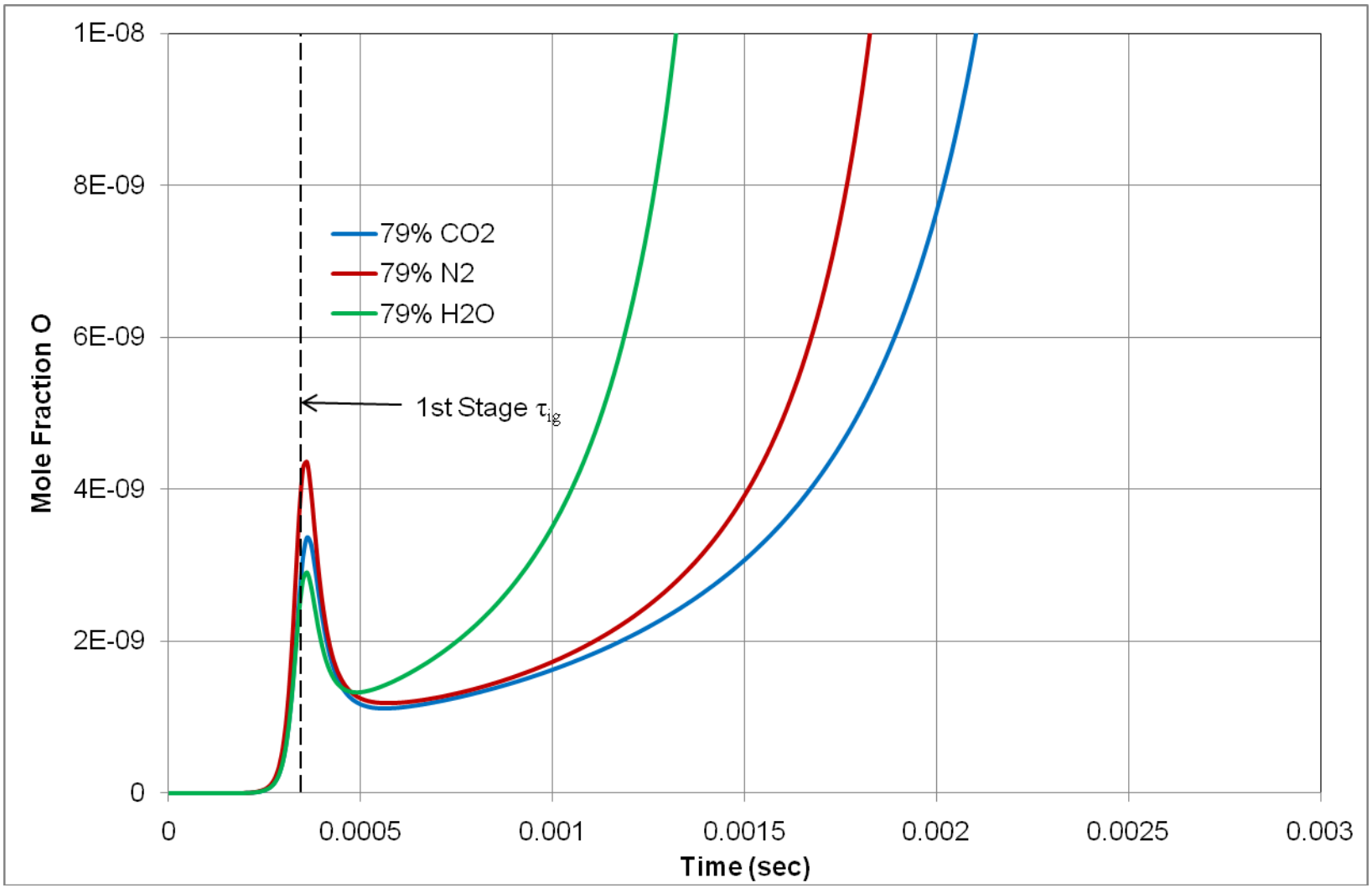

Figure 6.38: Mole Fraction O vs. Time, PRF 20, y_{O2} = 0.205, P_{in} = 40 atm, T_{in} = 900 K, Fuel/O_2 Equivalence Ratio = 0.4.

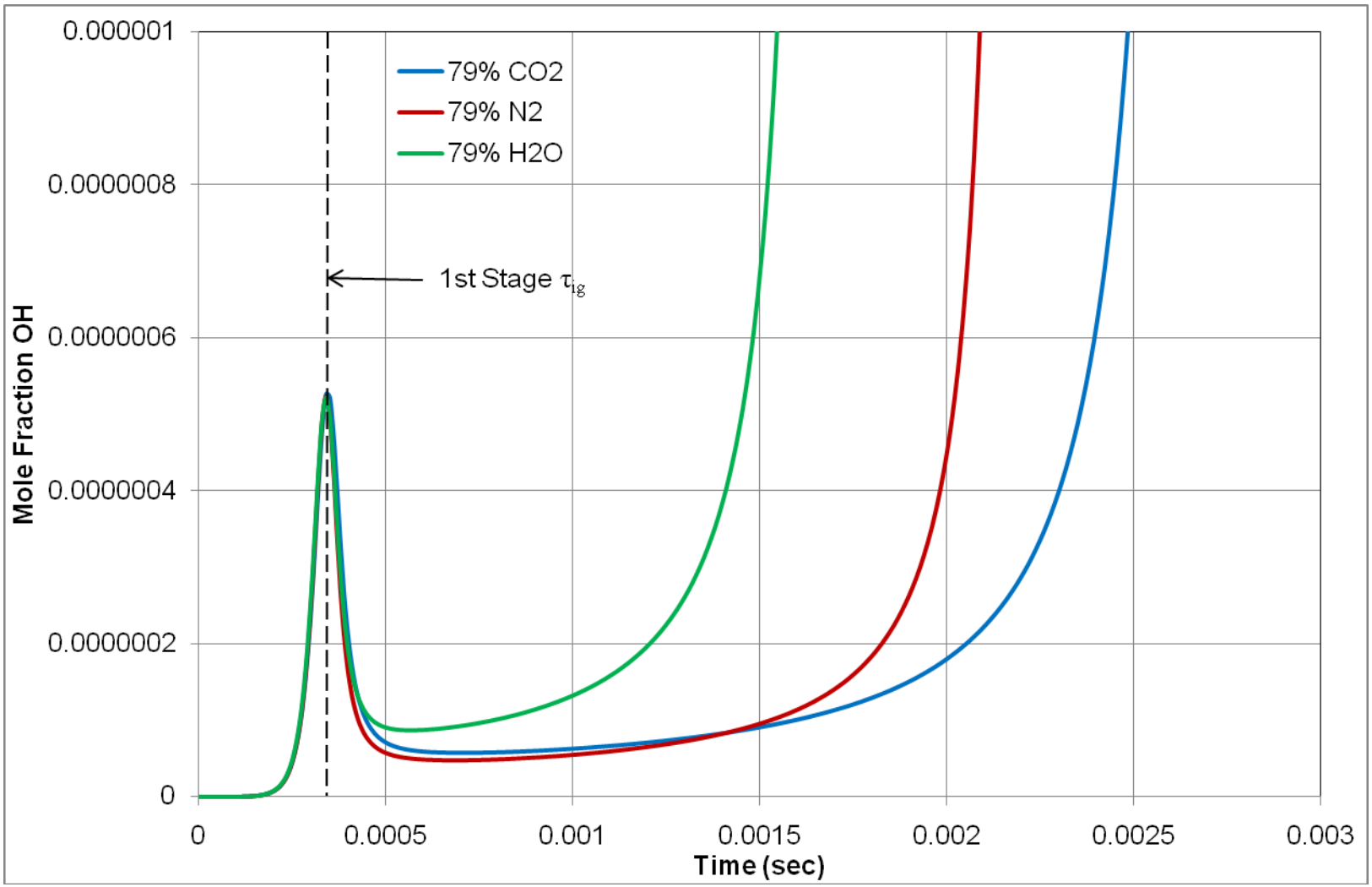

Figure 6.39: Mole Fraction OH vs. Time, PRF 20, $y_{O_2} = 0.205$, $P_{in} = 40$ atm, $T_{in} = 900$ K, Fuel/O_2 Equivalence Ratio = 0.4.

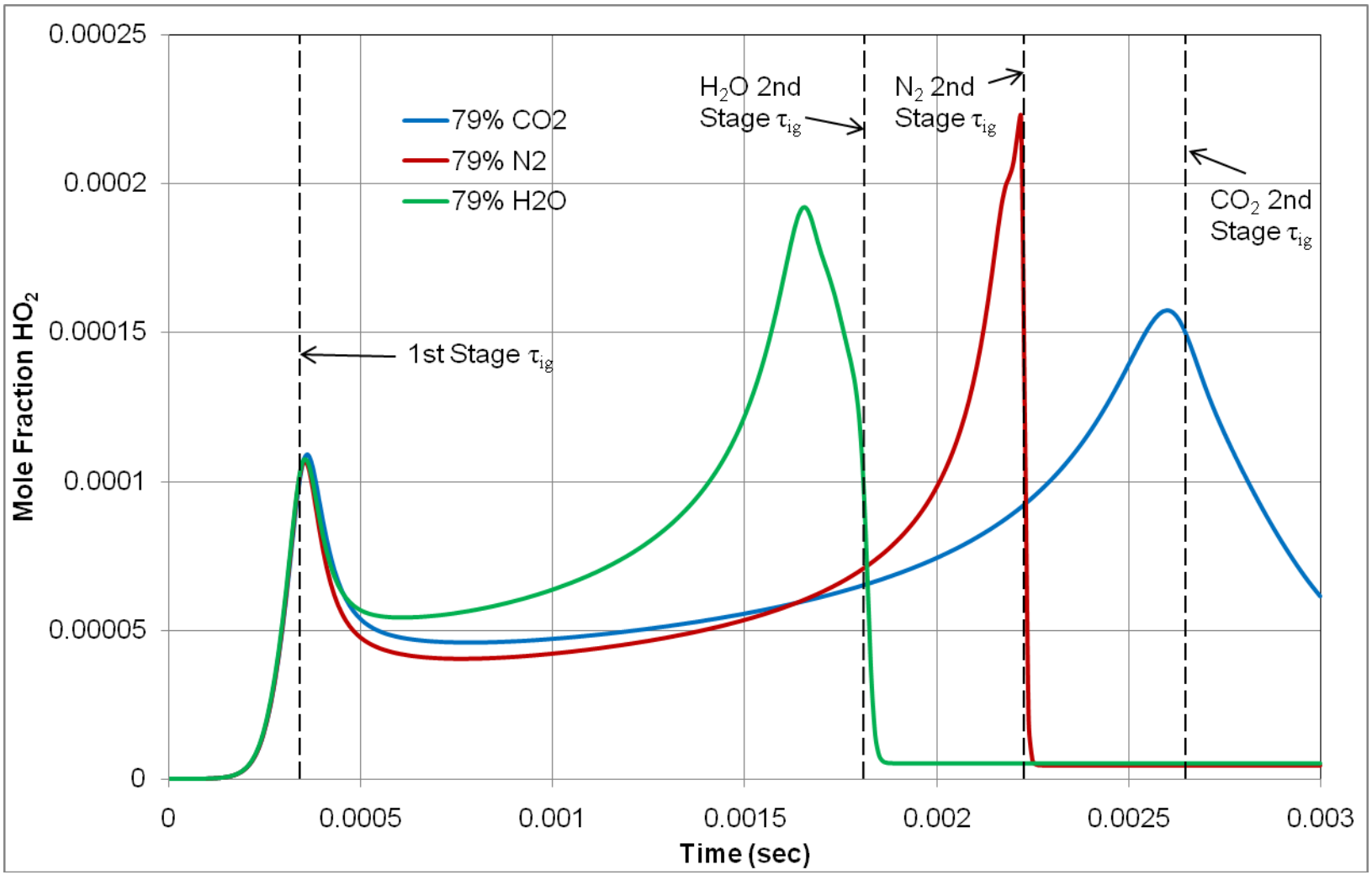

Figure 6.40: Mole Fraction HO_2 vs. Time, PRF 20, $y_{O2} = 0.205$, $P_{in} = 40$ atm, $T_{in} = 900$ K, Fuel/O_2 Equivalence Ratio = 0.4.

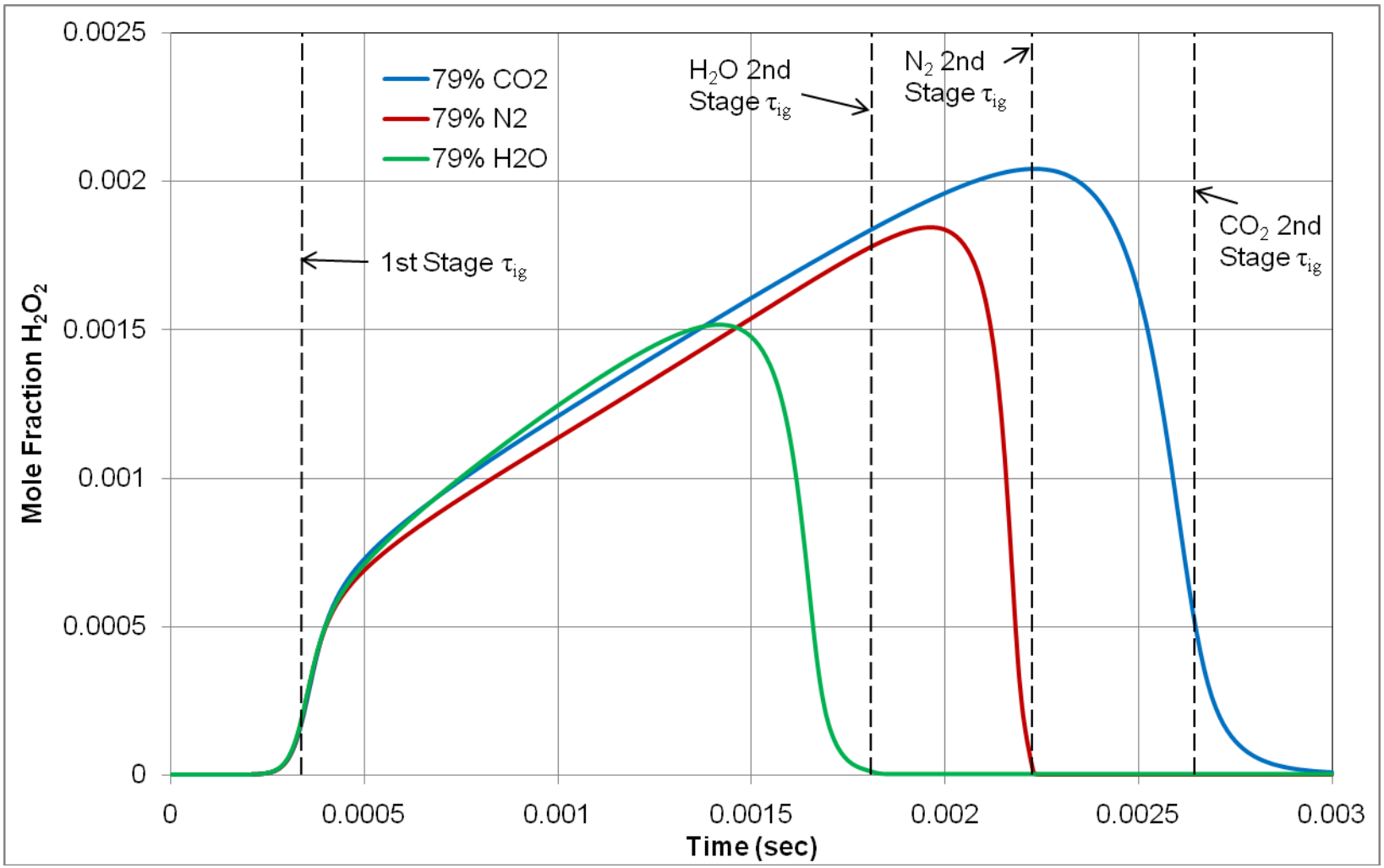

Figure 6.41: Mole Fraction H_2O_2 vs. Time, PRF 20, $y_{O_2} = 0.205$, $P_{in} = 40$ atm, $T_{in} = 900$ K, Fuel/O_2 Equivalence Ratio = 0.4.

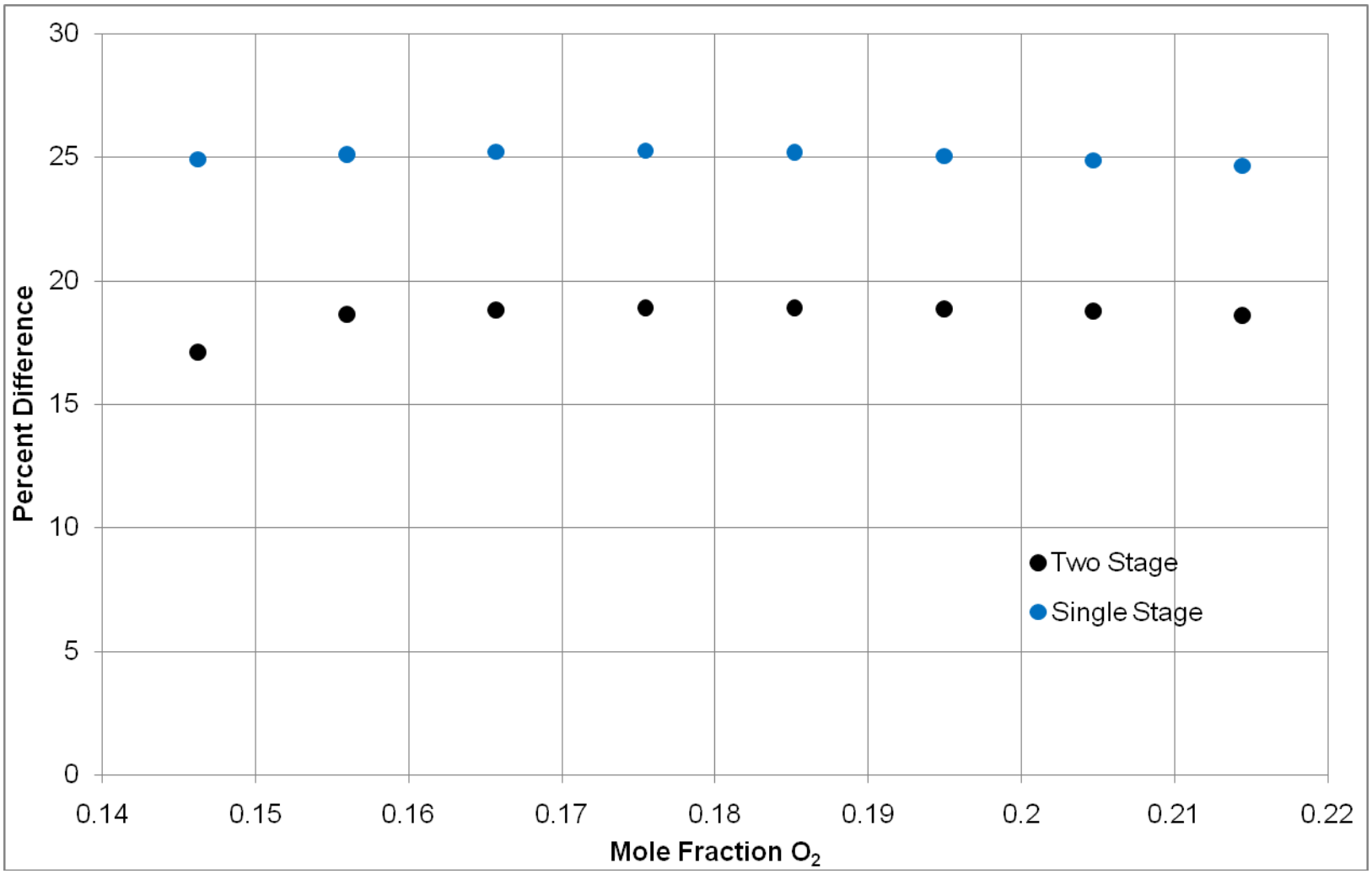

Figure 6.42: % Difference of N_2 and H_2O Ignition Delay vs. y_{O_2}, PRF 20, P_{in} = 40 atm, Fuel/O_2 Equivalence Ratio = 0.4.

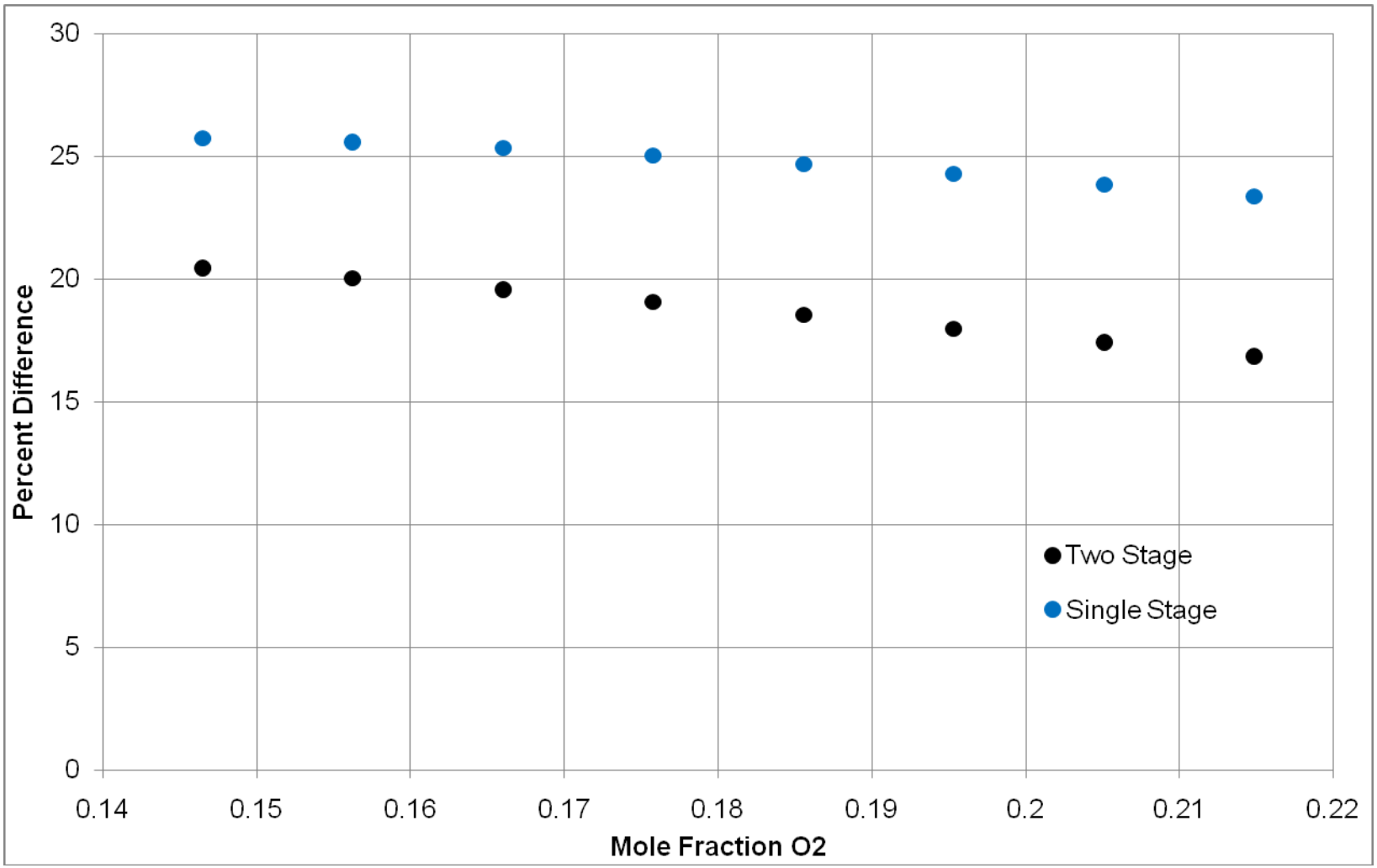

Figure 6.43: % Difference of N_2 and H_2O Ignition Delay vs. y_{O_2}, PRF 84, P_{in} = 40 atm, Fuel/O_2 Equivalence Ratio = 0.4.

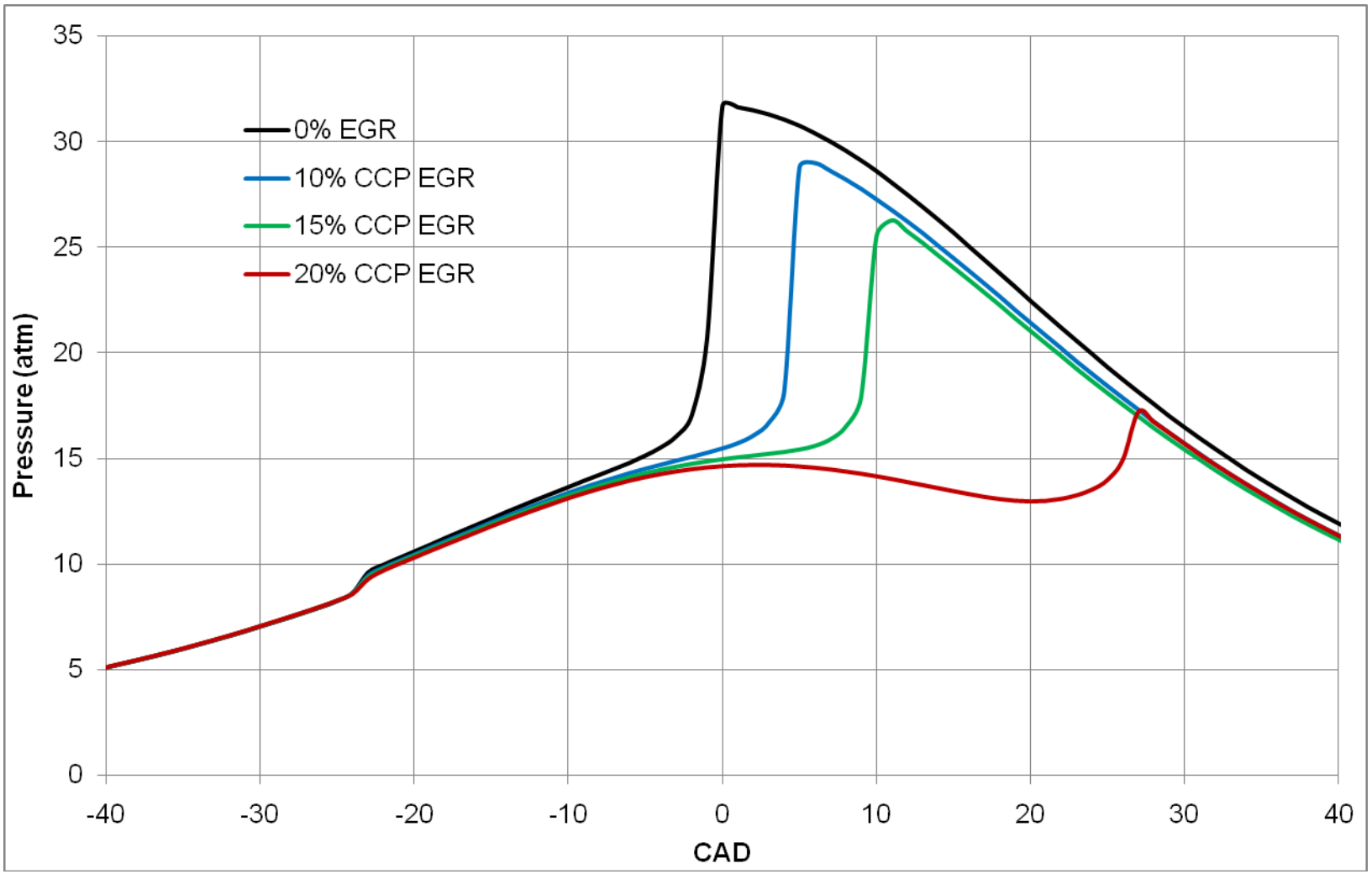

Figure 6.44: Pressure vs. CAD at Varying CCP EGR Rates Modeling the PRF 20 Engine.

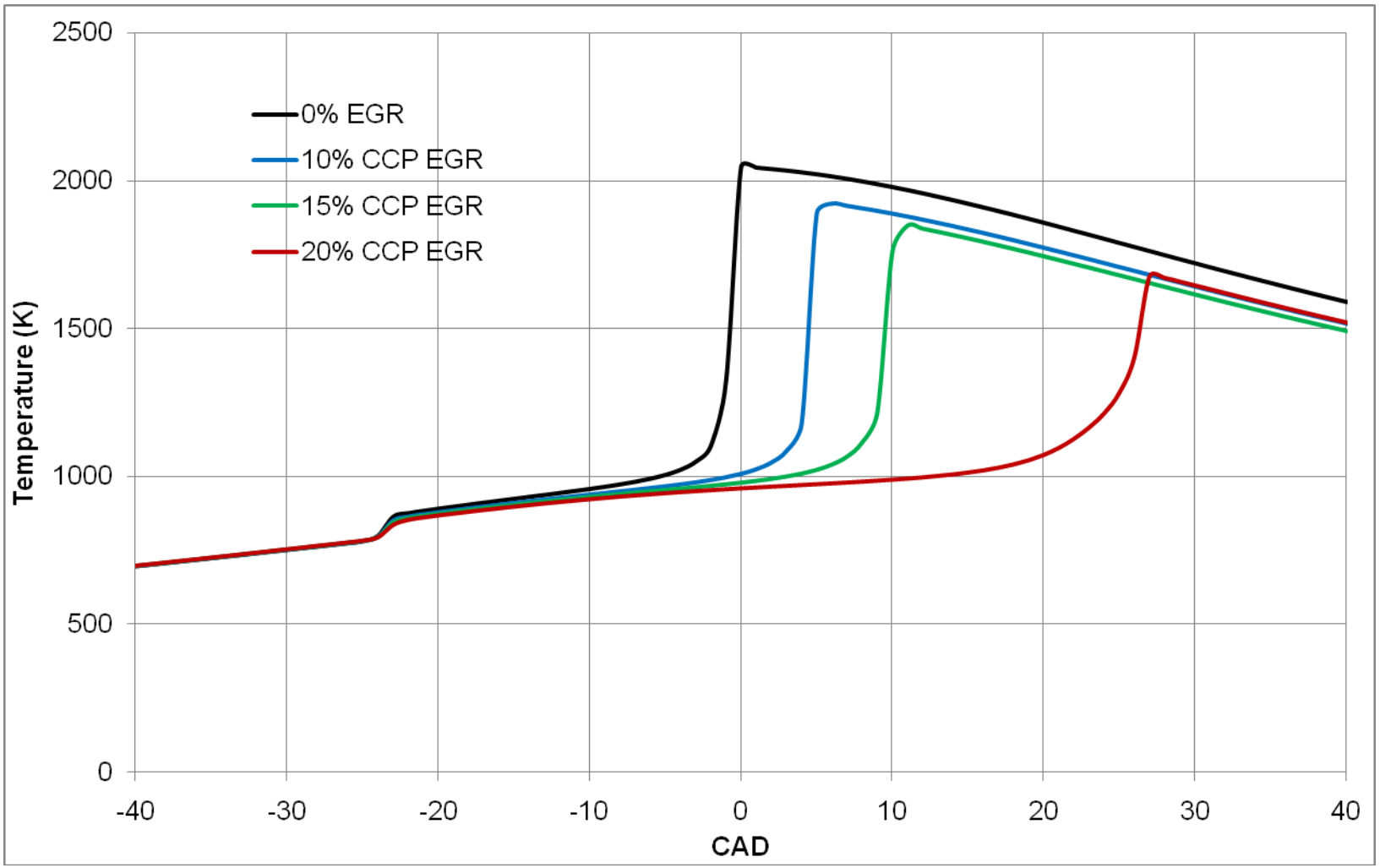

Figure 6.45: Temperature vs. CAD at Varying CCP EGR Rates Modeling the PRF 20 Engine.

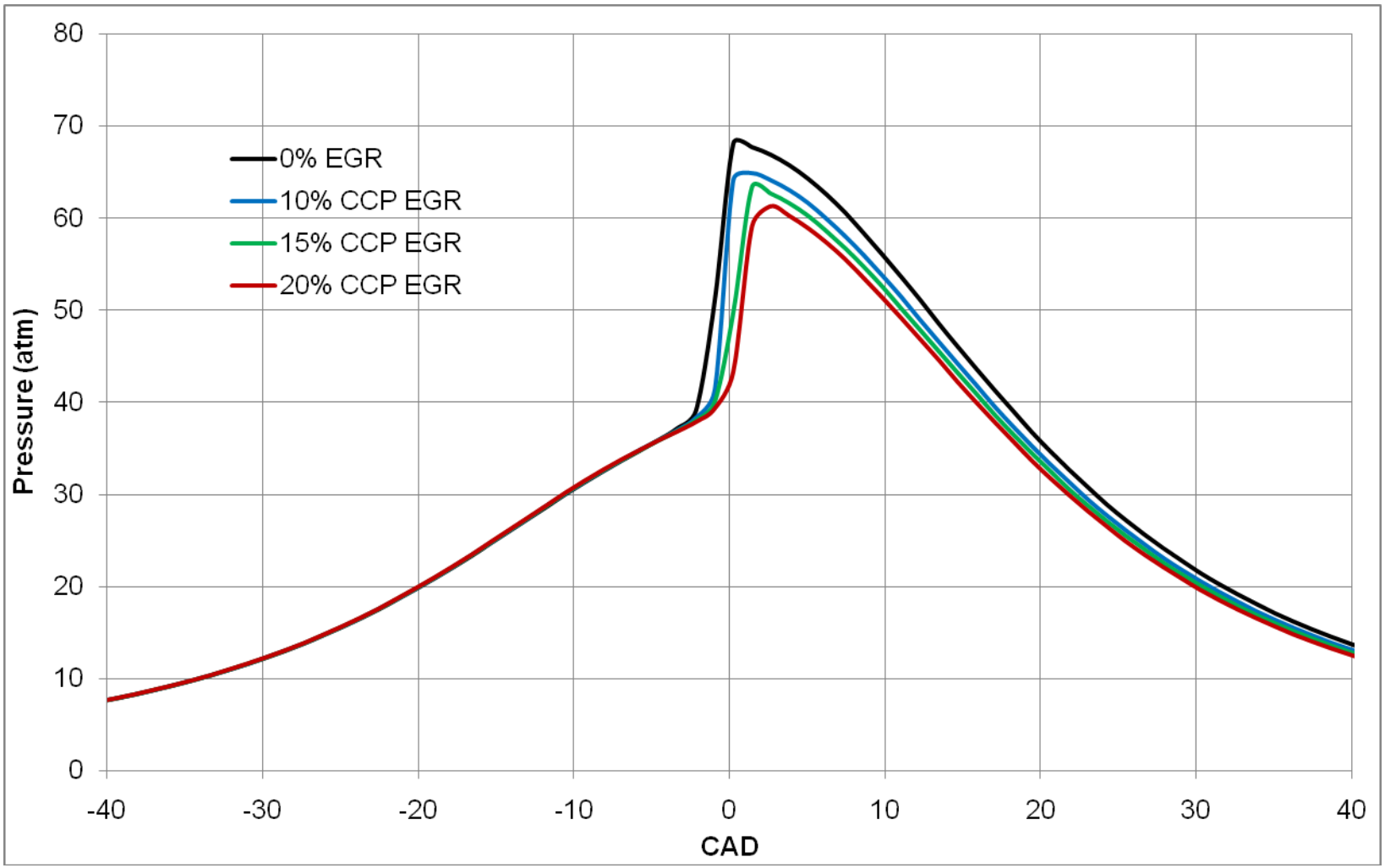

Figure 6.46: Pressure vs. CAD at Varying CCP EGR Rates Modeling the PRF 84 Engine.

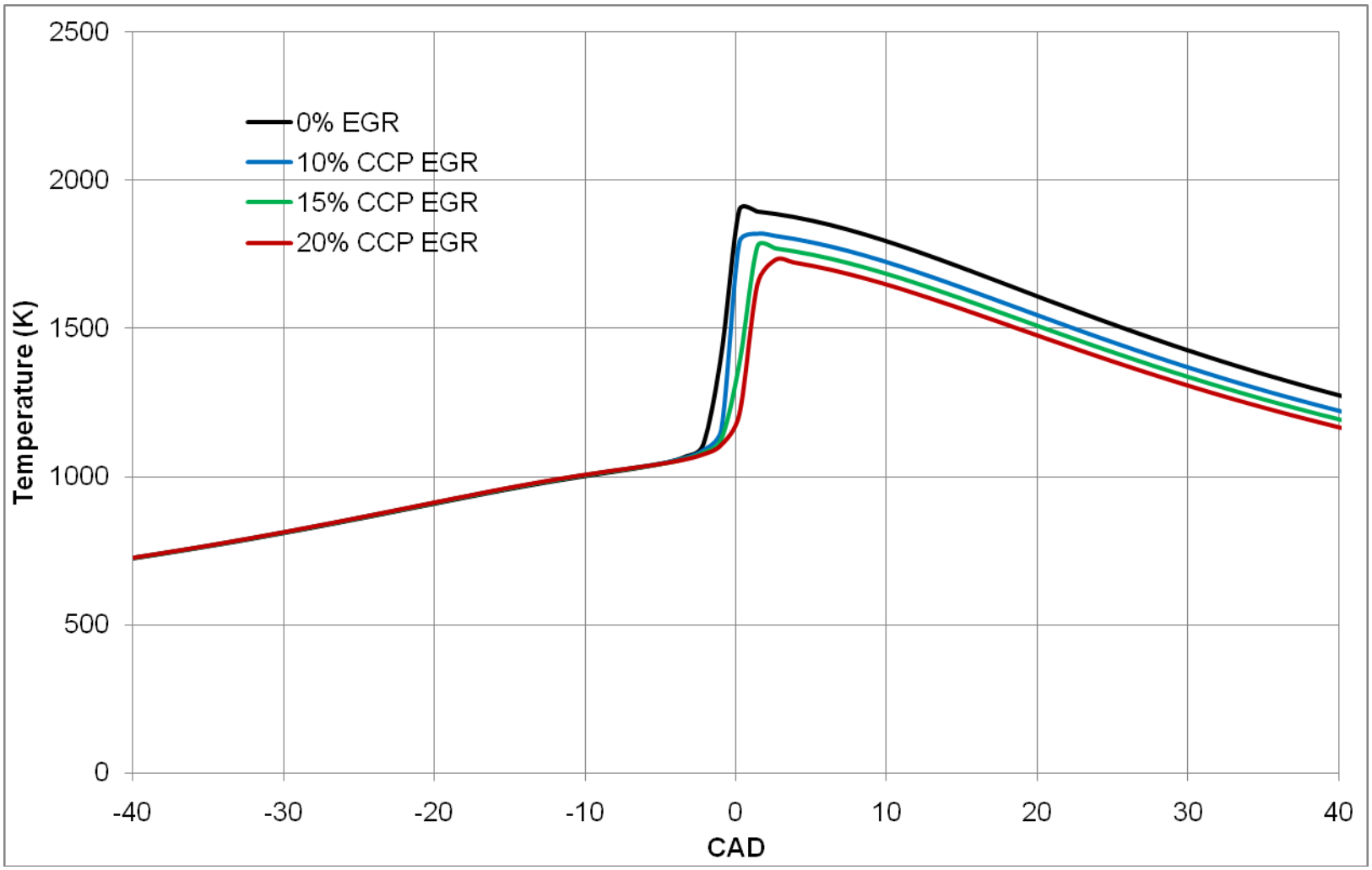

Figure 6.47: Temperature vs. CAD at Varying CCP EGR Rates Modeling the PRF 84 Engine.

CHAPTER 7

CONCLUSION

An investigation of the autoignition characteristics of Primary Reference Fuels (PRFs) using a detailed kinetics mechanism has been conducted. The modeling package CHEMKIN (2006) was used to facilitate the solution of the kinetic model by Curran *et al*. (2002) in constant volume and variable volume (IC engine) reactors. The kinetic model was first compared with experimental data of shock tube ignition delay times and then homogeneous charge compression ignition (HCCI) engine data. It was observed that the model consistently predicted longer ignition delay than the shock tube data; however, trends with varying temperature were captured over a wide range of octane number (ON). There was some difficulty in modeling the HCCI engine combustion, and this was primarily credited to non-ideal conditions of the real engine combustion such as temperature inhomogeneities. Regardless, it was observed that many of the experimental trends could be reproduced with the model and baseline conditions were established to facilitate a parametric study. The constant volume adiabatic reactor was first used to isolate effects of the parameter being studied, and a parametric investigation in the HCCI engine model followed. The effects of inlet pressure P_{in}, inlet temperature T_{in}, ON, equivalence ratio ϕ, and exhaust gas recirculation (EGR) were studied. The following is an itemized list of significant observations.

- The hot (explosive) ignition temperature is approximately constant independent of P_{in}, T_{in}, or ON.
- The induction time between the first and second stages of two-stage ignition is dependent upon the energy released during the first stage ignition. A larger first stage energy release results in a shorter induction time.
- For two-stage ignition, a higher P_{in} or lower T_{in} results in larger first stage energy release.
- The temperature at the conclusion of the first stage in two-stage ignition (that is the temperature where degenerate branching overcomes the first stage reactions) is independent of T_{in}.
- Fuels with lower ON exhibit larger first stage energy release for two-stage ignition. This is due to a higher percentage of n-C_7H_{16} in the fuel composition.
- Fuels with a range of ON = 0 – 100 can exhibit single or two-stage ignition for given P_{in} and ϕ. The critical T_{in} separating single and two-stage ignition decreases approximately linearly with an increase in ON.
- The total energy release increases with ϕ for the range studied here (ϕ = 0.2 – 0.6). For two-stage ignition, the first stage energy release also increases with ϕ, and the burn rate decreases significantly with decreasing ϕ, particularly below ϕ = 0.4.
- The total ignition delay, single or two-stage, is correlated with n-C_7H_{16}/O_2 ratio and not with i-C_8H_{18}/O_2.
- EGR can have both thermodynamic and chemical effects on ignition.

- The thermodynamic effect of EGR is due to changes in the mixture specific heat c_p. Addition of a diluent with higher c_p than air will inhibit temperature increases and delay ignition. This is the case for the thermodynamic effects of CO_2 and H_2O; however, N_2 has a slightly lower c_p than air and thus can decrease ignition delay.
- The reduction of O_2 mole fraction as a result of EGR introduction is a chemical effect that increases ignition delay and occurs regardless of diluent.
- An additional chemical effect of H_2O was identified that enhances ignition. The kinetic model predicts this effect is stronger for single stage ignition than two-stage.

This study has identified a number of characteristics of the autoignition of PRF mixtures with varying reactor types and inlet condtions according to the kinetic model. It has been shown that reproducing experimental HCCI combustion data with CHEMKIN's IC Engine model is not without difficulty and at this point fails to accurately reproduce the complete measured pressure and temperature profiles. It should be noted that although the kinetic model has been tested extensively by its authors and is among the most widely used in literature to describe PRF oxidation, the data generated in this study does not represent actual experiments and therefore is subject to flaws. Nonetheless, the material presented here can be useful for identifying mechanisms that affect PRF autoignition.

LIST OF REFERENCES

Andrae, J., Johansson, D., Bjornbom, P., Risberg, P., and Kalghatgi, G., 2005, "Co-Oxidation in the Auto-Ignition of Primary Reference Fuels and *n*-Heptane/Toulene Blends," *Combustion and Flame* **140**, 267-286.

Benson, S. W., 1976, "Thermochemical Kinetics," Wiley, NY.

Benson, S. W., 1981, "The Kinetics and Thermochemistry of Chemical Oxidation with Application to Combustion and Flames," *Progress in Energy and Combustion Science* **7**, 125-134.

Brüstle, C. and Hemmerlein, N., 1994, "Exhaust Gas Turbocharged SI Engines and Their Ability of Meeting Future Demands," *IMechE* Paper C484/039/94.

Chang, J., Güralp, O., Filipi, Z., Assanis, D., Kuo, T., Najt, P., and Rask, R., 2004, "New Heat Transfer Correlation for an HCCI Engine Derived from Measurements of Instantaneous Surface Heat Flux," *SAE* Paper 2004-01-2996.

Chase, M. W., Jr., 1998, "NIST-JANAF Thermochemical Tables, Fourth Ed., American Chemical Society/American Institute of Physics, Washington, DC.

CHEMKIN Release 4.1, 2006, Reaction Design, San Diego, CA.

Cox, R. A. and Cole, J. A., 1985, "Chemical Aspects of the Autoignition of Hydrocarbon-Air Mixtures," *Combustion and Flame* **60**, 109-123.

Curran, H. J., Gaffuri, P., Pitz, W. J., and Westbrook, C. J., 2002, "A Comprehensive Modeling Study of iso-Octane Oxidation," *Combustion and Flame* **129**, 253-280.

Diana, S., Giglio, V., Iorio, B., and Police, G., 1996, "A Strategy to Improve the Efficiency of Stoichiometric Spark Ignition Engines," *SAE* Paper 961953.

Dryer, F. L., 1991, "The Phenomenology of Modeling Combustion Chemistry," *Fossil Fuel Combustion-A Source Book*, 121-213, Bartok, W. and Sarofim, A. F., Eds., Wiley, NY.

Dryer, F. and Glassman, I., 1978, "Combustion Chemistry of Chain Hydrocarbons," *Progress in Astronautics and Aeronautics* **62**, 255-306.

Epping, K., Aceves, S., Bechtold, R., and Dec, J., 2002, "The Potential of HCCI Combustion for High Efficiency and Low Emissions," *SAE* Paper 2002-01-1923.

Fieweger, K., Blumenthal, R., and Adomeit, G., 1997, "Self-Ignition of S.I. Engine Model Fuels: A Shock Tube Investigation at High Pressures," *Combustion and Flame* **109**, 599-619.

Fristrom, R. and Westenberg, A., 1965, "Flame Structure," McGraw-Hill, NY.

Glassman, I., 1996, "Combustion," Third Ed., Academic Press, CA.

Grandin, B., Ångström, H., Stålhammar, P., and Olofsson, E., 1998, "Knock Suppression in a Turbocharged SI Engine by Using Cooled EGR," *SAE* Paper 982476.

Gu, X. J., Emerson, D. R., and Bradley, D., 2003, "Modes of Reaction Front Propagation from Hot Spots," *Combustion and Flame* **133**, 63-74.

Heywood, J., 1988, "Internal Combustion Engine Fundamentals," McGraw-Hill, NY.

Hu, H. and Keck, J., 1987, "Autoignition of Adiabatically Compressed Combustible Gas Mixtures," *SAE* Paper 872110.

Kalghatgi, G., Risberg, P., and Angstrom, H., 2003, "A Method of Defining Ignition Quality of Fuels in HCCI Engines," *SAE* Paper 2003-01-1816.

Kee, R. J., Rupley, F. M., and Miller, J. A., 1987, "The Chemkin Thermodynamic Data Base," *Sandia National Laboratories*, Report SAND87-8215B.

Knyazev, V. D. and Slagle, I. R., 1998, "Thermochemistry of the R-O_2 Bond in Alkyl and Chloroalkyl Peroxy Radicals," *The Journal of Physical Chemistry A* **102**, 1770-1778.

Lay, T. H. and Bozzelli, J. W., 1997, "Enthalpies of Formation and Group Additivity of Alkyl Peroxides and Trioxides," *The Journal of Physical Chemistry A* **101**, 9505-9510.

Lay, T. H., Bozzelli, J. W., Dean, A. M., and Ritter, E. R., 1995, "Hydrogen Atom Bond Increments for Calculation of Thermodynamic Properties of Hydrocarbon Radical Species," *The Journal of Physical Chemistry* **99**, 14514-14527.

Lewis, B. and von Elbe, G., 1951, "Combustion, Flames and Explosions of Gases," Academic Press, Inc., NY.

McBride, B. J., Zehe, M. J, and Gordon, S., 2002, "NASA Glenn Coefficients for Calculating Thermodynamic Properties of Individual Species," NASA Glenn Research Center, TP-2002-211556.

Moran, M. J. and Shapiro, H. N., 2004, "Fundamentals of Engineering Thermodynamics," Fifth Ed., Wiley, NJ.

Nakagawa, Y., Takagi, Y., Itoh, T., and Iijima, T., 1984, "Laser Shadowgraphic Analysis of Knocking in S.I. Engine," *SAE* Paper 845001.

Ritter, E. R. and Bozzelli, J. W., 1991, "THERM: Thermodynamic Property Estimation for Gas Phase Radicals and Molecules," *International Journal of Chemical Kinetics* **23**, 767-778.

Semenov, N. N., 1958, "Some Problems in Chemical Kinetics and Reactivity," Princeton University Press, Princeton, NJ.

Simmie, J. M., 2003, "Detailed Kinetic Models for the Combustion of Hydrocarbon Fuels," *Progress in Energy and Combustion Science* **29**, 599-634.

Sjöberg, M., Dec, J. E., and Hwang, W., 2007, "Thermodynamic and Chemical Effects of EGR and Its Constituents on HCCI Autoignition," *SAE* Paper 2007-01-0207.

Smith, J. R., Green, R. M., Westbrook, C. K., and Pitz, W. J., 1984, "An Experimental and Modeling Study of Engine Knock," *Proceedings of the Twentieth International Symposium on Combustion*, 91-100, The Combustion Institute.

Tanaka, S., Ayala, F., and Keck, J. C., 2003, "A Reduced Chemical Kinetic Model for HCCI Combustion of Primary Reference Fuels in a Rapid Compression Machine," *Combustion and Flame* **133**, 467-481.

Tanaka, S., Ayala, F., Keck, J. C., and Heywood, J. B., 2003, "Two-Stage Ignition in HCCI Combustion and HCCI Control by Fuels and Additives," *Combustion and Flame* **132**, 219-239.

Thring, R. H., 1989, "Homogeneous Charge Compression Ignition (HCCI) Engines," *SAE* Paper 892068.

Woschni, G., 1967, "Universally Applicable Equation for the Instantaneous Heat Transfer Coefficient in the Internal Combustion Engine," SAE Paper 670931, *SAE Transactions* **76**, 3065-3083.

Würmel, J., Silke, E. J., Curran, H. J., Ó Conaire, M. S., and Simmie, J. M., 2007, "The Effect of Diluent Gases on Ignition Delay Times in the Shock Tube and in the Rapid Compression Machine," *Combustion and Flame* **151**, 289-302.

Zheng, J., Miller, D. L., and Cernansky, N. P., 2004, "A Global Reaction Model for the HCCI Combustion Process," *SAE* Paper 2004-01-2950.

Zheng, J., Yang, W., Miller, D. L., and Cernansky, N. P., 2002, "A Skeletal Chemical Kinetic Model for the HCCI Combustion Process," *SAE* Paper 2002-01-0423.